Selective Sequestration of Carbon dioxide in Natural Gas Hydrates – Role of Third Gas

A thesis

submitted for the Degree of

Doctor of Philosophy

by

Satyam Singh

(18CHPH10)



School of Chemistry
University of Hyderabad
Hyderabad – 500 046, INDIA

August, 2023

Dedicated to my Parents, Family Members and special thanks to My Grandfather and Brother

CONTENTS

Statement	1
Certificate	ii
Coursework Certificate	iii
Acknowledgements	iv
Abbreviations	vi
Chapter 1 – Introduction	1
Chapter 2 – Role of Polyatomic Gases in CO ₂ -CH ₄ Exchange in NGHs	40
Chapter 3 – Role of Monatomic Gases in CO ₂ -CH ₄ Exchange in NGHs	58
Chapter 4 – Role of Flue Gases and Noble Gases in CO ₂ -CH ₄ exchange in NGHs	79
Chapter 5 – Role of Hydrate Promoter (EDTA Bisamides) in CO ₂ -CH ₄ Exchange	
in NGHs in Presence of Monatomic and Polyatomic Gases	100
Chapter 6 – Future Directions	123

STATEMENT

I hereby declare that the matter embodied in the thesis entitled "Selective Sequestration of Carbon dioxide in Natural Gas Hydrates – Role of Third Gas" is the result of investigation carried out by me in the School of Chemistry, University of Hyderabad, India, under the supervision of Dr. Manju Sharma.

In keeping with the general practice of reporting scientific investigations, acknowledgement have been made wherever the work described based on the finding of other investigators.

17/08/2023

Date

200

Signature of candidate

CERTIFICATE



School of Chemistry University of Hyderabad Hyderabad, 500046 Telangana, India

This is to certify that the research work contains in this thesis, entitled "Selective Sequestration of Carbon dioxide in Natural Gas Hydrates – Role of Third Gas" submitted by Satyam Singh, (Reg. No. 18CHPH10), in partial fulfilment of the requirements for the award of Doctor of Philosophy in Chemistry is a bonafide work carried out by him under my supervision and guidance. This thesis is free from plagiarism and has not been submitted previously in part or in full to this University or any other University or Institution for award of any degree or diploma.

Part of this thesis have been communicated:

Role of Third Gas in Enhancing Methane-Carbon Dioxide Exchange in Natural Gas Hydrates, Satyam Singh and Manju Sharma* (*Under Review*).

Role of Mixture of Flue Gases and Noble Gases in Methane-Carbon dioxide Exchange in Natural Gas Hydrates. Satyam Singh and Manju Sharma* (*Under Review*).

Part of this thesis to be communicated:

Xenon and EDTA Bisamides Enhanced CO2 Selectivity in Natural Gas Hydrates. Satyam Singh and Manju Sharma* (Under Preparation).

He has also made presentations in the following conferences:

Poster presentation, Titled "CO₂-CH₄ exchange in Natural Gas Hydrate – Role of Hydrate Promoters" in **Theoretical Chemistry Symposium (TCS-2019)**.

Poster presentation, Titled "CO₂-CH₄ exchange in Natural Gas Hydrate – Role of Hydrate Promoters" in **Annual In-House Symposium CHEMFEST 2019**.

Attended the Mumbai Workshop on Quantum Chemistry (MWQC 2019).

Participated in DAE Symposium on current Trends in Theoretical Chemistry (CTTC-2020).

Oral Presentation, Titled "Role of Small Gas Molecules in CO₂-CH₄ Exchange in Natural Gas Hydrates" in Annual In-House Symposium CHEMFEST 2023.

Further, the student has passed the following courses towards fulfilment of coursework requirement for PhD.:

Sl. No.	Course	Title	Credits	Pass/Fail
1	CY801	Research Proposal	4	Pass
2	CY805	Instrumental Methods- A	4	Pass
3	CY806	Instrumental Methods- B	4	Pass

Final Result: Passed

Hyderabad

August 2023

Dr. Manju Sharma

(Thesis Supervisor)

MANJU SHARMA Assistant Professor School of Chemistry University of Hyderabad Hyderabad - 500 046.

Dean SCHOOL OF CHEMISTRY University of Hyderabad School of ChemistryHyderabad-500 046

ACKNOWLEDGEMENTS

With a genuine pleasure, I would like to express profound respect and gratitude to my PhD Supervisor, **Dr Manju Sharma**, for her valuable guidance, continuous support, suggestions and inspiration throughout my research work. I am very thankful to be a student under her supervision and will always be in debt to her for values to approach and deal with research problems that would help me throughout my life. I feel inspired from her scientific research standards, writing and communication skills. I would like to convey my special thanks to her for constant support during ups and downs in my personal life. This endeavour would have not completed without her suggestions and inspiration.

I would like to express my heartfelt gratitude to my DRC committee members - Prof. Samar Kumar Das and Prof. Susanta Mahapatra for their suggestions and encouragement.

I thank the present and former Deans of School of Chemistry for providing me a great environment for study and discussion, non-teaching staff and staff in administrative building for their help at different occasions.

My special thanks to lab mates: Shyam, Shampita and Nisha to provide a friendly environment in the lab. We spent golden-times together, shared lot of good memories and they helped me a lot in all the phases during PhD. I am thankful to Shyam and Shampita for discussions and suggestions while learning FORTRAN programming, analysis of research work. I learnt a lot of things from Shyam when I joined this lab.

My special thanks to chai buddies: Daradi, Sachin, Asif, Aishwarya and Shyam. Especial thanks to Daradi and Sachin for numerous help and support at various events during tough times.

I would like to extend my thanks to Dr. Pranchi and Dr. Arun to guide me while writing the synopsis and thesis.

I would like to extend my thanks my roommates: Dr. Bhupendra, Dr. Mithilesh and Sameer for a friendly and supportive environment during early phase of PhD.

I would like to thank all my friends: Ajay, Intzar, Janish, Alamgiri, Rani, Shruti, Shrinivash, Shridatri, Praveen, Dr. Jaykrishna, Kirti, Nitai Da, Anjali, Divyanshu, Shekher, Sudarshan, Jishu, Abhisek, Sumit, Dr. Surrender, Irfan for support during various events. My sincere thanks to friends from cricket group: Shyam, Abinash, Manoj, Raajkiran, Koneti, Dr. Bilal, Dr. Ashfaque, Ashwini, Dr. Manas, Daud, Rakshit, Vinay, Vinod, Hasan, Liyaqat, Dr. Shubham, Hashan for Sunday cricket.

I would like to thank CMSD and DST SERB for computational facilities and UGC for the fellowship.

August, 2023 (Satyam Singh)

Hyderabad, 500 046

Abbreviations

CV Collective Variables

CP Cyclopentane

DFT Density Functional Theory

EDTA Ethylene Diamine Tetraacetic Acid

EG Ethylene Glycol

FES Free Energy Surface

HBL Hydrate Bearing Layer

KHPs Kinetic Hydrate Promoters (KHPs)

LAMMPS Large-scale Atomic/Molecular Massively Parallel Simulator

MC Monte Carlo

MD Molecular Dynamics

NGHs Natural Gas Hydrates

F4 OP F4 Order Parameter

OPLS-AA Optimized Potentials for liquid Simulations All-Atom

PPPM Particle-Particle Particle-Mesh

sI Structure I

sII Structure II

SDS Sodium Dodecyl Sulfate

sH Structure H

TBAB Tetra Butyl Ammonium Bromide

THPs Thermodynamic Hydrate Promoters

THF Tetrahydrofuran

TIP4P/2005 4-site Transferable Intermolecular Potential 2005 Model

VACF Velocity Autocorrelation Function

ZPE Zero Point Energy

Chapter 1

Introduction

1.1 Natural Gas Hydrates

Natural gas hydrates (NGHs) are non-stoichiometric solids, ice-like crystalline structure that are formed at low temperatures and high pressure and have polyhedral cages formed by hydrogen bonded (H- bond) network of water molecules and these cages are stabilized due to encapsulation of small molecules (CH₄, C₂H₆ and C₃H₈). The gas molecules that are entrapped into the cages are called the guest molecules and cages formed due to hydrogen bonded network of water molecules are called the hosts in gas hydrates as shown for methane hydrate in Figure 1.1. The interactions in gas hydrates are non-covalent in nature where interaction between the water molecules is due to hydrogen bonding and guests trapped inside the water cages interact *via* van der Waals interactions ¹⁻³. Gas hydrates have broad range of applications that range from methane recovery as a clean energy source ³⁻⁶, carbon dioxide sequestration ⁷, stabilization of hydrate reservoirs due to rising environment temperature ⁸, gas storage (164 cubic feet of CH₄ contains in 1 cubic foot of methane hydrates, transportation ⁹⁻¹¹ and separation methods ¹²⁻¹³. Recently natural gas hydrates have been proposed to be one of the alternatives for clean energy to meet the every-growing demands for energy and limited availability of the fossil fuels ¹⁴.

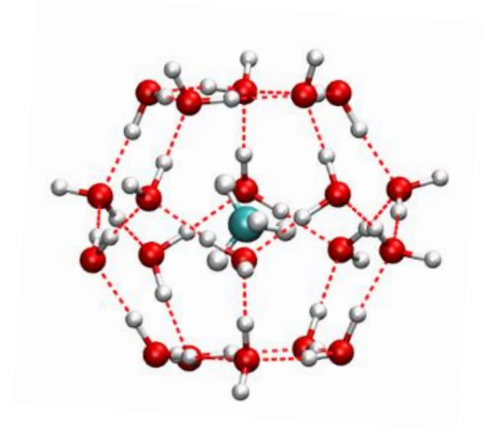


Figure 1.1: Small cage of methane hydrate with methane (cyan – C, red - O and white – H) in the centre of cage.

1.2 Type of Natural Gas Hydrates

There are mainly three types of natural gas hydrates (structure I (sI, cubic); structure II (sII, cubic) and structure H (sH, hexagonal)) that differ in stoichiometry and size of cages that form the unit cells in NGHs. sI-NGHs are the most abundant NGHs among all the NGHs ². There are five different types of hydrate cages and can be represented as X^Y where X and Y represent number of edges and faces in a hydrate cage as shown in Figure 1.2. Two or more cages combine in a specific patten and form the crystal structure.

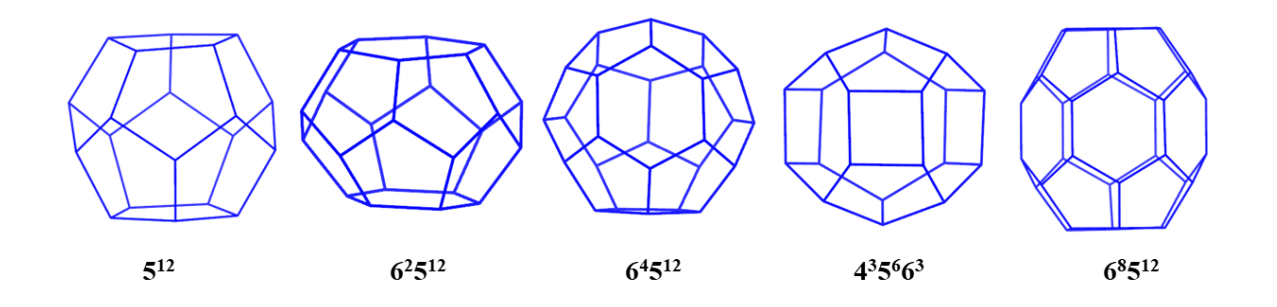


Figure 1.2: Five types of hydrate cages that exist in nature; (a) pentagonal dodecahedron (b) tetracaidecahedron (c) hexacaidecahedron (d) icosahedron and (f) irregular dodecahedron. (Reproduced from reference [1]).

1.2.1 Structure I (sI) NGHs

sI-NGH of ethylene oxide was first reported by McMullan and Jeffrey in 1965 ¹⁵. It is formed by combination of two small pentagonal dodecahedron (5¹²) and six large tetracaidecahedron (6²5¹²) cages with average cavity radii of 3.95Å and 4.33Å respectively as shown in Figure 1.3. A pentagonal dodecahedron cages has 12 planar pentagonal faces and tetracaidehedral cages has 12 pentagonal and 2 hexagonal faces with vertices shared between 5¹² blocks. A primitive unit cell lattice is formed by total eight guest molecules that are entrapped inside two 5¹² and six 6²5¹² cages formed by 46 hydrogen bonded water molecules. The dimensions of a sI unit cell is 12.0Å in all the three-dimensions. The quantitative formula of sI unit cell is 6A.2B.46H₂O where A and B are the number of guest molecules entrapped inside small and large cages of sI hydrate. The coordination numbers of water molecules for small and large cages are 20 and 24, respectively. The naturally occurring sI-NGHs mainly encapsulate small

gas molecules like CH_4 and C_2H_6 . The ideal hydrate number for sI unit cell is 5.75 which is the ratio of number of host molecules to number of guest molecules as reported in Eq. 1.1 ¹⁻².

Ideal hydrate number =
$$\frac{\text{Number of water molecules in the unit cell (46)}}{\text{Number of guest molcules in the unit cell (8)}} = 5.75$$
 Eq. (1.1)

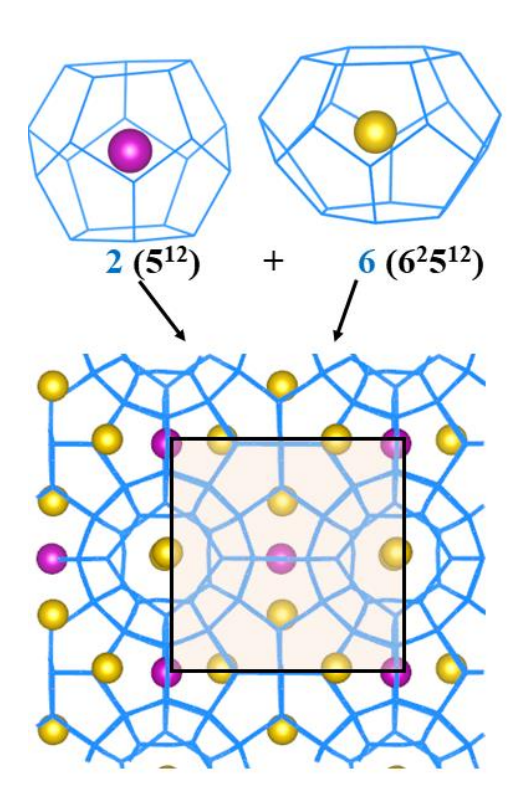


Figure 1.3: Schematic of a sI unit cell formation from small (5^{12}) and large (6^25^{12}) cages where magenta and golden spheres represent guests in small and large cages respectively. (Reproduced from reference [2]).

1.2.2 Structure II (sII) NGHs

sIIThe structure hydrate was first reported Mak McMullan for and tetrahydrofuran/hydrogen sulfide hydrate in 1965 16. A face centred cubic unit cell is formed by combination of 16 pentagonal dodecahedron (5¹², small cages) and 8 hexakaidecahedron (6⁴5¹², large cages) with average cavity radii of 3.91Å and 4.73Å respectively as shown in Figure 1.4. A unit cell consists of 32 guest molecules entrapped inside small and large cages formed by 136 hydrogen-bonded water molecules with an ideal hydrate number of 5.67. The dimensions of a unit cell is 17.3Å in all the three-dimensions. The quantitative formula of sII unit cell is 16A.8B.136H₂O, where A and B are the guest molecules entrapped in small and large cages. The coordination numbers for small and large cage is 20 and 28, respectively. sII-hydrates mainly encapsulate large guest molecules like propane and isobutane along-with small molecules such as CH_4 and H_2S $^{1-2}$.

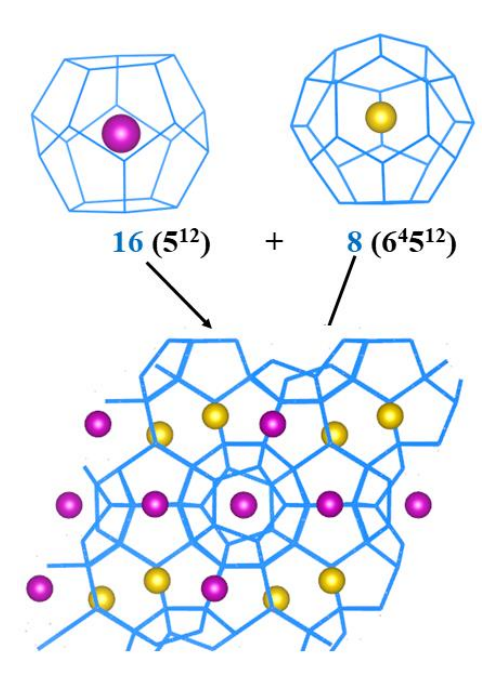


Figure 1.4: Schematic of a sII-NGH unit cell formation from small (5^{12}) cage and large (6^45^{12}) cages. (Reproduced from reference [2]).

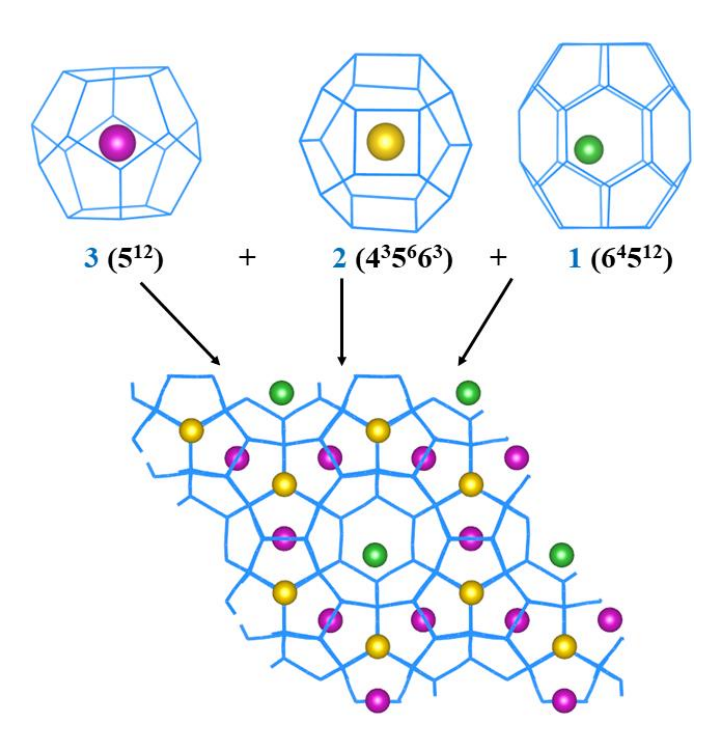


Figure 1.5: Schematic of a unit cell of sH NGH with small (5^{12}), medium ($4^35^66^3$) and large (6^85^{12}) cages. (Reproduced from reference [2]).

1.2.3 Structure H (sH) NGHs

The structure of sH unit cell was reported by Ripmeester *et. al.* in 1987 for 2,2-dimethylpentane, 5(Xe, H₂S).34H₂O hydrate that was synthesized using a mixture of 2,2-dimethylpentane, Xe and H₂S in ice ¹⁷. A hexagonal unit cell of sH hydrate is formed by three pentagonal dodecahedron (5¹², small cages), two irregular dodecahedron (4³5⁶6³, medium cage) and one icosahedron (6⁸5¹², large cage) with cavity radii of 3.91Å, 4.06Å and 5.71Å respectively as shown in Figure 1.5. The unit cell of sH-NGH consists of 6 guest molecules encapsulated into a network of cages formed by 34 water molecules. The quantitative formula of a sH unit cell is 3A.2B.1C.136H₂O where A, B and C are the guest molecule entrapped in small, medium and large cages, respectively. sH hydrates encapsulate small (CH₄, CO₂ and ethane) as well as large guest molecules like cyclopentane and neohexene ¹⁻².

1.3 Classification of hydrate reservoirs

NGH reservoirs are classified based on the coexistence of NGHs with other phases such as free water or free gas. These reservoirs are divided into three classes: Class 1, Class 2 and Class 3 as shown in Figure 1.6 ¹⁸⁻²¹. Class 1 reservoirs are formed with hydrate bearing layer (HBL) underlying a free gas zone as shown in Figure 1.6a. The free zone and thermodynamic conditions are close to equilibrium phase of NGHs thus, making Class 1 reservoirs as the most promising reservoirs for hydrate production. Depressurization is the most suitable technique for gas hydrate production in these reservoirs as it is simple and cost-effective technique. Class 1 reservoirs exist in Russia (Messoyokha field) and Alaska (Sagavanirktok region) ²⁰⁻²¹. Class 2 reservoirs are formed with HBL underlying on free water zone as shown in Figure 1.6b, while in Class 3, there is only a HBL as shown in Figure 1.6c. Class 2 and Class 3 reservoirs are less promising in term of gas production as thermodynamic conditions, stability zones and economic considerations are not well defined. Depressurization is a less effective technique for Class 2 reservoirs due to continuous supply of water from free water zone. Similarly, depressurization is least effective for Class 3 reservoirs as there is absence of free gas or free water ²⁰⁻²¹. Beside these three reservoirs, Class 4 reservoirs consist of less saturated and unconfined geological layer zones and are widely distributed at ocean floor ²⁰⁻²¹.

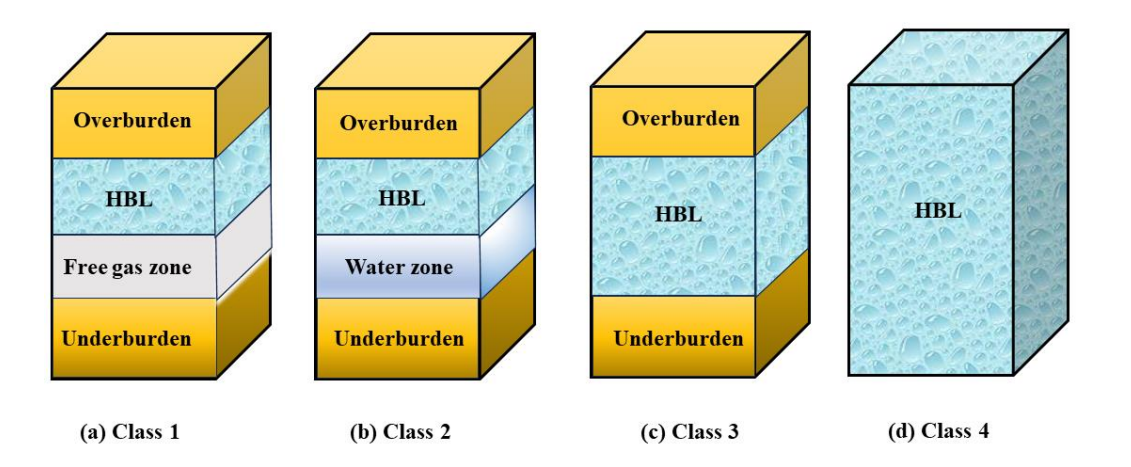


Figure 1.6: Schematic diagram of different classes of hydrate reservoirs: (a) Class 1 (b) Class 2 (c) Class 3 and (d) Class 4. (Reproduced from reference [20]).

1.4 Methane Extraction Techniques

Traditionally, different conventional techniques are employed to recover CH₄ from NGH reservoirs such as thermal simulation, depressurization and chemical inhibitor injection. We present a brief introduction to these techniques in the following section.

1.4.1 Thermal Simulation Technique

The temperature of NGH reservoir is increased by heating or steam injection in thermal simulation technique ^{21, 23-27}. Therefore, temperature of reservoir turns above the phase equilibrium temperature at a local pressure as shown in Figure 1.7a. As a result, natural gas starts releasing along-with water due to hydrate dissociation. McGuire reported that thermal simulation as an effective technique in early stage of gas production from Class 2 NGH reservoirs with high permeability for gas production ². Later, in 1982, feasibility and effectiveness of this technique was further evaluated by Holed et. al. ²⁴. Eventually, numerous thermal simulation studies were reported and are categorized in three sets; (I) Hot water circulation, (II) Wellbore heating and (III) Hot water huff and puff methods. Tung et. al. ²⁵ reported hot water injection method in unconsolidated sediment by using one dimensional experimental setup where the temperature of injected water, injection rate and hydrate saturation were the controlling factors. The results showed that high hydrate saturation, lower water injection rate and temperature provides higher energy ratio. In case of wellbore heating

technique, wellbore is heated by different methods such as electric heating, which was first introduced by Islam in 1990 ²⁶; it is considered as *situ* approach. Herein, heat loss during heat flow through well could be controlled, as a result, this method could achieve higher energy efficiency. Hot water huff and puff method is performed in three stages: heat injection, soaking and gas production. In the first stage, hot water is injected into the system for a particular time, as a result, pressure will start rising in the second step and when the pressure of system will stop rising, the production of gas will start. These three steps make a cycle and thus, this technique is performed in cycles ²⁷.

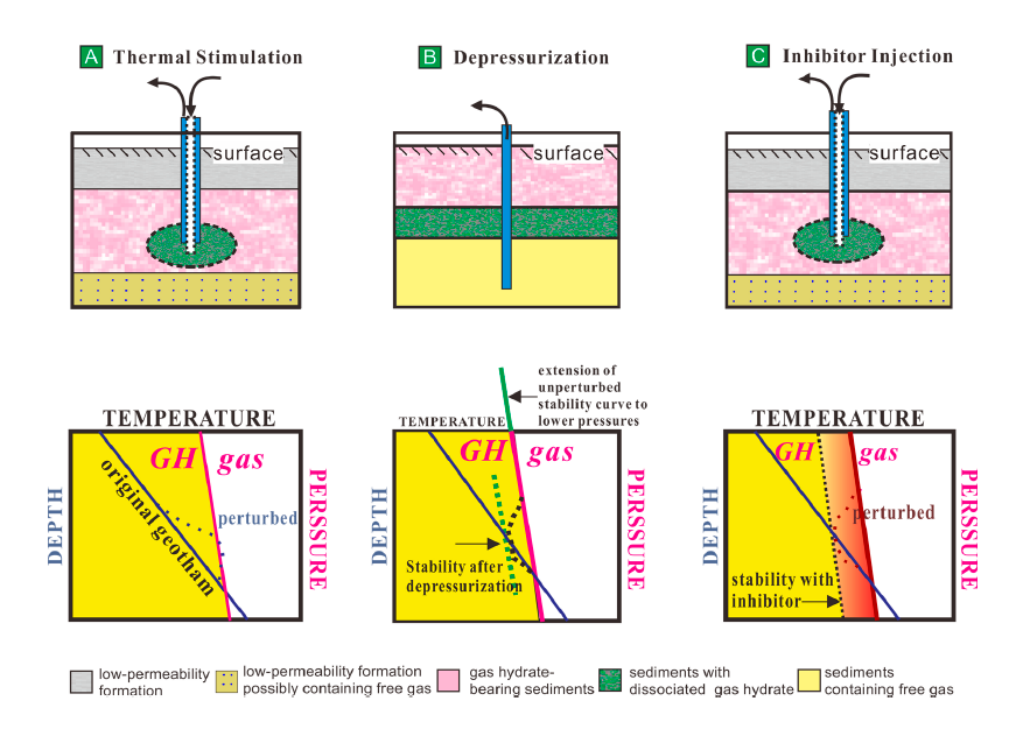


Figure 1.7: Schematic representation of three conventional techniques and their effect on phase equilibrium of gas hydrate reservoir; (a) Thermal Stimulation (b) Depressurization and (c) Chemical Inhibitor Injection. (Taken from reference [22]).

1.4.2 Depressurization

Depressurization reduces the equilibrium pressure of NGH reservoirs at the local temperature ^{21, 28-29}. The pressure difference causes dissociation of hydrate cages leading to production of gas and water as shown in Figure 1.7b. Hydrate dissociation is an endothermic process that results in lowering of local temperature of hydrate reservoirs and dissociation of hydrate cages.

The dissociation of cages might reduce when the local temperature reaches equilibrium temperature at a given pressure. Hence, heat must be required for continuation of this process. Hence, first hydrate dissociation starts near the well leading to release of natural gas and water ²¹. The early studies on gas production *via* depressurization method at a laboratory scale showed that hydrate dissociation that leads to gas production positively changed with time and showed some buffering due to endothermic hydrate dissociation ³⁰. Heat flow is considered to be the controlling factor for hydrate dissociation in thermal injection method; however, pressure difference is considered to be a driving force for hydrate dissociation in depressurization method ²⁹⁻³⁰. The rate of hydrate dissociation above 273.15K is governed by intrinsic dissociation reaction ³¹⁻³³. However, at temperature below 273K, hydrate dissociation is controlled by gas diffusion in a mixture of hydrate and ice. It was noticed in the later process that free water molecules due to hydrate dissociation would rapidly turn into ice at the hydrate surface. As a result, hydrate dissociation below 273.15K is considered as a process of moving ice-hydrate boundary ³⁴. Tang et. al. reported hydrate depressurization at different conditions, where they compared both gas production and propagation of dissociation of gas hydrate with respect to time ³⁵. The results showed that hydrate dissociation is controlled by pressure difference between the outlet and equilibrium. If the pressure difference is high, hydrate dissociation will be low. However, rate of hydrate dissociation was found to be the highest when pressure difference is near to equilibrium pressure. In conclusion, heat supply is considered to be a controlling factor for hydrate dissociation in depressurization technique. The efficiency of gas recovery might be restricted if heat supply is added in the later stages when temperature starts to reduce because of endothermic process.

1.4.3 Chemical Hydrate Inhibitor

Chemical hydrate inhibitors alter the phase equilibria of NGH reservoirs to low pressure and high temperature and thus, destabilize NGHs as shown in Figure 1.7c ^{21, 36-37}. Chemical inhibitors are generally categorized as thermodynamic and kinetic inhibitors where thermodynamic inhibitors shift the phase equilibrium, while kinetic inhibitors prolong the rate of hydrate formation. Methanol and Ethylene Glycol (EG) are the two most common hydrate inhibitors available in the market that have low toxicity and good performance. Sira et. al. showed that hydrate dissociation rate was controlled by inhibitor concentration, injection rate,

local pressure and contact area of interface and inhibitor and similar results were observed with brines in presence of hydrate inhibitors ³⁶⁻³⁷.

1.5 CO₂-CH₄ exchange

CO₂-CH₄ exchange in NGHs is being explored over past few decades and is to have certain advantages over conventional methane extraction technologies 2, 38-41. First, conventional technologies exploit the stability of hydrates for gas production and could destabilize the hydrate reservoirs as large-scale melting of hydrates could lead to geological disasters. However, CO₂-CH₄ exchange process replaces natural gas i.e., CH₄ with CO₂ that would help to sequestrate CO₂ which is one of the major global warming gases ⁴². Thermodynamically, enthalpy for CO₂ hydrate formation (≈ -57.98 kJ/mol) is lower than the enthalpy for CH₄ hydrate formation (≈ -54.49 kJ/mol) which would stabilize the gas hydrate reservoirs during CH₄-CO₂ exchange process ⁴³. CO₂-CH₄ exchange in NGHs has been confirmed by several experiments where liquid CO₂, pure CO₂ gas and CO₂ emulsion were fed into water ⁴²⁻⁵⁰. The molecular dynamics simulations studies showed that Gibbs free energy for CH₄ replacement by $CO_2 \approx -12.00$ kJ/mol ⁵¹. The mechanism of CO_2 -CH₄ exchange is widely covered by *situ* Raman spectroscopy and there are two exchange processes proposed for CO₂-CH₄ exchange ⁵²⁻⁵⁴; first process where CO₂-CH₄ exchange occurs in two independent steps; CH₄ hydrate dissociates and CO₂ hydrate forms with release of CH₄ as gas and in second process, Tung et. have reported that CH₄ replacement occurs at the interface by direct swap of CH₄ with CO₂ due to breaking and re-formation of cages at the interface as shown in Figure 1.8 55. However, far from interface, replacement occurs through transient co-occupation of both CH₄ and CO₂ in the same cavity.

CO₂ molecules have larger molecular radius (2.56Å) as compared to CH₄ (2.18Å) molecules and thus, CO₂ prefers to replace CH₄ molecules from large cages ². Hence, ideally, 75% of CH₄ could be replaced by CO₂, however, only 45% replacement is observed at laboratory scale. Furthermore, exchange efficiency and rate of exchange are low and there is significant delay in replacement with time as mixed hydrates of CO₂-CH₄ are formed that are more stable compared to pure gas hydrates and block the exchange process ⁴³⁻⁵⁰. Uchida *et. al.* performed Raman spectroscopy analysis for CO₂-CH₄ exchange using gaseous CO₂ and showed that rate of gas hydrate replacement is quite slow and induction period occurred over several days ⁵⁶. Le

et. al. reported that CO₂-CH₄ exchange rate was slow due to formation of new CO₂ hydrate that act as a wrap on the surface of CH₄ hydrate and prevents the replacement process ⁵⁷. Ota et. al. reported that amount of CH₄ decomposition is proportional to CO₂ hydrate formation during CO₂-CH₄ replacement using liquid CO₂ ⁵⁸. They showed that activation energy of 14.5 kJ/mol is involved in the dissociation of CH₄ hydrate whereas activation energy of 73.3 kJ/mol is required for the formation of CO₂ hydrates using a kinetic model. Similarly, Zhang et. al. reported that though the CH₄ decomposition and CO₂ hydrate formation are similar in porous sediment but maximum replacement of upto 45% occurs in 124h ⁵⁹⁻⁶⁰. Ors and Sinayuc showed that CH₄-CO₂ swap occurred mainly at the surface of the system when gaseous CO₂ was injected into a sand pack system ⁶¹.

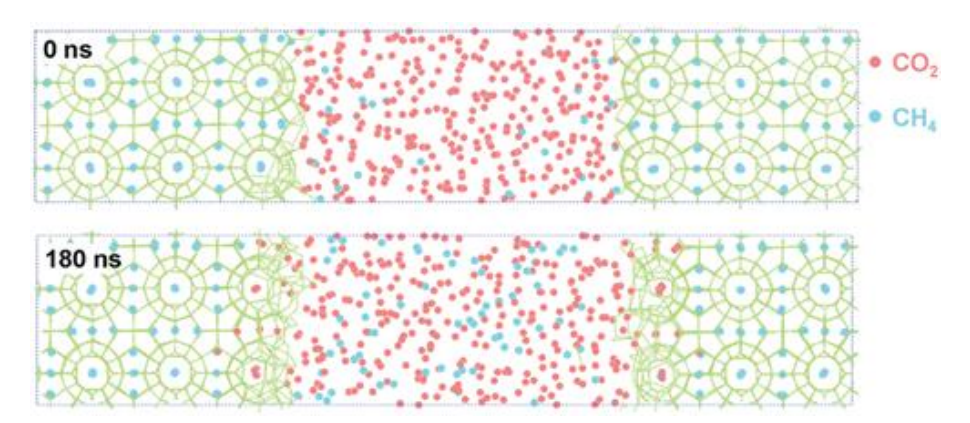


Figure 1.8: Schematic representation for direct CO₂-CH₄ exchange in hydrate. (Taken from reference [55]).

1.5.1 Mixture of CO₂ and N₂

Inclusion of flue gases like N_2 , H_2S , N_2O and SO_2 along-with CO_2 in bulk phase showed enhancement in CH_4 - CO_2 exchange in NGHs $^{62-73}$. The molecular diameter of N_2 (4.1Å) is smaller than CH_4 (4.36Å) that suggests N_2 can occupy large number of small cages in NGHs than CH_4 ². Park et al. first reported that N_2 along with CO_2 enhances methane recovery by 85% and 92% in sI and sII hydrates respectively, as compared to 64% CH_4 recovered using pure CO_2 system 74 . However, rate of methane recovery depends on concentration of N_2 in a system as 85% of CH_4 is recovered in sI hydrate only with 20:80 (mol%) mixture of N_2 and 20 CO_2 . The quantitative analysis showed that $\sim 23\%$ of CH_4 in hydrate was replaced with N_2 and 62% of CH_4 was replaced with CO_2 . Koh et. al. also reported similar studies for CH_4 recovery from gas hydrates intercalated within natural sediments using mixture of CO_2 (80 mol%) and

N₂ (20 mol%) ⁷⁵. Zhou et. al. reported Raman spectroscopic analysis of CH₄ recovery from NGHs by using mixture of CO₂ and N₂ and confirmed that CO₂ and N₂ prefer to driver out CH₄ from large and small cages respectively ⁷⁶. Yasue et. al. reported that CH₄ recovery was most effective when 30-40 mol% of CO₂ concentration was chosen in CO₂/N₂ gas mixture ⁷⁷. Shin et al. reported that CH₄ recovery is maximum (> 90%) in sH hydrates as compared to sI and sII hydrates in presence of mixture of CO₂ and N₂ ⁷⁸.

1.6 Nucleation in NGHs

Nucleation is a rare-event phenomenon and current state-of-art of experiments have spatiotemporal limitations to explore nucleation phenomenon in small molecular systems. In this direction, simulation techniques are a vital tool that could provide atomic level insights into different phenomena and classical molecular dynamics techniques are adequate to explore nucleation in hydrates as the nucleation barrier is low in these systems.

1.6.1 Labile cluster hypothesis

Labile cluster hypothesis was proposed by Sloan et. al. as shown in Figure 1.9 ⁷⁹⁻⁸¹. Initially, there are no gas molecules dissolved in water and with time when gas molecules dissolve in water, there is formation of labile clusters. The water molecules in labile clusters can exchange with bulk water molecules and the size of labile cluster depends upon the dissolved gas molecules. Hydrophobic clustering is the key step in the formation of agglomerates of labile clusters, where, dissolved gas molecules attract each other. These agglomerates are in quasi-equilibrium with each other; thus, they grow or shrink until they reach a critical size that forms nucleus once critical size is exceeded as shown in Figure 1.9d.

1.6.2 Local Cluster Mechanism

Radhakrishnan and Trout proposed the "local cluster mechanism" based on formation of CO₂ hydrates using molecular simulation techniques ⁸². Herein, thermal fluctuations lead to local ordering of gas and water molecules and thus, formation of hydrate cages. When the local ordering of gas molecules exceeds that of a critical nucleus, there is relaxation of gas and water molecules stabilize the free energy hypersurface, leading to the formation of hydrate nucleus.

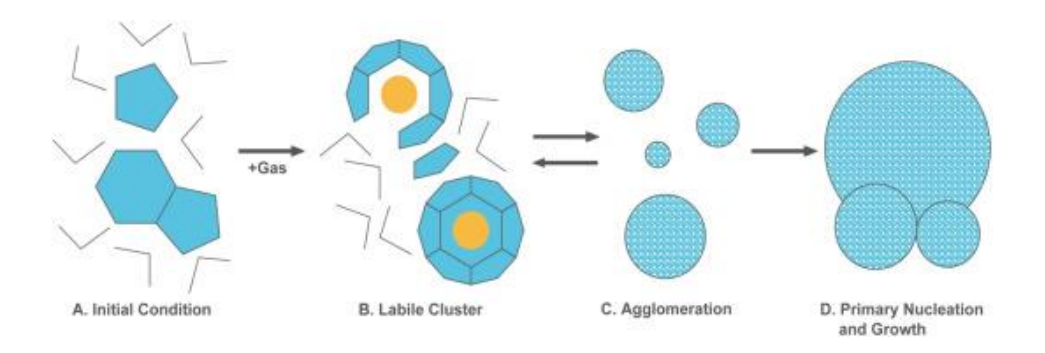


Figure 1.9: Schematic representation of labile cluster hypothesis. (Taken from reference [81]).

1.6.3 Blob Mechanism

Jacobsen et. al. proposed the "blob mechanism" which is a three-step mechanism where in first step, gas molecules form long-lived dynamical equilibrium amorphous clusters called blobs that are separated by water molecules as shown in Figure 1.10(a-b); in the second step, these clathrate cages continuously form and dissociates until a cluster turns into an amorphous clathrate nucleus (Figure 1.10c) which is in metastable state and in a subsequent state, amorphous hydrate turns into a crystalline hydrate nucleus that leads to hydrate formation (Figure 1.10 d) ⁸³.

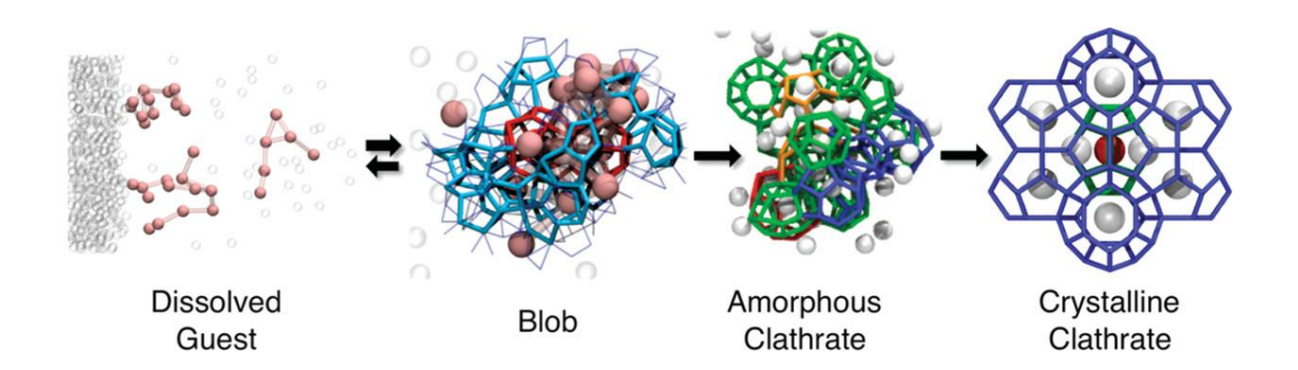


Figure 1.10: Schematic representation of blob mechanism; (a) guests dissolve in water (b) blob in dynamic equilibrium, (c) blob turns to the amorphous clathrate and (d) formation of crystalline clathrate. (Taken from reference [81]).

1.6.4 Multiple Cluster Hypothesis

Multiple Cluster hypothesis was proposed based on simulation studies using coarse-grained model of water where hydrate nucleation either occurs through an amorphous hydrate as an intermediate that transforms into ordered high degree of crystalline nucleus or due to direct formation of a well-ordered hydrate nucleus as shown in Figure 1.11 ^{84, 85}.

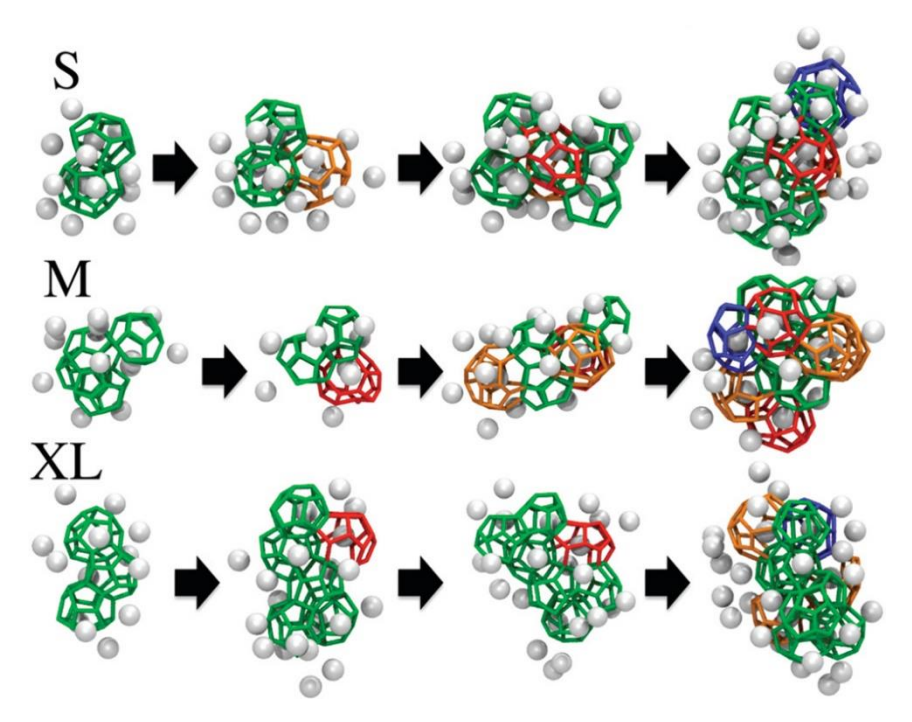


Figure 1.11: Schematic of multiple cluster hypotheses. S, M, XL stand for size of guests. S (small) solute fills all types of cages, M (Medium) solute primarily fills the large cages, however, XL fills only large cages. All the cages are demonstrated as; small cages (5¹², green) and large (5¹²6², Blue; 5¹²6³, red and 5¹²6⁴, orange) cages. (Taken from [85]).

1.7 Gas hydrate nucleation and Growth using MD

Theoretical insights into nucleation in hydrates are mainly reported for a single gas system or mixture of two gases; CH₄ [86-88, 93], CO₂ [89-90], H₂S [91] and CO₂-CH₄ [92]. Walsh et. al. [87] reported insights into homogeneous nucleation of methane hydrates using molecular dynamics where methane adsorbs on the planner face of H-bonded water ring that leads to spontaneous nucleation and growth of methane hydrate at 250K and 50MPa. The face sharing partial cages showed the characteristic of sII hydrate and nucleation of both sI and sII hydrates

were linked by 5¹²6³ cages. Sarupria and Debenedetti [88] reported methane hydrate nucleation at 250K and 200bar using MD simulations, where they reported the presence of 5¹²6³ and 5¹²6⁴ cages during sI hydrate nucleation. Hu et al. [93] reported that formation of a three-body aggregate is key step to nucleation of sI hydrates where a triangular pattern was formed by the central methane molecules and two methane molecules were located at two neighboring five membered ring and were separated by distance of ~6.7Å. The presence of three-membered aggregates reduced the hydrate nucleation time. The affinity of methane gas to liquid-hydrate interface, solubility of gas in water and diffusivity of gases are important factors in methane hydrate growth [94-97]. Vatamanu and Kusalik reported that incomplete cages at the interface shows strong affinity for methane [95-96]. Tung et al. [97] observed that solubility of methane in liquid phase, diffusion of methane gas and partial cages at the interface are the major factory for hydrate growth. Liu et al. [98] reported that super-saturation of CH₄ in solution phase has primary impact on the hydrate crystalline and high content of CH₄ in the system helps in rapid hydrate growth, however, in contrast, if content of CH₄ is low in the system, it takes more time for hydrate growth *via* formation of direct crystalline hydrate.

Hydrate growth of pure H₂S system is significantly faster compared to CH₄ hydrates in homogeneous medium [91]. Lu et al. [99] reported that during heterogeneous nucleation of CH₄ and H₂S increase in concentration of H₂S led to diffusion of more guest molecules from hydrate into water and consequently, high rate of hydrate growth and shrinking of the bubble radius was observed in system. During nucleation, H₂S preferred to initialize cage formation and stabilized the cages as molecular size of H₂S provides enough driving force for hydrate growth in the mixture. Matsui et al. [100] reported that in a mixture of CO₂/N₂, N₂ gas has higher tendency to penetrate in hydrate crystal and replace the CH₄ via decompositionreformation mechanism, however, excess presence of N₂ collapses the hydrate structure. Song et al. [101] reported that in CO₂/N₂ mixture, gas diffusion rate of CO₂ is doubled in replacement process. Wu et al. [102] reported that at the beginning of CO₂-CH₄ exchange process, replacement occurs but is later CH₄ showed co-growth because of low stabilization energy. Tadapalli and Kumar [103] used NH₃ as supportive gas in CO₂-CH₄ replacement but it causes defect in hydrate crystal due to hydrogen bonding that helped in CO₂-CH₄ replacement in hydrates. However, the penetration effect of NH₃ is dependent upon concentration and NH₃ destabilized hydrate at high concentration.

1.8 Hydrate Promoters

Hydrate equilibrium curve in a system depends on the composition of the gas and additives in a system ¹⁰⁴. If additives enhance the hydrate formation in a system, they are considered as hydrate promoters and are generally categorized into two groups; (I) Thermodynamic Hydrate Promoters (THPs) and Kinetic Hydrate Promoters (KHPs). THPs shifts the hydrate equilibrium curve to low pressure and high temperature and thus, mild conditions are required to form gas hydrate as compared to systems without THPs ¹⁰⁴. Tetrahydrofuran, cyclopentane, propane and tetrabutylammonium bromide are some of the common and widely used THPs for CO2 and CH₄ hydrates ¹⁰⁴⁻¹⁰⁸. Similarly, cyclohexane, acetone and methylcyclohexane act as THPs for other gases ^{104, 109-110}. However, in some systems, THF could itself form hydrates at ~277.5K and ambient pressure where it is trapped in large (5¹²6⁴) cages of sII hydrate ¹⁰⁵. On the other hand, KHPs do not participate in hydrate structures, therefore, they do not show significant shift in the hydrate equilibrium curve. KHPs promote hydrate nucleation by reducing the induction time and accelerating the hydrate formation process ¹⁰⁴. KHPs are more diverse and include surfactants (anionic, cationic and nonionic) 111-113, amino acids 114, nanoparticles 115, metal oxides ¹¹⁶, cellulose derivatives ¹¹⁷, cyclodextrins ¹¹⁸ and starches ¹¹⁹. Sodium dodecyl sulfate, SDS is a well-known example of KHPs ¹¹¹. Albert et. al. reported MD study of SDS for both CO₂ and CH₄ hydrates ¹²⁰⁻¹²¹. They found that SDS-CO₂ interactive behavior is different than SDS-CH₄ where CO₂ strongly interacts with SDS that inhibit them from forming suitable hydrate cages ¹²¹. However, there is no strong interaction between SDS and CH₄, therefore, it helps to drive H2O molecules to form suitable cages ¹²⁰.

1.9 Molecular Dynamics Simulation Techniques

Molecular dynamics (MD) simulation techniques are a classical simulation technique where dynamics of a particle is evaluated as per Newton's equations of motion and helps to explore energetics, conformations and dynamics of particles at an atomic level ¹²²⁻¹²³. It was first introduced by Alder and Wainwright in 1957 to study the dynamics of hard sphere systems ¹²⁴. However, first MD simulation studies on realistic material systems was reported by Vineyard and Brookhaven in 1960 and A. Rahman reported the first liquid systems MD simulations on Ar system in 1964 by modelling Ar atoms as Lennard-Jones particles ¹²⁵⁻¹²⁶. Harp and Ben

reported the linear- and angular autocorrection function and memory functions in liquid CO system using MD simulation techniques ¹²⁷⁻¹²⁸. Barker and Watts simulates the liquid water using Monte Carlo (MC) simulation techniques in 1969 ¹²⁹. However, Rahman and Stillinger simulate liquid water at 34.3°C using MD simulation techniques in 1971 where water molecules were modelled as rigid asymmetric rotors ¹³⁰. Water is one of the most tedious liquid system to model using classical simulation techniques and several models and MD studies have been reported over decades to simulate liquid water ¹²⁹⁻¹³². Currently, molecular dynamics simulation techniques are employed to study a wide-range of systems from materials to biomolecular systems ¹²².

Molecular Dynamics simulation techniques are based on Newton's equations of motion and are solved for each particle in a system as shown in Eq. 1.1 where m is the mass of the ith particle, $\vec{r_i}$ and $\vec{F_l}$ are the position and force coordinates in a N-particle system:

$$m\frac{\partial^2 \vec{r_i}}{\partial t^2} = \vec{F_i}$$
 where, $i = 1...N$

The force acting on a particle is negative derivative of potential function, $V(r_1, r_2, \dots, r_n)$ as reported in Eq. 1.3

$$\overrightarrow{\mathbf{F}_{i}} = -\frac{\partial \mathbf{V}}{\partial \overrightarrow{\mathbf{r}_{i}}}$$
 Eq. (1.3)

Herein, initial configuration is chosen and position coordinates and velocities are assigned. The forces on each particle with respect to particles in the system is calculated based on the chosen potential parameters for interactions (force field). The position, velocities and accelerations of particles are updated as a function of time using integration scheme that follows Newton's equation of motion. These steps are repeated till system reaches equilibrium and further the coordinates, velocities and forces are saved to calculate properties of interest.

1.9.1 Force Field

Force fields are a set of mathematical expressions that describe the energy of a system based on the coordinates of its particles. They are employed to calculate the intermolecular interaction

energies between the particles (e.g., van der Waals and electrostatic) and intramolecular energy within the particles (i.e., bond, angle and torsion) as shown in Figure 1.12. The parameters used in these expressions are usually obtained from theoretical calculations (i.e., *ab initio*), semi-empirical calculations or fitting parameters into experimental data such as spectroscopic data (Raman, Infrared, NMR, X-ray and Neutron diffraction data) ¹³³. There are two categories of force fields; Class I and II force fields where Class I force fields are based on harmonic potential between the particles and in Class II force field potential due to anharmonic interactions is considered by including cross-terms between bond-angle, bond-torsion and angle-torsion potentials ¹³⁴⁻¹³⁶. We have chosen Class I force field to model gas hydrates in the present work as Class I force fields are computational cheaper than Class II force fields and force fields for water at different temperatures and pressures are available in Class I force fields.

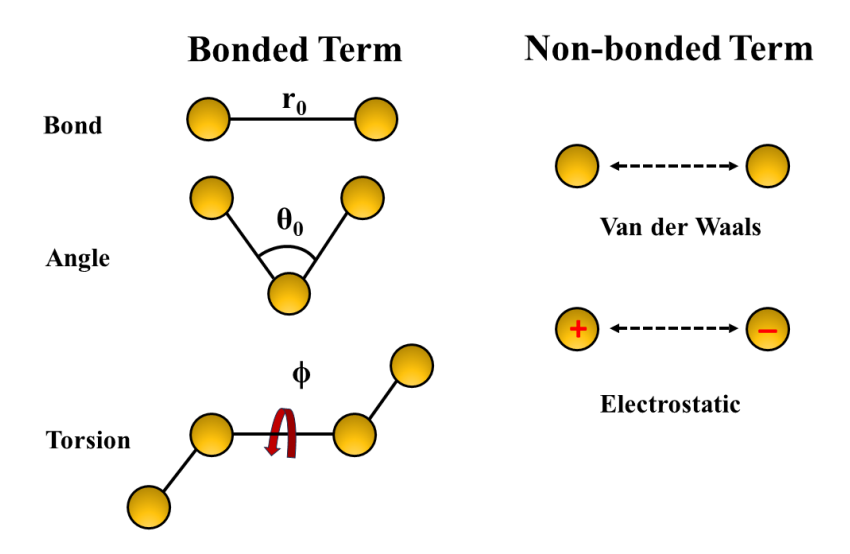


Figure 1.12: Schematic representation of bonded (bond, angle and torsion) and non-bonded (van der Waals and electrostatic) interaction terms.

The expression for potential energy in Class I force field is given as shown in Eq. 1.3.

$$V(r) = \sum_{bonds} \frac{1}{2} k_r (r - r_0)^2 + \sum_{angles} \frac{1}{2} k_{\theta} (\theta - \theta_0)^2 + \sum_{torsions} \frac{V_n}{2} [1 + d \cos(n\emptyset)]$$

$$+\sum_{i=1}^{N-1} \sum_{j\neq i}^{N} \left[4\epsilon_{ij} \left\{ \left(\frac{\sigma_{ij}}{r_{ij}} \right)^{12} - \left(\frac{\sigma_{ij}}{r_{ij}} \right)^{6} \right\} + \frac{q_{i}q_{j}}{\epsilon r_{ij}} \right]$$
Eq. (1.3)

where, k_r and r_0 are force constant and equilibrium bond distance for bond potential; k_{θ} and θ_0 are

force constant and equilibrium bond distance for angle potential; V_n is the force constant for torsion potential ($\mathbf{n}=1,2,3,4$ and $\mathbf{d}=+1$ or -1) for harmonic style; ϵ_{ij} and σ_{ij} are well depth and diameter between \mathbf{i}^{th} and \mathbf{j}^{th} particle; \mathbf{q}_i and \mathbf{q}_j are atomic charges on \mathbf{i}^{th} and \mathbf{j}^{th} particle and \mathbf{r}_{ij} is the distance between \mathbf{i}^{th} and \mathbf{j}^{th} particle.

1.10 Integration schemes

The Newton's equations of motion are solved numerically using integration schemes where integration timestep (Δt) is $\approx 1 \, \text{fs}$ in systems modelled with all-atom force fields. There are several integration schemes (Verlet, Leap-frog, Velocity-Verlet and Gear-Predictor Algorithm) based on the accuracy, number of variables and amount of data to be stored per integration step. In general, a good integration scheme should be simple, fast, and less expensive, should replicate the classical trajectory of system as accurately as possible even with long time step, should be time reversible and follow the laws of conservation of energy and momentum 123 .

1.10.1 Verlet Algorithm

Verlet Algorithm is one of the most widely used integration schemes in molecular dynamics simulations ^{123,137}. It considers Taylor's expansion of the position of particle, one step forward and one step backward to the current step as shown in Equations 1.4 and 1.5 ¹²³.

$$r(t + \Delta t) = r(t) + v(t)\Delta t + \frac{1}{2}a(t)\Delta t^2 + \frac{1}{6}b(t)\Delta t^3 + O(\Delta t^4)$$
 Eq. (1.4)

$$r(t - \Delta t) = r(t) - v(t)\Delta t + \frac{1}{2}a(t)\Delta t^2 - \frac{1}{6}b(t)\Delta t^3 + O(\Delta t^4)$$
 Eq. (1.5)

where adding Eq. 1.4 and 1.5 gives Eq. 1.6

$$r(t + \Delta t) + r(t - \Delta t) = 2r(t) + a(t)\Delta t^2 + O(\Delta t^4)$$
 Eq. (1.6)

Rearranging the Eq. 1.6 gives

$$r(t + \Delta t) = 2r(t) - r(t - \Delta t) + a(t)\Delta t^2 + O(\Delta t^4)$$
 Eq. (1.7)

Eq. 1.7 suggests that particle position is updated at $(t + \Delta t)$ without the velocity term.

However, updated velocity, $v(t + \Delta t)$ is required to update properties like temperature thus, it is calculated from difference of Eq.s 1.5 and 1.6.

$$r(t + \Delta t) - r(t - \Delta t) = 2v(t)\Delta t + O(\Delta t^{2})$$
 Eq. (1.8)

Thus, velocity at time t is given as

$$v(t) \approx \frac{r(t+\Delta t)-r(t-\Delta t)}{2\Delta t}$$
 Eq. (1.9)

The updated coordinates and velocities have an error of order of $O(\Delta t^4)$ and $O(\Delta t^2)$ respectively though velocity accuracy can be improved by adding more variables of order of $O(\Delta t^2)$ but could be computationally expensive. Moreover, calculation of velocity at time t, requires position of the next step $(t + \Delta t)$ as showed in Eq. 1.9.

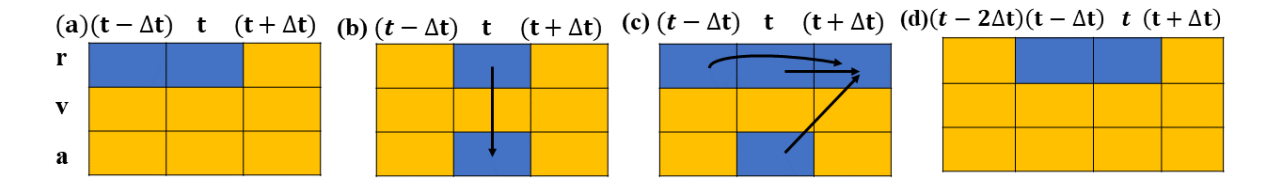


Figure 1.13: Schematic representation of Verlet Algorithm; (a) previous and current coordinates, **r** (b) computes the acceleration, **a** of current step using current position (c) compute the next position using previous position, current position and current acceleration and (d) current position becomes previous step position in next step and next position becomes current position and steps (a-c) are repeated to calculate the trajectory. Velocities, **v** are calculated using the position coordinates of previous and next steps. (Reproduced from reference [123]).

1.10.2 Leapfrog Algorithm

Leapfrog algorithm is computationally economical than Verlet algorithm and reduces the order of error in position and velocity as compared to Verlet algorithm ¹²³.

$$v\left(t + \frac{1}{2}\Delta t\right) = v\left(t - \frac{1}{2}\Delta t\right) + a(t)\Delta t$$
 Eq. (1.10)

$$r(t + \Delta t) = r(t) + \Delta t vt \left(t + \frac{1}{2}\Delta t\right)$$
 Eq. (1.11)

The velocity of next half step is calculated initially using the velocity of previous half step and acceleration of current step as shown in Eq. 1.10 and Figure 1.14(a-b), which is further used to calculate the position of the next step as shown in Eq. 1.11 and Figure 1.14 (c-d).

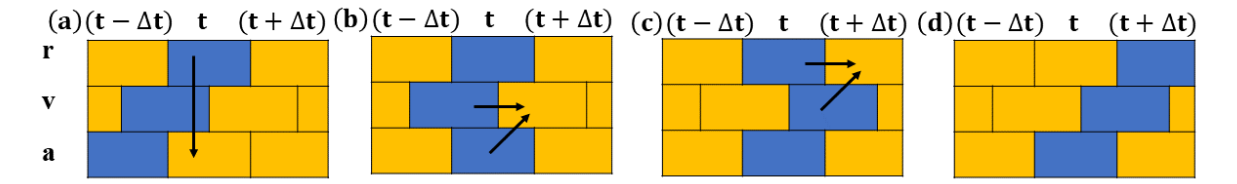


Figure 1.14: Schematic representation of Leapfrog Algorithm; (a) current position coordinates, **r** used to calculate the current acceleration, (b) current acceleration, **a** and previous half step velocity used to compute the next half-step velocity, (c) next half step velocity and current position used to calculate the next position and (d) steps (a-c) repeated to calculate the next step position coordinates. Velocity, **v** of current step are calculate using the previous and next half time-step (Eq. 1.12). (Reproduced from reference [123]).

The velocity of current step is calculated as shown in Eq. 1.12.

$$v(t) = \frac{1}{2} \left[v \left(t - \frac{1}{2} \Delta t \right) + v \left(t - \frac{1}{2} \Delta t \right) \right]$$
 Eq. (1.12)

Algebraically Eq. 1.9 and 1.12 are equivalent but Eq 1.12 explicitly includes velocity. The Leapfrog algorithm calculates the half-step velocity throughout the trajectory and Eq. 1.12 is required to calculate the full-step velocity.

1.10.3 Velocity-Verlet Algorithm

Velocity-Verlet algorithm is most widely used algorithm compared to the other two algorithms ^{123, 138}. It calculates the position, velocity and acceleration at the same time without effecting the precision. The mathematical equations for velocity-Verlet algorithms are as follows:

$$v\left(t + \frac{1}{2}\Delta t\right) = v(t) + \frac{1}{2}\Delta t \,a(t)$$
 Eq. (1.13)

$$r(t + \Delta t) = r(t) + \Delta t \, v\left(t + \frac{1}{2}\Delta t\right)$$
 Eq. (1.14)

$$v(t + \Delta t) = V\left(t + \frac{1}{2}\Delta t\right) + \frac{1}{2}\Delta t \ a(t + \Delta t)$$
 Eq. (1.15)

It is three-step process; first, velocity of next half-time step is calculated using velocity and acceleration of current time step as reported in Figure 1.15b using positions, velocities and accelerations of the current step, t; secondly, velocity of previous step and position of current step compute the position of next step (Figure 1.15c); position of next time step directly gives the acceleration of next timestep (Figure 1.15d) and in the end, velocity of half-time step and acceleration of next timestep gives the velocity of full step (Figure 1.15e).

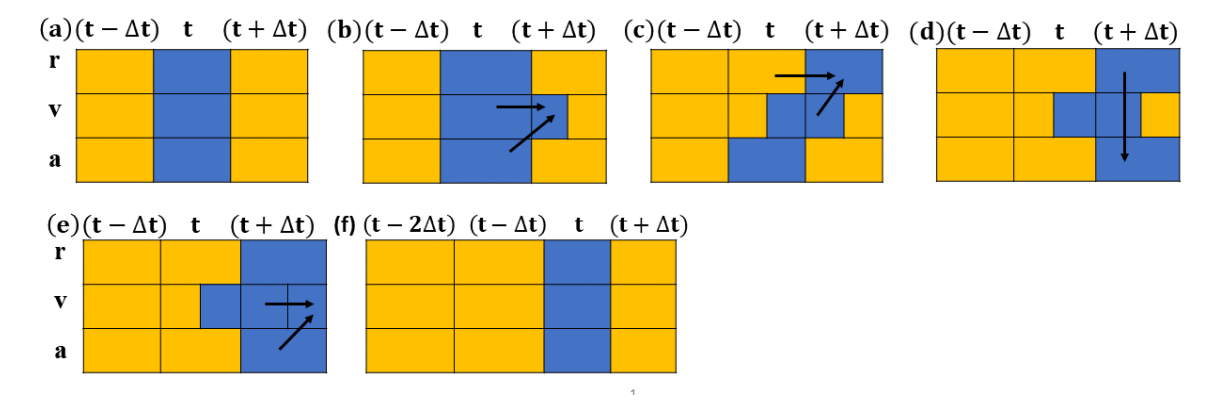


Figure 1.15: Schematic representation of velocity-Verlet Algorithm. (a) position, velocity and acceleration at time, t; (b) compute velocity of next half timestep using velocity and acceleration of current step; (c) compute next step position using previous position and velocity of previous step; (d) compute the acceleration of next timestep using position of next timestep and (e) half timestep velocity and next timestep acceleration gives full-step velocity and these steps are repeated. (Reproduced from reference [123]).

1.11 MD Analysis

The data from the molecular dynamics simulations was analysed to calculate different properties and a brief discussion on few of the common analysis methods is given below.

1.11.1 Hydrate Cage Analysis

GRADE code is an open-source software that identifies the clathrate hydrate structures in a system using oxygen coordinates of water within a cut-off distance, where cut-off distance of two neighbour water molecules must be less than or equal to 3.5Å ¹⁴¹. A guest is considered the part of cage if the centre of mass of cage and encapsulated guest is less than 2.0Å else cage is considered as an empty cage. GRADE identifies the 5¹², 6²5¹² and 6⁴5¹² cages in a system. When these cages combine in a specific pattern, code can identify sI and sII NGHs. GRADE code work in a sequence where initially rings are identified, connectivity between rings identifies cups and combination of cups give rise to cages.

Rings: Rings are primary unit in a cage. It is formed by connecting the neighbouring water molecules to each other. Suppose, i, j, k, l and m are water molecules that form a ring, then, m and j are first neighbours of i; j and l are first neighbour of k; i and l are first neighbour of m. The size of a ring depends upon the number of water molecules participating in a ring. In the above example, we considered 5 water molecules (i.e., i, j, k, l and m), therefore, it is a 5 membered ring. The GRADE algorithm starts with one water molecules and explores all the nearest neighbouring water molecules of starting water molecule before tracking to other molecules as shown in Figure 1.16. The bottleneck of this code is that it excludes all the deformed rings which cannot form the stable cups or cages. This code identifies two types of deformation in the rings: (I) related to convexity and (II) related to planarity.

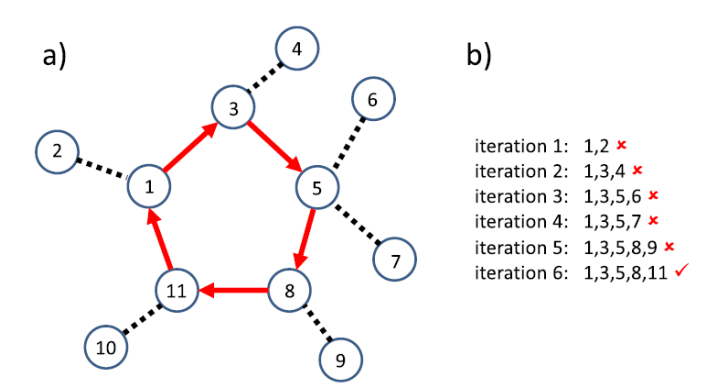


Figure 1.16: Schematic representation of cage search algorithm to identify the ring in a system; (a) all water molecules are represented by nodes and first-neighbour nodes are connected to each other by a dashed line, red arrows are used to represent the first neighbour nodes that form the five membered ring and (b) The six iterations are required to search the five membered ring in a panel starting from node 1. (Taken from reference [141]).

Cups: If two vertices (i.e., one edge) are common in two rings then the number of edges which are common to reference ring i are called the coordination number of the reference ring. When the coordination number is equal to number of edges of a ring then that ring is called a fully coordinated ring and its neighbouring rings are called as lateral rings. Hence, a cup is formed when a set of water molecules contains the fully coordinated ring and their lateral rings where, lateral rings must be neighbour to each other as shown in Figure 1.17(a-c). The fully coordinated or six membered rings are represented with red colour and lateral rings are shown in black colour. The nomenclature used is:

- (a) 5⁶ Cup where, 5 stands for the size of fully coordinated lateral rings and upper index 6 stands for number of five membered rings.
- (b) 6^15^6 Cup where, 6 and 5 stand for full coordinated six and five membered lateral ring, respectively. Upper indexes stand for number of five and six membered rings.

Cages: A cage is formed by combination of two of more cups of same kind, where lateral cage of one cup is neighbour to two lateral cages of other cups.

There are three types of cages identified by GRADE code.

- 5^{12} cage is formed by combining of two 5^6 cups (Figure 1.17a).
- 6^26^{12} cage is formed by combining of two 6^15^6 cups (Figure 1.17b).
- 6^46^{12} cage is formed by combining of four 6^15^6 cups (Figure 1.17c).

1.11.2 F4 Order Parameter

F4 Order parameter (OP) is used to distinguish the phase change in a system based on the arrangement of water molecule in a hydrate, ice or liquid water. The expression for F4 OP is given in Eq. 1.16 ^{81, 142}

$$F4 = \frac{1}{N} \sum_{i=1}^{N} \cos 3\phi_i$$
 Eq. 1.16

where, \emptyset_i represents the torsion angle between two oxygen atoms of water molecules that have distance between the outermost hydrogen atoms of both the water molecules within 3.5Å as

shown in Figure 1.18a. F4 OP value for hydrate, ice and liquid water are 0.7, -0.4 and -0.04 respectively. Figure 1.18b shows the phase change in a system where the system goes from liquid phase to hydrate phase at 30ns of simulation time.

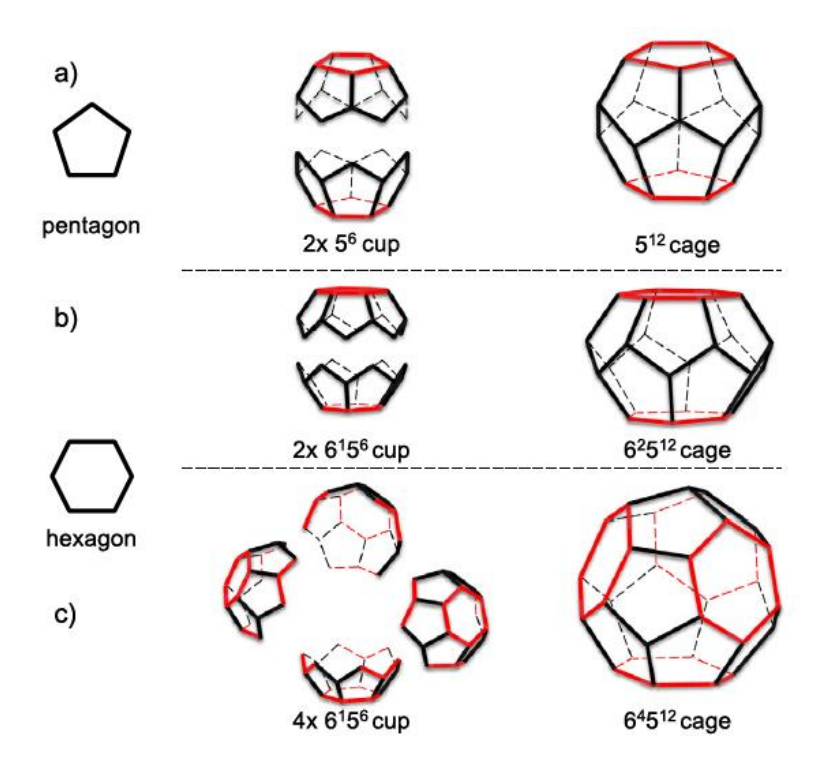


Figure 1.17: Schematic representation of cage formation. (a) five membered ring, two 5^6 cups and 5^{12} cage (b) five and six membered ring, two 6^16^5 cups and 6^25^{12} cages (c) five and six membered ring, four 6^15^6 cups, 6^45^{12} cages. (Taken from reference [141]).

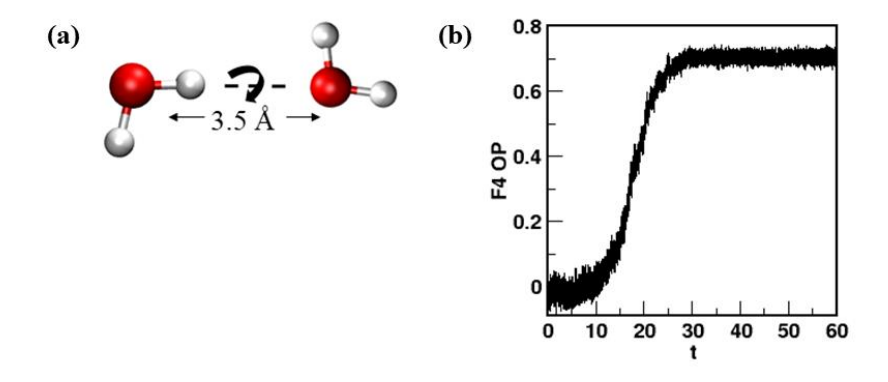


Figure 1.18: (a) Distance criteria between water molecules to calculate F4 OP (b) F4 OP as a function of time for hydrate growth in a system (from present work).

1.11.3 Velocity Autocorrelation Function

Velocity Autocorrelation Function (VACF) provides insights into how the dynamics of particles is correlated with their environment and it is a time dependent autocorrelation function of velocity as shown in Eq. 1.17 ¹⁴³

$$C_v(t) = \langle \mathbf{v}_i(t), \mathbf{v}_i(0) \rangle$$
 Eq. 1.17

where, $\mathbf{v}_i(0)$ and $\mathbf{v}_i(t)$ are the velocities of i^{th} particle at time 0 and t and $C_v(t)$ is averaged over time and number of particles in the system. If the particles have highly correlated motion, then a slow decay with a negative VACF region called cage effect due to the slow motion of particles is observed as reported in Figure 1.19.

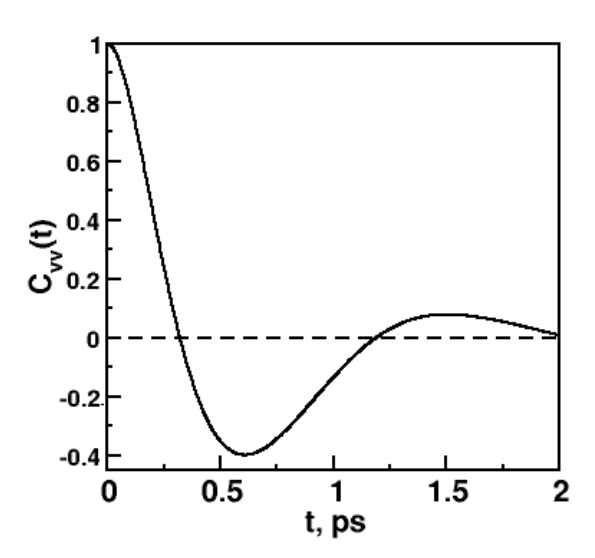


Figure 1.19: Velocity autocorrelation function as a function of time in a system (from present work) where negative region is due highly correlated motion of particles.

1.11.4 Metadynamics

Metadynamics is a powerful technique to enhance sampling of energetically-forbidden regions in MD simulations by adding a history dependent bias potential in the system based on the collective variables (CV) where collective variables are a group of variables that govern the progress of a reaction ¹³⁹. The biased added on CV can be single or multiple depending on the

complexity of the system of the interest for e.g., if a set, S of CV of d functions depends on the microscopic coordinates, R they can be expressed in mathematical form as shown in Eq. 1.16

$$S(R) = (S_1(R), S_2(R), \dots, S_d(R))$$
 Eq. (1.16)

The expression of biased potential which was added to the Hamiltonian, H of a system with time through CV can be written as reported in Eq. 1.17.

$$V_{G}(S,t) = \int_{0}^{t} dt' \omega \exp\left(-\sum_{i=1}^{d} \frac{(S_{i}(R) - S_{i}(R(t')))^{2}}{2\sigma_{i}^{2}}\right)$$
 Eq. (1.17)

where, ω is energy rate constant that depends upon the Gaussian height (W) and a deposition stride. It is expressed as $\omega = \frac{W}{\tau_G}$. σ_i which is the Gaussian width for an ith CV. In a simulation, bias potential is updated stepwise. So, for a computationally implemented form, update is discretised into τ intervals and delta (δ) function is replaced by Kernel function. Hence, in a simulation, bias potential become the sum of the kernel functions cantered at the instantaneous collective variable, S_i at time τ_i as

$$V_G(S(R),t) \approx \tau \sum_{j=0}^{n} \omega K(|\vec{S} - \vec{S_j}|)$$
 Eq. (1.18)

where, $n = \left\lfloor \frac{t_{sim}}{\tau} \right\rfloor$ is a scalar factor and bias potential continuously is updated based on its value. As the simulation proceeds, for an infinitively long simulation time i.e., $t \to \infty$, aggregated bias potential converse to Free Energy Surface (FES) as

$$V_G(S, t \to \infty) = -F(S) + C$$
 Eq. (1.19)

where, C is an irrelevant additive constant and the free energy F(S) is expressed as

$$F(S) = -\frac{1}{6} \left(\int dR \, \delta(S - S(R)) e^{-\beta U(R)} \right)$$
 Eq. (1.20)

where, $\beta = \frac{1}{k_B T}$, k_B is the Boltzmann constant. T is the temperature of system. U(R) is the potential energy function. The potential wells are filled with biased potential and push the system from away from local energy minima that accelerates the rare event sampling, explores new reaction paths and does not require *a prior* information of free energy landscape. However, metadynamics cannot control the amount of bias potential to be added to explore the system to stop the simulation. Well-tempered metadynamics solves this problem by introducing the decrease in rate of bias potential with metadynamic-simulation time ¹⁴⁰. This is achieved by rescaling the Gaussian hight W in the following Eq. 1.21

$$W = \omega \exp\left(-\frac{V_G(s,t)}{\Delta T}\right) \tau_G$$
 Eq. (1.21)

where, ω is initial bias deposition rate, τ_G represents the time interval for Gaussian stride, ΔT is the input parameter with the dimension of temperature. This parameter tunes the amplitude of biased deposits which causes the potential of system converge smoothly and is expressed in using Eq. 1.22

$$V_G(S, t \to \infty) = -\frac{\Delta T}{T + \Delta T} F(S) + C$$
 Eq. (1.22)

where, C is an immaterial constant. The limiting cage of above equation is when $\Delta T \rightarrow 0$, where biased potential is zero and Eq. 1.22 turns to ordinary molecular dynamics or when $\Delta T \rightarrow \infty$ and deposition rate is constant, Eq. 1.22 corresponds to standard metadynamics and the extent of Free Energy Surface (FES) can be regulated in between by tunning ΔT .

References

- Sloan, E. D.; Koh, C. A. Clathrate Hydrates of Natural Gases, 3rd ed.; CRC Press: Boca Raton, FL, 2008.
- 2. Sloan, E. D. Fundamental Principles and Applications of Natural Gas Hydrates. Nature 2003, 426, 353–363.
- 3. Walsh, M. R.; Beckham, G. T.; Koh, C. A.; Sloan, E. D.; Wu, D. T.; Sum, A. K. Methane Hydrate Nucleation Rates from Molecular Dynamics Simulations: Effects of Aqueous

- Methane Concentration, Interfacial Curvature, and System Size. *J. Phys. Chem. C* **2011**, 115, 21241–21248.
- 4. Boswell, R.; Collett, T. S. Current Perspectives on Gas Hydrate Resources. *Energy Environ. Sci.* **2011**, 4, 1206–1215.
- 5. Makogon, Y.; Holditch, S.; Makogon, T. Natural Gas-Hydrates –A Potential Energy Source for the 21st Century. *J. Pet. Sci. Eng.* **2007**, 56, 14–31.
- 6. Milkov, A. V. Global Estimates of Hydrate-Bound Gas in Marine Sediments: How Much Is Really out There? *Earth Sci. Rev.* **2004**, 66, 183–197.
- 7. Park, Y.; Kim, D. Y.; Lee, J. W.; Huh, D. G.; Park, K. P.; Lee, J.; Lee, H. Sequestering Carbon Dioxide into Complex Structures of Naturally Occurring Gas Hydrates. *Proc. Natl. Acad. Sci. U.S.A.* **2006**, 103, 12690–12694.
- 8. Zhang, Y.; Cui, M.; Xin, G.; Li, D. Microscopic insights on the effects of flue gas components on CH4 –CO2 replacement in natural gas hydrate. *Gas Science and Engineering* **2023**, 112, 204947.
- 9. Lang, X.; Fan, S.; Wang, Y. Intensification of Methane and Hydrogen Storage in Clathrate Hydrate and Future Prospect. *J. Nat. Gas Chem.* **2010**, 19, 203–209.
- 10. Struzhkin, V. V.; Militzer, B.; Mao, W. L.; Mao, H.-K.; Hemley, R. J. Hydrogen Storage in Molecular Clathrates. *Chem. Rev.* **2007**, 107, 4133–4151.
- 11. Lee, H.; Lee, J.; Kim, D.; Park, J.; Seo, Y.; Zeng, H.; Moudrakovski, I.; Ratcliffe, C.; Ripmeester, J. Tuning Clathrate Hydrates for Hydrogen Storage. *Nature* **2005**, 434, 743–746.
- 12. Cha, I.; Lee, S.; Lee, J. D.; Lee, G. W.; Seo, Y. Separation of SF6 from Gas Mixtures Using Gas Hydrate Formation. *Environ. Sci. Technol.* **2010**, 44, 6117–6122.
- 13. Peng, X. M.; Hu, Y. F.; Liu, Y. S.; Jin, C. W.; Lin, H. J. Separation of Ionic Liquids from Dilute Aqueous Solutions Using the Method Based on CO2 Hydrates. *J. Nat. Gas Chem.* **2010**, 19, 81–85.
- 14. Mu, L.; Solms, N. v. Experimental Study on Methane Production from Hydrate-Bearing Sandstone by Flue Gas Swapping. *Energy Fuels* **2018**, 32, 8167–8174.
- 15. McMuLLAN, R. K; JEFFREY, G. A. Polyhedral Clathrate Hydrates. IX. Structure of Ethylene Oxide Hydrate. *J. Chem. Phys.* **1965**, 42, 2725–2732.
- 16. Mak; T. C. W.; McMullan, R. K. Polyhedral Clathrate Hydrates. X. Structure of the Double Hydrate of Tetrahydrofuran and Hydrogen Sulfide. *J. Chem. Phys.* **1965**, 42, 2732–2737.

- 17. Ripmeester, J.A.; Tse, J.S.; Ratcliffe, C.I.; Powell, B.M. A new clathrate hydrate structure. *Nature* **1987**, 325, 135.
- 18. Moridis G. J.; Collett TS, Boswell R, Kurihara M, Reagan MT, Koh C, Toward production from gas hydrates: current status, assessment of resources, and simulation-based evaluation of technology and potential. *SPE Reserv Eval Eng.* **2009**, 12, 745–71.
- Moridis, G.; Collet, T. Strategies for gas production from hydrate accumulation under various geologic conditions. LBNL-52568, TOUGH symposium 2003 Berkeley, CA, 2003, May 12-14.
- 20. Lee, J. Y.; Ryu, B. J.; Yun, T. S.; Lee, J.; Cho, G.-C. Review on the Gas Hydrate Development and Production as a New Energy Resource. *KSCE Journal of Civil Engineering* **2011**, 15,4, 689-696.
- 21. Li, X.-S.; Xu, C.-G.; Zhang, Y.; Ruan, X.-K.; Li, G.; Wang, Y. Investigation into gas production from natural gas hydrate: A review. *Applied Energy*, **2016**, 172, 286–322.
- 22. Sun, Z.; Xin, Y.; Sun, Q.; Ma, R.; Zhang, J.; Lv, S.; Cai, M.; Wang, H. Numerical Simulation of the Depressurization Process of a Natural Gas Hydrate Reservoir: An Attempt at Optimization of Field Operational Factors with Multiple Wells in a Real 3D Geological Model. *Energies* **2016**, 9, 714, 1-20.
- 23. McGuire, P. L. Recovery of Gas From Hydrate Deposits Using Conventional Technology. SPE/DOE 10832.
- 24. Holder, G. D.; Angert, P. F.; John, V. T.; Yen, S. A Thennodynamic Evaluation of Thennal Recovery of Gas From Hydrates in the Earth. *J Petrol Technol* **1982**, 34,1127–32.
- 25. Tang, L. G.; Xiao, R.; Huang, C.; Feng, Z. P.; Fan, S. S. Experimental Investigation of Production Behavior of Gas Hydrate under Thermal Stimulation in Unconsolidated Sediment. *Energy & Fuels* **2005**, *19*, 2402-2407.
- 26. Islam, M. R.; Chakma, A. Comprehensive Physical and Numerical Modeling of a Horizontal Well. *Society of Petroleum Engineers Inc.* **1990**, 111-123.
- 27. Li, B.; Li, G.; Li, X.-S.; Li, Q.-P.; Yang, B.; Zhang, Y.; Chen, Z.-Y. Gas Production from Methane Hydrate in a Pilot-Scale Hydrate Simulator Using the Huff and Puff Method by Experimental and Numerical Studies. *Energy Fuels* **2012**, 26, 7183–7194.
- 28. Collett, T. S; Ginsburg, G. D. Gas hydrates in the Messoyakha gas field of the west Siberian basin a re-examination of the geologic evidence. *Int Offshore Polar E* **1997**, 96–103.
- 29. Collett, T. S.; Kuuskraa V. A. Hydrates contain vast store of world gas resources. *Oil Gas J* **1998**, 96, 90–95.

- 30. Yousif, M.; Li P.; Selim, M.; Sloan E. Depressurization of natural gas hydrates in Berea sandstone cores. *J Inclusion Phenom Mol Recognit Chem.* **1990**, 8, 71–88.
- 31. Ohgaki, K.; Nakano, S.; Matsubara, T.; Yamanaka. S. Decomposition of CO₂, CH₄ and CO₂-CH₄ Mixed Gas Hydrates. *J. Chem. Eng. Jpn.* **1997**, 30, 310–314.
- 32. Xiong, L.; Li, X.; Wang, Y.; Xu, C. Experimental Study on Methane Hydrate Dissociation by Depressurization in Porous Sediments. *Energies* **2012**, *5*, 518-530.
- 33. Kim, H. C.; Bishnoi, P. R.; Heidemann, R. A.; Rizvi, S. S. H. Chemical kinetics of hydrate decomposition. *Eng. Sci.* **1987**, 42, 1645–1653.
- 34. Sun, C. Y.; Chen G. J. Methane hydrate dissociation above 0 °C and below 0 °C. *Fluid Phase Equilib.* **2006**, 242, 123–128.
- 35. Tang L. G.; Li X. S.; Feng Z. P.; Li G. Fan S. S.; Control mechanisms for gas hydrate production by depressurization in different scale hydrate reservoirs. *Energy Fuels* **2007**, 21, 227–233.
- Li G.; Li X. S.; Tang L. G.; Zhang Y. Experimental investigation of production behavior of methane hydrate under ethylene glycol injection in unconsolidated sediment. *Energy Fuels* 2007, 21, 3388–3393.
- 37. Sira, J. H.; PatH, S. L.; Kamath, V. A. Study of Hydrate Dissociation by Methanol and Glycol Injection. *Society of Petroleum Engineers Inc.* **1990**, 977,984.
- 38. Liu, Y.; Wang, P.; Yang, M.; Zhao, Y.; Zhao, J.; Song, Y. CO₂ sequestration in depleted methane hydrate sandy reservoirs. *J. Nat. Gas Sci. Eng.* **2018**, 49, 428–434.
- 39. Zhao, J.; Xu, K.; Song, Y.; Liu, W.; Lam, W.; Liu, Y.; Xue, K.; Zhu, Y.; Yu, X.; Li, Q. A review on research on replacement of CH4 in natural gas hydrates by use of CO2. *Energies* **2012**, 5, 399–419.
- 40. Tsypkin, G. G. Analytical study of CO2eCH4 exchange in hydrate at high rates of carbon dioxide injection into a reservoir saturated with methane hydrate and gaseous methane. *Energy* **2021**, 233, 121115.
- 41. Koh, D.-Y.; Kang, H.; Lee, J.-W.; Park, Y.; Kim, S.-J.; Lee, J.; Lee, J. Y.; Lee, H. Energy-efficient natural gas hydrate production using gas exchange. *Applied Energy* **2016**, 162, 114–130.
- 42. Stanwix, P. L.; Rathnayake, N. M.; Obanos, F. P. P. D. O.; Johns, M. L.; Aman, Z. M.; May. E. F. Characterising thermally controlled CH4–CO2 hydrate exchange in unconsolidated sediments. *Energy Environ. Sci.* **2018**, 11, 1828.

- 43. Goel, N. In situ methane hydrate dissociation with carbon dioxide sequestration: current knowledge and issues. *J Petrol Sci Eng* **2006**, 51, 169–184.
- 44. Ota, M.; Saito, T.; Aida, T.; Watanabe, M.; Sato, Y.; Jr., R. L. S.; Hiroshi Inomata, H. Macro and Microscopic CH4–CO2 Replacement in CH4 Hydrate Under Pressurized CO2. *AIChE Journal* 2007, 53, 10.
- 45. Heeschen, K. U.; Deusner, C.; Spangenberg, E.; Priegnitz, M.; Kossel, E.; Strauch, B.; Bigalke, N.; Luzi-Helbing, M.; Haeckel, M.; Schicks, J. M. Production Method under Surveillance: Laboratory Pilot-Scale Simulation of CH4–CO2 Exchange in a Natural Gas Hydrate Reservoir. *Energy Fuels* **2021**, 35, 10641–10658.
- 46. Jadhawar, P.; Yang, J.; Chapoy, A.; Tohidi, B.; Subsurface Carbon Dioxide Sequestration and Storage in Methane Hydrate Reservoirs Combined with Clean Methane Energy Recovery. *Energy Fuels* **2021**, 35, 1567–1579.
- 47. Boswell, R.; Schoderbek, D.; Collett, T. S.; Ohtsuki, S.; White, M; Anderson, B. J. The Ignik Sikumi Field Experiment, Alaska North Slope: Design, Operations, and Implications for CO2–CH4 Exchange in Gas Hydrate Reservoirs. *Energy Fuels* **2017**, 31, 140–153.
- 48. Chen, Y.; Gao, Y.; Chen, L.; Wang, X.; Liu, K.; Sun, B. Experimental investigation of the behavior of methane gas hydrates during depressurization-assisted CO2 replacement. *Journal of Natural Gas Science and Engineering* **2019**, 61, 284–292.
- 49. Lee, S.; Lee, Y.; Lee, J.; Lee, H.; Seo, Y.; Experimental Verification of Methane–Carbon Dioxide Replacement in Natural Gas Hydrates Using a Differential Scanning Calorimeter. *Environ. Sci. Technol.* **2013**, 47, 13184–13190.
- 50. Zhou, X.; Lin, F.; Liang, D.; Multiscale Analysis on CH4–CO2 Swapping Phenomenon Occurred in Hydrates. *J. Phys. Chem. C* **2016**, 120, 25668–25677.
- 51. Ohgaki K.; Takano K.; Sangawa H.; Matsubara T.; Nakano S. Methane exploitation by carbon dioxide from gas hydrates. Phase equilibria for CO2–CH4 mixed hydrate system. *J Chem Eng Jpn* **1996**, 29, 478–83.
- 52. Qi, Y.; Ota, M.; Zhang, H. Molecular dynamics simulation of replacement of CH4 in hydrate with CO2. *Energy Conversion and Management* **2011**, 52, 2682–2687.

- 53. Yoon, J.-H.; Kawamura, T.; Yamamoto, Y.; Komai, T. Transformation of Methane Hydrate to Carbon Dioxide Hydrate: In Situ Raman Spectroscopic Observations. *J. Phys. Chem. A* **2004**, *108*, 5057-5059.
- 54. Seo, Y.; Lee, S.; Lee, J. Experimental Verification of Methane Replacement in Gas Hydrates by Carbon Dioxide. *Chem Engineer Trans.* **2013**, 32, 163–168.
- 55. Tung, Y.-T.; Chen, L.-J.; Chen, Y.-P.; Lin, S.-T. In Situ Methane Recovery and Carbon Dioxide Sequestration in Methane Hydrates: A Molecular Dynamics Simulation Study. *J. Phys. Chem. B* **2011**, 115, 15295–15302.
- 56. Uchida T.; Takeya S.; Ebinuma T.; Replacing methane with CO2 in clathrate hydrate: observations using Raman spectroscopy. In: Proceedings of the fifth international conference on greenhouse gas control technologies, Cairns, Austrian; 2000.Williams DJ, Durie RA, McMullan P, Paulson CAJ, Smith AY. Collingwood, Australia: CSIRO Publishing; 2001.
- 57. Lee H.; Seo Y.; Seo Y. T.; Moudrakovski IL, Ripmeester JA. Recovering methane from solid methane hydrate with carbon dioxide. *Angew Chem Int Ed* **2003**, 42,5048–5051.
- 58. Ota M.; Abe Y.; Watanabe M.; Smith R. L.; Inomata H. Methane recovery from methane hydrate using pressurized CO2. *Fluid Phase Equilib.* **2005**, 228, 553–559.
- 59. Zhang Y.; Xiong L. J.; Li X. S.; Chen Z. Y.; Xu C. G. Replacement of CH4 in hydrate in porous sediments with liquid CO2 injection. *Chem Eng Technol.* **2014**, 37, 12, 2022–2029.
- 60. Ota M.; Morohashi K.; Abe Y.; Watanabe M.; Smith R. L. Inomata H. Replacement of CH4 in the hydrate by use of liquid CO2. *Energy Convers Manage* **2005**, 46, 1680–1691.
- 61. Ors, O.; Sinayuc, C. An experimental study on the CO₂–CH₄ swap process between gaseous CO₂ and CH₄ hydrate in porous media. *Journal of Petroleum Science and Engineering* **2014**, 119, 156–162.
- 62. Gambelli, A. M.; Presciutti, A.; Rossi, F. Review on the characteristics and advantages related to the use of flue-gas as CO2/N2 mixture for gas hydrate production. *Fluid Phase Equilibria* **2021**,541, 113077.
- 63. Park, Y.; Kim, D.-Y.; Lee, J.-W.; Huh, D.-G.; Park, K.-P.; Lee, J.; Lee, H. Sequestering carbon dioxide into complex structure of naturally occurring gas hydrates. *PNAS* **2006**, 103, 34, 12690 –12694.

- 64. Cha, M.; Shin, K.; Lee, H.; Moudrakovski, I. L.; Ripmeester, J. A.; Seo, Y. Kinetics of Methane Hydrate Replacement with Carbon Dioxide and Nitrogen Gas Mixture Using in Situ NMR Spectroscopy. *Environ. Sci. Technol.* **2015**, 49, 1964–1971.
- 65. Tupsakhare, S. S.; Castaldi, M. J. Efficiency enhancements in methane recovery from natural gas hydrates using injection of CO2/N2 gas mixture simulating in-situ combustion. *Applied Energy* **2019**,236, 825–836.
- 66. Zhou, X.; Liang, D.; Liang, S.; Yi, L.; Lin, F. Recovering CH4 from Natural Gas Hydrates with the Injection of CO2–N2 Gas Mixtures. *Energy Fuels* **2015**, 29, 1099–1106.
- 67. Chaturvedi, K. R.; Sinha, A. S. K.; Nair, V. C.; Sharma, T. Enhanced carbon dioxide sequestration by direct injection of flue gas doped with hydrogen into hydrate reservoir: Possibility of natural gas production. *Energy*, **2021** 227, 120521.
- 68. Yasue, M.; Masuda, Y.; Liang, Y.; Estimation of Methane Recovery Efficiency from Methane Hydrate by the N2–CO2 Gas Mixture Injection Method. *Energy Fuels* **2020**, 34, 5236–5250.
- 69. Shin, K.; Park, Y.; Cha, M.; Park, K.-P.; Huh, D.-G.; Lee, J.; Kim, S.-J.; Lee, H. Swapping Phenomena Occurring in Deep-Sea Gas Hydrates. Energy & *Fuels* **2008**, 22, 3160–3163.
- 70. Lim, D.; Ro, H.; Seo, Y.; Seo, Y.-J.; Lee, J. Y.; Kim, S.-J.; Lee, J.; Lee, H. Thermodynamic stability and guest distribution of CH4/N2/CO2 mixed hydrates for methane hydrate production using N2/CO2 injection. *J. Chem. Thermodynamics* **2017**, 106, 16–21.
- 71. Liu, J.; Yan, Y.; Xu, J.; Li, S.; Chen, G.; Zhang, J. Replacement micro-mechanism of CH4 hydrate by N2/CO2 mixture revealed by ab initio studies. *Computational Materials Science* **2016**, 123, 106–110.
- 72. Panter, J. L.; Ballard, A. L.; Sum, A. K.; loan, E. D.; Koh, C. A. Hydrate Plug Dissociation via Nitrogen Purge: Experiments and Modeling. *Energy Fuels* **2011**, 25, 2572–2578.
- 73. Prasad, P. S. R.; Kiran, B. S.; Stability and exchange of guest molecules in gas hydrates under the influence of CH4, CO2, N2 and CO2+N2 gases at low-pressures. *Journal of Natural Gas Science and Engineering* **2020**, 78, 103311.
- 74. Park, Y.; Kim, D.-Y.; Lee, J.-W.; Huh, D.-G.; Park, K.-P.; Lee, J.; Lee, H. Sequestering carbon dioxide into complex structure of naturally occurring gas hydrates. *PNAS* **2006**, 103, 34, 12690 –12694.

- 75. Koh D. Y.; Kang H.; Kim D. O.; Park J.; Cha M.; Lee H. Recovery of methane from gas hydrates intercalated within natural sediments using CO2 and a CO2/N2 gas mixture. *ChemSusChem* **2012**, 5, 1443–1448.
- 76. Zhou, X.; Liang, D.; Liang, S.; Yi, L.; Lin, F. Recovering CH4 from Natural Gas Hydrates with the Injection of CO2–N2 Gas Mixtures. *Energy Fuels* **2015**, 29, 1099–1106.
- 77. Yasue, M.; Masuda, Y.; Liang, Y.; Estimation of Methane Recovery Efficiency from Methane Hydrate by the N2–CO2 Gas Mixture Injection Method. *Energy Fuels* **2020**, 34, 5236–5250.
- 78. Shin, K.; Park, Y.; Cha, M.; Park, K.-P.; Huh, D.-G.; Lee, J.; Kim, S.-J.; Lee, H. Swapping Phenomena Occurring in Deep-Sea Gas Hydrates. Energy & *Fuels* **2008**, 22, 3160–3163.
- 79. Sloan, E. D.; Fleyfel, F. "Molecular Mechanism for Gas Hydrate Nucleation from Ice," *AIChE J.*, **1991**, 37, 9, 1283-1292.
- 80. CHRISTIANSEN, R. L.; SLOAN, E. D. Mechanisms and Kinetics of Hydrate Formation. *Ann. N. Y. Acad. Sci.* **1994**, 715, 1, 283–305.
- 81. Cui, J.; Sun, Z.; Wang, X.; Yu, B.; Leng, S.; Chen, G; Sun, C. Fundamental mechanisms and phenomena of clathrate hydrate nucleation. *Chinese Journal of Chemical Engineering* **2019**, 27, 2014–2025.
- 82. Radhakrishnan, R.; Trout, B. L.; A new approach for studying nucleation phenomena using molecular simulations: Application to CO2 hydrate clathrates. *J. Chem. Phys.*, **2002**,117, 4, 1786–1796.
- 83. Jacobson, L. C.; Hujo, W.; Molinero, V. Amorphous precursors in the nucleation of clathrate hydrates. *J. Am. Chem. Soc.* **2010**, 132, 33, 11806–11811.
- 84. Zhang, Z.; Walsh, M. R.; Guo, G. J.; Microcanonical molecular simulations of methane hydrate nucleation and growth: Evidence that direct nucleation to sI hydrate is among the multiple nucleation pathways. *Phys. Chem. Chem. Phys.* **2015**, 17, 14, 8870–8876.
- 85. Jacobson, L. C.; Hujo, W.; Molinero, V. Nucleation pathways of clathrate hydrates: Effect of guest size and solubility. *J. Phys. Chem. B* **2010**, 114, 43, 13796–13807.
- 86. Moon, C.; Taylor, P. C.; Rodger, P. M. Molecular dynamics study of gas hydrate formation. *J. Am. Chem. Soc.*, **2003**, 125,16, 4706–4707.

- 87. Walsh, M. R.; Koh, C. A.; Sloan, E. D.; Sum, A. K.; Wu, D. T. Microsecond Simulations of Spontaneous Methane Hydrate Nucleation and Growth. *Science* **2009**, 326, 5956,1095-1098.
- 88. Sarupria, S.; Debenedetti, P. G. Homogeneous nucleation of methane hydrate in microsecond molecular dynamics simulations. *J. Phys. Chem. Lett.*, **2012**, 3, 20, 2942–2947.
- 89. He, Z.; Linga, P.; Jiang, J. What are the key factors governing the nucleation of CO₂ hydrate? *Phys. Chem. Chem. Phys.* **2hydrate**?4,15657–15661.
- 90. Arjun, A.; Bolhuis, P. G. Molecular Understanding of Homogeneous Nucleation of CO₂ Hydrates Using Transition Path Sampling. *J. Phys. Chem. B*, vol. **2021**, 125, 1, 338–349.
- 91. Liang, S.; Kusalik, P. G. Exploring nucleation of H₂S hydrates. *Chem. Sci.* **2011**, 2, 7, 1286–1292.
- 92. He, Z.; Gupta, K. M.; Linga, P.; Jiang, J. Molecular Insights into the Nucleation and Growth of CH₄ and CO₂ Mixed Hydrates from Microsecond Simulations. *J. Phys. Chem. C* **2016**, 120, 44, 25225–25236.
- 93. Hu, W.; Chen, C.; Sun, J.; Zhang, N.; Zhao, J.; Liu, Y.; Ling, Z.; Li, W.; Liu, W.; Song, Y. Three-body aggregation of guest molecules as a key step in methane hydrate nucleation and growth. *Commun. Chem.* 2022, 5, 1, 1–11.
- 94. Nada, H. Growth mechanism of a gas clathrate hydrate from a dilute aqueous gas solution: A molecular dynamics simulation of a three-phase system. *J. Phys. Chem. B* **2006**, 110, 33, 16526–16534.
- 95. Vatamanu, J.; Kusalik, P. G. Molecular insights into the heterogeneous crystal growth of sImethane hydrate. *J. Phys. Chem. B* **2006**, 110, 32,15896–15904.
- 96. Vatamanu, J.; Kusalik, P. G. Heterogeneous crystal growth of methane hydrate on its sII [001] crystallographic face. *J. Phys. Chem. B* **2008**, 112, 8, 2399–2404.
- 97. Tung, Y. T.; Chen, L. J.; Chen, Y. P.; Lin, S. T. The growth of structure I methane hydrate from molecular dynamics simulations. *J. Phys. Chem. B* **2010**, 114, 33, 10804–10813.
- 98. Liu, Y.; Chen, C.; Hu, W.; Li, W.; Dong, B.; Qin, Y. Molecular Dynamics Simulation Studies of Gas Hydrate Growth with Impingement. *Chem. Eng. J.* **2021**, 426, 130705.
- 99. Yi Lu, Y.; Lv, X.; Li, Q.; Yang, L.; Zhang, L.; Zhao, J.; Song, Y. Molecular behavior of hybrid gas hydrate nucleation: separation of soluble H₂S from mixed gas. *Phys. Chem. Chem. Phys.* **2022**, 24, 16, 9509–9520.
- 100. Matsui, H.; Jia, J.; Tsuji, T.; Liang, Y.; Masuda, Y. Microsecond simulation study on the replacement of methane in methane hydrate by carbon dioxide, nitrogen, and carbon dioxide–nitrogen mixtures. *Fuel*, **2020**, 263, 116640.

- 101. Song, W.; Sun, X.; Zhou, G.; Huang, W.; Lu, G.; Wu, C.; Molecular Dynamics Simulation Study of N2/CO2 Displacement Process of Methane Hydrate. *ChemistrySelect.* **2020**, 5, 44, 13936–13950.
- 102. Wu, G.; Tian, L.; Chen, D.; Niu, M.; Ji, H. CO2 and CH4 Hydrates: Replacement or Cogrowth? *J. Phys. Chem. C* **2019**, 123, 22, 13401–13409.
- 103. Tadepalli, K. M.; Kumar, R. Can Ammonia Be Used to Enhance the CO2 Sequestration in Methane Hydrates: A Molecular Dynamics Perspective. *Energy Fuels* 2022, 36, 10583–10590.
- 104. Majid, A. A. M.; Worley, J.; Koh, C. A. Thermodynamic and Kinetic Promoters for Gas Hydrate Technological Applications. **Energy Fuels 2021**, 35, 19288–19301.
- 105. de Deugd, R. M.; Jager, M. D.; de Swaan Arons, J. Mixed Hydrates of Methane and Water-Soluble Hydrocarbons Modeling of Empirical Results. AIChE J. 2001, 3, 47, 693-704.
- 106. Lee, Y.-J.; Kawamura, T.; Yamamoto, Y.; Yoon, J.-H. Phase Equilibrium Studies of Tetrahydrofuran (THF) + CH4, THF + CO2, CH4+CO2, and THF + CO2+CH4 Hydrates. J. Chem. Eng. Data 2012, 57, 3543–3548.
- 107. Khan, M. N.; Peters, C. J.; Koh, C. A. Desalination using gas hydrates: The role of crystal nucleation, growth and Separation. *Desalination* **2009**, 468,114049.
- 108. Arjmandi, M.; Chapoy, A.; Tohidi, B. Equilibrium Data of Hydrogen, Methane, Nitrogen, Carbon Dioxide, and Natural Gas in Semi-Clathrate Hydrates of Tetrabutyl Ammonium Bromide. *J. Chem. Eng. Data* **2007**, *52*, 2153-2158.
- 109. Mohammadi, A. H.; Richon, D. Phase Equilibria of Binary Clathrate Hydrates of Nitrogen+ Cyclopentane/Cyclohexane/Methyl Cyclohexane and Ethane+Cyclopentane/Cyclohexane/Methyl Cyclohexane. *Chemical Engineering Science* 2011, 66, 4936–4940.
- 110. Seo, Y.-T.; Kang, S.-P.; Lee, H. Experimental determination and thermodynamic modeling of methane and nitrogen hydrates in the presence of THF, propylene oxide, 1,4-dioxane and acetone. *Fluid Phase Equilib.* **2001**, 189, 99–110.
- 111. Pavelyev, R. S.; Gainullin, S. E.; Semenov, M. E.; Zaripova, Y. F.; Yarkovoi, V. V.; Luneva, A. I.; Farhadian, A.; Varfolomeev, M. A. Dual Promotion–Inhibition Effects of Novel Ethylenediaminetetraacetic Acid Bisamides on Methane Hydrate Formation for Gas Storage and Flow Assurance Applications. *Energy Fuels* 2022, 36, 290–297.

- 112. Asadi, F.; Nguyen, N. N.; Nguyen, A. V. Synergistic Effects of Sodium Iodide and Sodium Dodecyl Sulfate at Low Concentrations on Promoting Gas Hydrate Nucleation. *Energy Fuels* **2020**, 34, 9971–9977.
- 113. He, Y.; Sun, M.-T.; Chen, C.; Zhang, G.-D.; Chao, K.; Lin, Y.; Wang, F. Surfactant-based promotion to gas hydrate formation for energy storage. *J. Mater. Chem. A* **2019**, 7, 21634-21661.
- 114. Bhattacharjee, G.; Choudhary, N.; Kumar, A.; Chakrabarty, S.; Kumar, R. Effect of the Amino Acid L-Histidine on Methane Hydrate Growth Kinetics. *J. Nat. Gas Sci. Eng.* **2016**, 35, 1453–1462.
- 115. Arjang, S.; Manteghian, M.; Mohammadi, A. Effect of Synthesized Silver Nanoparticles in Promoting Methane Hydrate Formation at 4.7 MPa and 5.7 MPa. *Chem. Eng. Res. Des.* **2013**, 91, 1050–1054.
- 116. Liu, G.-Q.; Wang, F.; Luo, S.-J.; Xu, D.-Y.; Guo, R.-B. Enhanced Methane Hydrate Formation with SDS-Coated Fe3O4 Nanoparticles as Promoters. *J. Mol. Liq.* **2017**, 230, 315–321.
- 117. Mohammad-Taheri, M.; Moghaddam, A. Z.; Nazari, K.; Zanjani, N. G. Methane Hydrate Stability in the Presence of Water-Soluble Hydroxyalkyl Cellulose. *J. Nat. Gas Chem.* **2012**, 21, 119–125.
- 118. Asadi, F.; Metaxas, P. J.; Lim, V. W. S.; Nguyen, T. A. H.; Aman, Z. M.; May, E. F.; Nguyen, A. V. Cyclodextrins as Eco-Friendly Nucleation Promoters for Methane Hydrate. *Chem. Eng. J.* **2021**, 417, 127932.
- 119. Fakharian, H.; Ganji, H.; Naderi Far, A.; Kameli, M. Potato Starch as Methane Hydrate Promoter. *Fuel* **2012**, 94, 356–360.
- 120. Albertí, M; Costantini, A.; Laganá, A.; Pirani, F. Are Micelles Needed to Form Methane Hydrates in Sodium Dodecyl Sulfate Solutions? *J. Phys. Chem. B* **2012**, 116, 4220–4227.
- 121. Albertí, M.; Pirani, F.; Laganà, A. Carbon Dioxide Clathrate Hydrates: Selective Role of Intermolecular Interactions and Action of the SDS Catalyst. *J. Phys. Chem. A* **2013**, 117, 6991–7000.
- 122. Hollingsworth, S. A.; Dror, R. O. Molecular Dynamics Simulation for All. *Neuron* **2018**, 99, 1129-1143.
- 123. Allen, M. P., Tildesley, D. J. *Computer Simulation of Liquids*. Oxford University Press. **1987**.

- 124. Alder, B. J.; Wainwright, T. E. Phase Transition for a Hard Sphere System. *J. Chem. Phys.* **1957**, 27, 1208–1209.
- 125. GIBSON, J. B.; GOLANDP, A. N.; MILGRAM, M.; VINEYARD, G. H. Dynamics of Radiation Damage. *PHYSICAL REVIEW*, **1960**, 4, 120, 1229-1253.
- 126. RAHMAN, A. Correlations in the Motion of Atoms in Liquid Argon. *PHYSICAL REVIEW* **1994**, 2A, 136, A 405-411.
- 127. HARP, G. D.; BERNE, B. J. Linear- and Angular-Momentum Autocorrelation Functions in Diatomic Liquids. *J. Chem. Phys.* **1968**, 49, 1249-1254.
- 128. HARP, G. D.; BERNE, B. J. Time-Correlation Functions, Memory Functions, and Molecular Dynamics. *Phys. Rev. A*, **1970**, 2,975-996.
- 129. BARKER, J. A.; WATTS, R. O. STRUCTURE OF WATER; A NIONTE CARLO CALCULATION. *Chem. Phys. Lett.* **1969**, 3, 144-145.
- 130. RAHMAN, A.; STILLINGER, F. H.; Molecular Dynamics Study of Liquid Water. *J. Chem. Phys.* **1971**, 55, 3336-3339.
- 131. Morse, M. D.; Rice, S. A. Tests of effective pair potentials for water: Predicted ice Structures. *J. Chem. Phys.* **1982**, 76, 650-660.
- 132. Abascal, J. L. F.; Vega, C. A general purpose model for the condensed phases of water: TIP4P/2005. *J. Chem. Phys.* **2005**, 123, 234505.
- 133. González, M. A. Force fields and molecular dynamics simulations. *Collection SFN* 2011, 12, 169–200.
- 134. Jorgensen, W. L.; Tirado-Rives, J. Potential energy functions for atomic-level simulations of water and organic and biomolecular systems. *PNAS*, **2005**, 102, 19. 6665–6670.
- 135. Hwang, M. J.; Stockfiscb, T. P.; Hagler, A. T. Derivation of Class II Force Fields. 2. Derivation and Characterization of a Class II Force Field, CFF93, for the Alkyl Functional Group and Alkane Molecules. *J. Am. Chem. SOC.* **1994**, 116, 2515-2525.
- 136. Sun, H.; Mumby, S. J.; Maple, J. R.; Hagler, A. T. An ab Initio CFF93 All-Atom Force Field for Polycarbonates. *J. Am. Chem. Soc.* **1994**, 116, 2978-2987.
- 137. Verlet, L. Comyuter "Exyeriments" on Classical Fluids. I. Thermodynamical Properties of Lennard, -Jones Molecules. *Phys. Rev.* **1967**, 159, 98-103.
- 138. Swope, W. C.; Andersen, H. C.; Berens, P. H.; Wilson, K. R. A computer simulation method for the calculation of equilibrium constants for the formation of physical clusters of molecules: Application to small water clusters. *J. Chem. Phys.* **1982**, 76, 637–649.
- 139. Barducci, A.; Bonomi, M.; Parrinello, M. Metadynamics. WIREs Comput. Mol. Sci. 2011, 1, 826–843.

- 140. Barducci, A.; Bussi, G.; Parrinello, M. Well-Tempered Metadynamics: A Smoothly Converging and Tunable Free-Energy Method. *Phys. Rev. Lett.* **2008**, 020603.
- 141. Mahmoudinobar, F.; Dias, C. L. GRADE: A code to determine clathrate hydrate structures. *Computer Physics Communications* **2019**, 244, 385–391.
- 142. Rodger, P. M.; Forester, T. R.; Smith, W. Simulations of the methane hydrate / methane gas interface near hydrate forming conditions. *Fluid Phase Fxluilibria* **1996**,116, 326-332.
- 143. Jiang, H.; Jordan, K. D. Comparison of the Properties of Xenon, Methane, and Carbon Dioxide Hydrates from Equilibrium and Nonequilibrium Molecular Dynamics Simulations. *J. Phys. Chem. C* **2010**, *114*, 5555–5564.

Chapter 2

Role of Polyatomic Gases in CO₂-CH₄ Exchange in NGHs

Introduction

Ever-increasing demand for energy and limited availability of fossil fuels has turned worldwide focus towards alternative resources of clean energy. Natural Gas Hydrates (NGHs) are one of the most abundant natural and clean energy resources that contain twice the amount of carbon than the fossil fuels ¹⁻³. Conventional techniques like depressurization and steam technology are employed at a limited scale to extract methane from sI hydrates to avoid any geological hazards ⁴. The replacement of CH₄ hydrates with CO₂ hydrates is proposed to be an alternative to avoid geological catastrophes by simultaneously extracting CH₄ and sequestrating CO₂ in NGHs ⁴⁻⁷. However, one of the major challenges in this process is the formation of CH₄-CO₂ mixed hydrates that reduces the rate of methane recovery ⁵. Recently, mixture of CO₂ with polyatomic (flue) gases such as like N₂, H₂S and SO₂ have shown to improve CH₄-CO₂ exchange (MCE) process but rate of CO₂ sequestration depends on the concentration of flue gases 8-13. Commercially, methane-carbon dioxide exchange process is a heterogeneous process and the formation of hydrate layer besides the interface slows down the recovery of methane, thus, multiphase recovery of methane has been proposed as an alternative to enhance the rate of methane extraction ^{5, 23-28}. The theoretical studies could provide microscopic insights into the factors that control hydrate growth unlike experiments that

currently have spatiotemporal restrictions to explore nucleation mechanisms. The hydrate nucleation in *homogeneous medium* has been theoretically proposed to occur either through formation of labile water-gas clusters; amorphous water-gas aggregates; local ordering of gas and water molecules due to thermal fluctuations ¹⁴⁻²⁰. On the other hand, hydrate nucleation in *heterogeneous medium* has been reported to occur either through the direct exchange of methane and carbon dioxide in hydrate cages or melting of methane cages due to the heat released from the exothermic formation of CO₂ hydrates ^{6,21-22}. Some of the challenges in this direction are: (i) what role do the polyatomic gases play in the MCE process? (ii) why does cage occupancy of N₂ change with change in the conc. of N₂ and CO₂ (iii) why is the sequestration of CO₂ dependent on the conc. of flue gases? and (iv) how can the sequestration of CO₂ be enhanced in the first layer that form beside the interface? In this work, we explore the role of polyatomic gases (H₂S, CO and N₂) in the formation of first hydrate layer beside the interface in heterogeneous medium during MCE process and effect of these gases on CO₂ sequestration using molecular dynamics simulation techniques.

Computational Details

We chose the following systems: *pure gas systems*; $(CH_4)_P$, $(CO_2)_P$ and $(H_2S)_P$ that have only one type of gas species both in the bulk phase and sI hydrate seed; *bulk CO₂ system*, $(CO_2)_B$ with CO_2 in the bulk phase and sI hydrate as seed; *third gas systems* (G_3) with sI hydrate seed and mixture of CO_2 and G_3 $(H_2S/N_2/CO)$ in bulk; where two concentrations of G_3 were studied: $CO_2(3):G_3(1)$ (*low*) and $CO_2(2):G_3(2)$ (*high*) ^{12,29}.

The model system consisted of sI hydrate seed (5x5x3 supercell)⁵² in the center of the simulation box with randomly placed supersaturated solution of gases in water (equivalent to

5 x 5 x 1.5 of sI hydrate) on either side of the seed along the z-axis as shown in Figure 2.1. The number of water and gas molecules in each bulk region were taken equivalent to 5x5x1.5 of sI hydrate where 1720 water molecules and 300 gas molecules were randomly placed in each bulk region. The supersaturation in the bulk region was obtained by replacing 5 H₂O molecules with 5 gas molecules in bulk regions. The relaxed systems of CO₂:G₃(3:1) systems were chosen as the initial configurations for CO₂:G₃(2:2) systems where relevant number of CO₂ molecules were replaced by G₃ as reported in Table 2.1. In order to generate (H₂S)_P and (CO₂)_P systems, the CH₄ molecules in (CH₄)_P system were replaced by H₂S and CO₂ respectively in both the bulk and in the hydrate seed. Hereon, all third gas systems are referred as G₃(3:1) for CO₂(3):G₃(1) and G₃(2:2) for CO₂(2):G₃(2) as CO₂ is the common gas in all these systems.

All the molecular dynamics (MD) simulations were performed using LAMMPS package ³¹ and all-atom forcefields were chosen for all the species; water (TIP4P-2005) ³²⁻³⁴, CH₄ ³⁵, CO₂ ³⁶, N₂ ³⁷, CO ³⁸ and H₂S ³⁹. A timestep of 1fs and three-dimensional periodic boundary conditions was chosen in all the systems. We chose cutoff distance of 12Å and 10Å for the van der Waals and electrostatic interactions. In G₃(3:1), (H₂S)_P and (CH₄)_P systems, NVT simulations were performed for 2ns at 250K followed by 10ns of NVT simulations at 300K to generate a uniform interface between bulk phase and hydrate seed ^{24,29-30,34}. In case of (CO₂)_P system, due to instability of hydrate seed at 300K, NVT simulations were not performed at 300K and the initial configuration was energy minimized by using steepest descent algorithm. Finally, all the systems were simulated for 60ns using NPT simulations at 250K and 15MPa (noble gases form clathrates at very high pressures and low temperature and CO₂ hydrate are stable in this T and P range) ^{18,29,42}. The relaxation times for Nose-Hoover thermostat and barostat were chosen as 0.06ps and 2ps respectively ⁴¹.

ANALYSIS: The velocities were stored every 2fs for initial 1.5ns of NPT simulation run for the calculation of velocity autocorrelation function. The free energy calculations on MD data were performed in PLUMED2 (LAMMPS) using the configuration 1ns prior to formation of growth synthon as the initial configuration ⁴⁵⁻⁴⁶. The restraint metadynamics was employed by constraining the dihedral angle between the four gas species of the growth synthon (details in Results and Discussions section) to 180° with a force constant between 50 kcal/mol to 200 kcal/mol in different systems. The width and height of Gaussians were chosen as 0.25kcal/mol and 0.50kcal/mol respectively. The Gaussians were deposited at every 100fs and data was analyzed using metadynminer package ⁴⁷. The last configuration of NPT simulation was used to calculate the total and CO₂ selectivities. The first hydrate layers (left and right side of interface) were chosen as 12Å along the z-axis from the interface (which is equivalent to unit cell dimension of sI hydrate). The cage analysis was done using GRADE code, where hydrogen bond distance between oxygens of hydrogen-bonded ordered water molecules in a cage is taken less than or equal to 3.0Å and guest is included in a cage if distance between center of mass of guest and center of cage in less than or equal to 2.0 Å and gases are assigned to small (5^{12} type cages) or large (5¹²6² type cages) ⁴⁸. All the snapshots were generated using VESTA or VMD software 49-50.

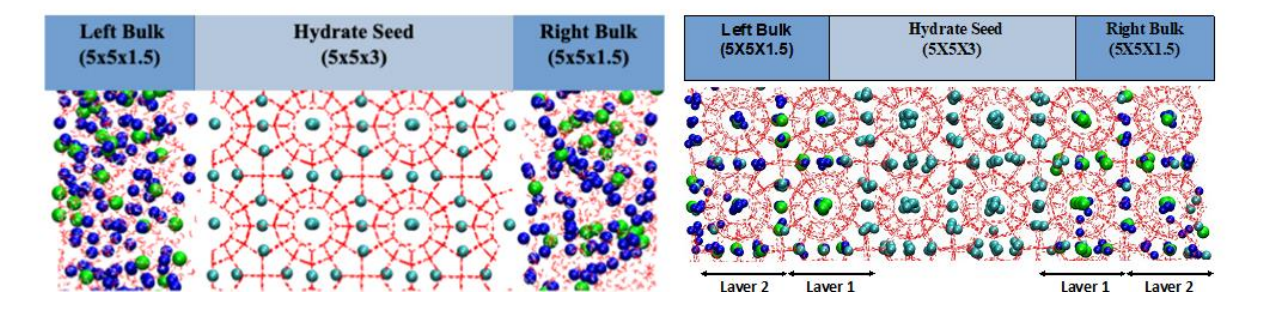


Figure 2.1: (Left) Schematic of initial configuration in a system with sI hydrate in the center of simulation box and gas species on either sides of the hydrate seed and (Right) Final configuration with two hydrate layers formed adjacent to the interface (Layer 1 and Layer 2) at the end of NPT simulation. Here cyan, green and blue represent center-of-masses of CH₄, CO₂ and flue gas or noble gas (atomic coordinates) respectively.

Table 2.1: Box dimensions and number of molecules/atoms in different systems where G_3 is the flue or noble gas, G_3 = H_2S , N_2 , CO, Ne, Ar, Kr and Xe; here $G_3(3:1)$ and $G_3(2:2)$ represent (CO2: G_3) in ratios of (3:1) and (2:2) respectively.

Systems	Box Dimensions (ų)	NH20	N сн4	Nco2	N _G 3
G ₃ (3:1) G ₃ (2:2) (CO ₂) _B	58.1 x 58.1 x 69.72	6890	600	458 306 610	152 304 0
(CH ₄) _P			1210	0	0
(CO ₂) _P			0	1210	0
(H ₂ S) _P			0	0	1210

Results and Discussions

We observed melting of hydrate seed layer besides the interface during NVT simulations at 300K with diffusion of \geq 80% in third gas systems and 60% of CH₄ molecules in pure CH₄ system into bulk solution as reported in Table 2.2. However, there was no further melting of the inner layers of the seed during the NPT simulations at 250K. There was no mass transfer barrier in the bulk phase in all the systems except for pure CH₄ system where a cluster of gas was observed in the bulk phase as reported in Figure 2.2 ^{24,26}. The results for pure CO₂ and pure CH₄ systems are consistent with the earlier reports that system size shrinks for CO₂ hydrate then CH₄ hydrate ⁵⁸. Figure 2.2(a-b) shows the growth of hydrate in different systems as a time plot of potential energy (PE) and F4 order parameter (OP) ⁴². F4 OP can quantitatively differentiate water in bulk water (-0.04), ice (0.4) and hydrate phase (0.70) and can be calculated as shown in Eq 2.1 ⁴²

$$F4 = \frac{1}{N} \sum_{i=1}^{N} \cos 3 \, \emptyset_i$$
 Eq (2.1)

where, Ø represents the torsion angle between two closed by oxygen atoms of water molecules within cutoff of 3.5Å and outermost hydrogen of both water molecules. There is a gradual decrease in PE and increase in F4 OP till former reached minimum and latter reached a value between 0.68-0.70 that indicated complete hydrate formation in all the systems within 60ns and as expected hydrate growth in heterogeneous medium is faster than induction time for methane hydrate nucleation in homogeneous medium $(0.1 \mu s)^{15,42}$. Interestingly, though most of the flue and noble gases form s-II hydrates in pure forms but they form sI hydrates in the presence of sI hydrate seed ^{24,42-44}. In general, heterogeneous nucleation could occur simultaneously from several nucleation sites, thus, we chose time for the formation of first hydrate layers besides the interface as the induction time for hydrate growth. Figure 2.2b reports the average induction time (t_{ind}) and total time (t_{tot}) for hydrate formation in different systems. Pure H₂S system is the fastest ($t_{ind} = 3$ ns, $t_{tot} = 21.5$ ns) growing system then CH₄ $(t_{ind} = 13 \text{ns}, t_{tot} = 56 \text{ns})$ and these results are consistent with the reports of faster hydrate growth in H₂S hydrates then CH₄ hydrates in homogeneous medium ³⁴. The induction time for $(CO_2)_P$ system $(t_{ind} = 18 \text{ns} \text{ and } t_{tot} = 26 \text{ns})$ is longer than $(H_2S)_P$ and $(CH_4)_P$ systems which is in agreement with large nucleation time for pure CO₂ hydrates in homogeneous medium ¹⁸-¹⁹. However, the total hydrate growth is faster in (CO₂)_P then (CH₄)_P system which is due to the formation of methane cluster in bulk phase of (CH₄)_P system. The bulk CO₂ system shows larger induction (30ns) and total hydrate formation (49ns) times which is in agreement with the earlier reports that hydrate growth is slow during MCE process ⁶. Among the polyatomic gas systems, $H_2S(2:2)$ is the fastest ($t_{ind} = 15$ ns) growing system and the systems with CO as the third gas showed the slowest hydrate growth. However, H₂S based systems (H₂S(3:1) and $H_2S(2:2)$) showed short t_{ind} but longer t_{tot} and vice-versa was observed for $N_2(3:1)$. We evaluated the role of dynamics of gases in hydrate growth by calculating the velocity autocorrelation function (VACF) of gases in different systems. The velocity autocorrelation function provides insights into the dynamics of particles with respect to their environment and is calculated as

$$C_v(t) = \frac{1}{N} \sum_{i=1}^{N} \frac{\langle v_i(t).v_i(0) \rangle}{\langle v_i(0).v_i(0) \rangle}$$
 Eq. (2.2)

where $v_i(0)$ and $v_i(t)$ are velocities of particle at time t = 0 and t as shown in Eq. 2.2 and Figure 2.3 shows that VACF plot of a gas is independent of the concentration of gas in a system (3:1 or 2:2 system) and depends only on the type of gas species. These anomalies are hard to answer based on diffusivity or size of the gas species.

Figure 2.4 shows the time plot of number of SCs and LCs formed by different gas species in a system during NPT simulations. Figure 2.4a shows that number of SCs and LCs are formed in a decreasing order in pure systems as $(H_2S)_P > (CH_4)_P > (CO_2)_P > (CO_2)_B$. However, we observe a sharp increase in the number of SCs in $(CO_2)_P$ after 15ns which is contradictory to the earlier reports that CO_2 occupies mainly LCs in sI hydrates 10 . The slow increase in the number of cages in $(CO_2)_B$ then $(CO_2)_P$ is consistent with the earlier reports that growth during MCE process is a slow process due to the formation of mixed CH_4 - CO_2 hydrates 6 . The preferential occupation of a cage by a gas in a third gas systems is evident only after t > 10ns. Among *the low conc. flue gas systems*, H_2S occupies larger number of SCs than CH_4 though the molecular diameter, d of $H_2S(d=4.58\text{Å})$ is larger than CH_4 (d=4.36Å) which is inconsistent with the reports that large gases lead to unstable SCs 1,3,34 . However, in N_2 system, N_2 and CO have similar sizes (d=4.1Å) but N_2 occupies more SCs then CH_4 which is consistent with the earlier reports $^{9-10}$, however, CO competes with CH_4 to occupy SCs. In *high conc. flue gas systems*, the flue gases dominate over CH_4 and compete with CO_2 to occupy cages where $H_2S(2:2) >$

 $CO(2:2) > N_2(2:2)$. These results are in agreement with the earlier reports that sequestration of flue gases is higher than CO_2 in hydrates when the conc. of flue gases is increased ¹²⁻¹³.

Table 2.2: Number of methane molecules diffused in the bulk phase at end of NVT simulations at 300K due to melting of hydrate cages during the formation of interface.

System	N _{CH4}	
Pure CH ₄	125	
Bulk CO ₂	167	
H ₂ S(3:1)	152	
N ₂ (3:1)	144	
CO(3:1)	152	
H ₂ S(1:1)	150	
N ₂ (1:1)	149	
CO(1:1)	147	

We elucidated the mechanism of hydrate formation based on the simulation trajectories during the total simulation time, t^* . There is formation of SCs or LCs with different gases during the beginning of the simulations, however, most of these cages breakdown within 1ns as shown in Figure 2.5 for H₂S(2:2) system. However, there is formation of stable, dual cages occupied by particular gas species that eventually leads to the formation of four-caged, Y-shaped growth synthon (GS, Figure 2.6c). The growth synthon consists of one large-large dual cage (LLDC) and three small-large dual cages (SLDC) and leads to the growth of unit cell. The growth synthon is observed in all the systems (Figure 2.6). The formation of GS in most of the systems occurs mainly via the following steps as shown for pure CH₄ in Figure 4(a) – formation of a (i) L cage (ii) LL dual cage (iii) LLS cluster and (iv) LLSL cluster except for pure H₂S system where SL forms at step (ii) and other steps are similar to other cases. Thus, thermal fluctuations lead to the formation of ordered cages though no amorphous cages or labile clusters that contribute to growth synthon are observed during heterogeneous nucleation of hydrates ¹⁵⁻²⁰.

There is clustering of CO₂ molecules (Figure 2.6b) during the formation of first L cage in pure CO₂ system and is consistent with the earlier reports of high conc. of CO₂ molecules in the vicinity of amorphous CO₂ cage in homogeneous medium ¹⁸.

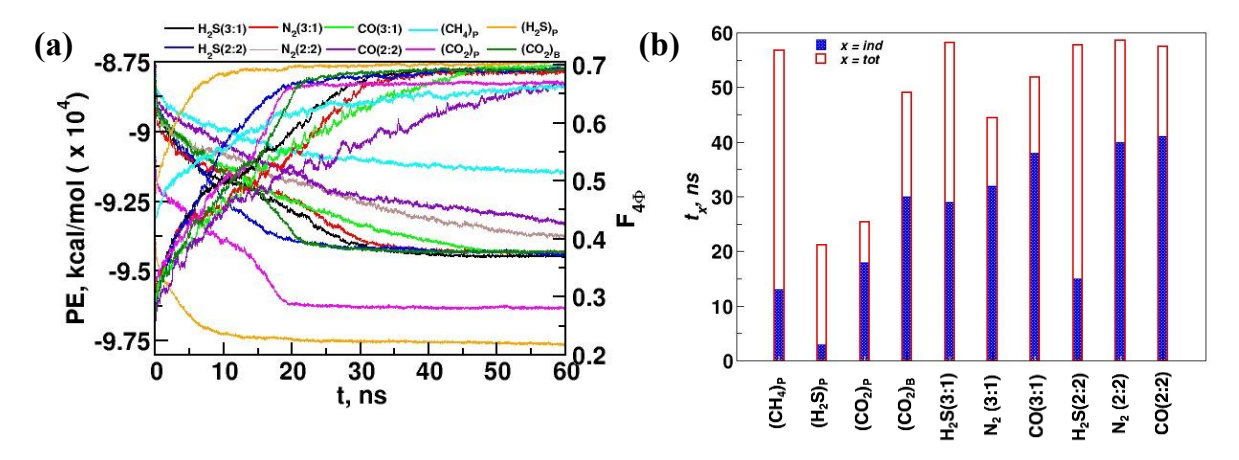


Figure 2.2: Potential energy and F4 order parameter of full system as a function of time for (a) systems with flue gas (H₂S, N₂ and CO) as third gas; pure gas systems ((CH₄)_P, (CO₂)_P and (H₂S)_P) and bulk CO₂ system (CO₂ in bulk water and methane sI hydrate seed, CO₂)_B) at 250K and 15 MPa, where third gas systems have two conc. of CO₂:G₃(3:1) and CO₂:G₃(2:2) referred here as G₃(3:1) and G₃(2:2); (b) average induction time (t_{ind}) for the formation of first hydrate layer near interface (and) total time (t_{tot}) for hydrate growth in different systems. The observed trend for t_{ind} is (H₂S)_P < (CH₄)_P < H₂S(2:2) < (CO₂)_P < (CO₂)_B < H₂S(3:1) < N₂(3:1) < CO(3:1) < CO(2:2) < N₂(2:2) and trend for t_{tot} is (H₂S)_P < (CO₂)_P < N₂(3:1) < (CO₂)_B < CO(3:1) < (CH₄)_P < H₂S(3:1) < H₂S(2:2) < N₂(2:2) < CO(2:2).

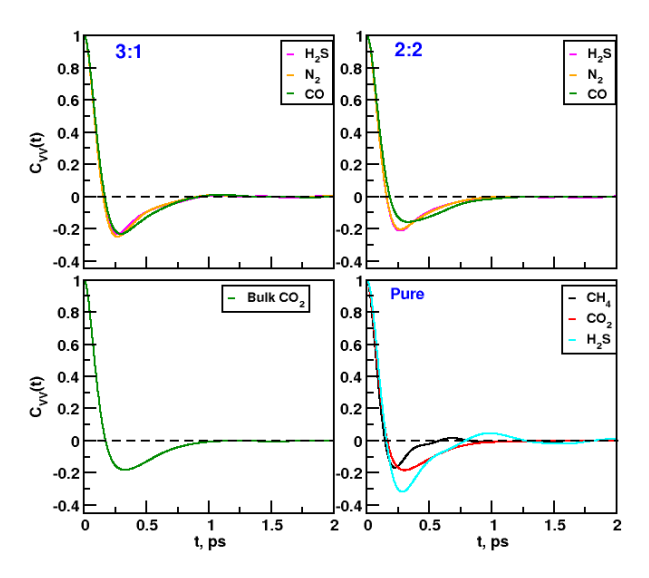


Figure 2.3: Velocity autocorrelation function plot of gases in different systems at 250K and 15MPa.

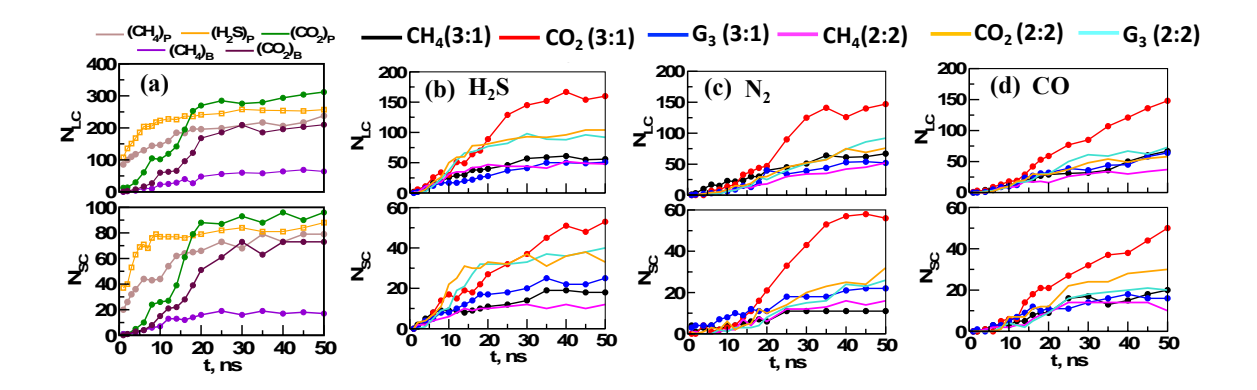


Figure 2.4: Number of gas species (methane, carbon dioxide and third gas) in small (N_{SC}) and large (N_{LC}) cages as a function of time during the simulation at 250K and 15MPa;(a) pure gas (CH₄, H₂S and CO₂) systems and bulk CO₂, third gas systems where third gas is (b) H₂S, (c) N₂ and (d) CO.

In a sI hydrate, SC and LC are formed by 20 and 24 water molecules respectively with an intermolecular distance of 6-8Å between the gas species 1,59 . The formation of GS was further quantified by calculating two coordination numbers; water-guest, N_{WG} (N_{GW} is 20 and 24 for SC and LC in a sI hydrate) and guest-guest, N_{GG} (N_{GG} =4 in a GS, where two gas species are within distance of 8Å) as a function of time (t^* where time from beginning of simulations (NVT, 250K) is considered) as shown in Figure 2.7. The cut-off distance between center of cage and center-of-mass of gas species was chosen as 5.8Å and 5.0Å for a gas to belong to large and small cage respectively. Figure 2.7a shows that values of N_{GW} and N_{GG} are 25 and 0 at 4ns in (CH₄)_P due to the formation of one LC with CH₄ molecule. Further, the value of N_{GG} changes to 2 (5.5ns), 3 (7ns) and 4 (7.5ns) and ordered fourth cage is formed at 16ns. In case of (CO₂)_P, formation of GS is a slow process; initially N_{GG} = 3 at 13ns with three CO₂ molecules within a distance of 8Å and one LC is formed (N_{GW} =23), all four cages are formed by 18ns though the fourth cage is ordered by 28ns only. Here, t^* = 28ns is equivalent to t (NPT) = 14ns [28ns – 14ns; where 14ns is NVT(250K, 2ns) + NVT(300K, 10ns)] and as growth synthon forms by

this time, there is enhanced growth in the number of small cages in pure CO₂ system as reported in Figure 2.4a.

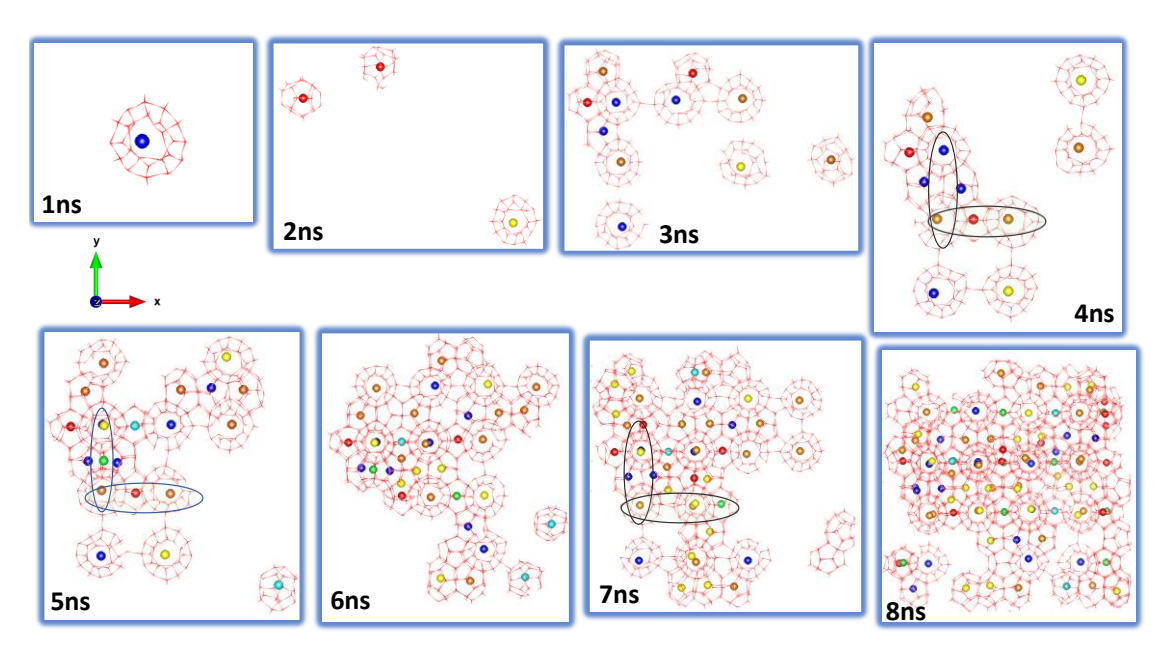


Figure 2.5: Snapshots of cages formed during NPT simulations in right side of interface in $H_2S(2:2)$ system; cyan, blue, green, yellow, red and orange represent CH_4 in SC, CH_4 in LC, CO_2 in SC, CO_2 in LC, H_2S in SC and H_2S in LC. Large cage of CH_4 formed at 1ns disappears at 2ns; Ovals represent the growth synthon.

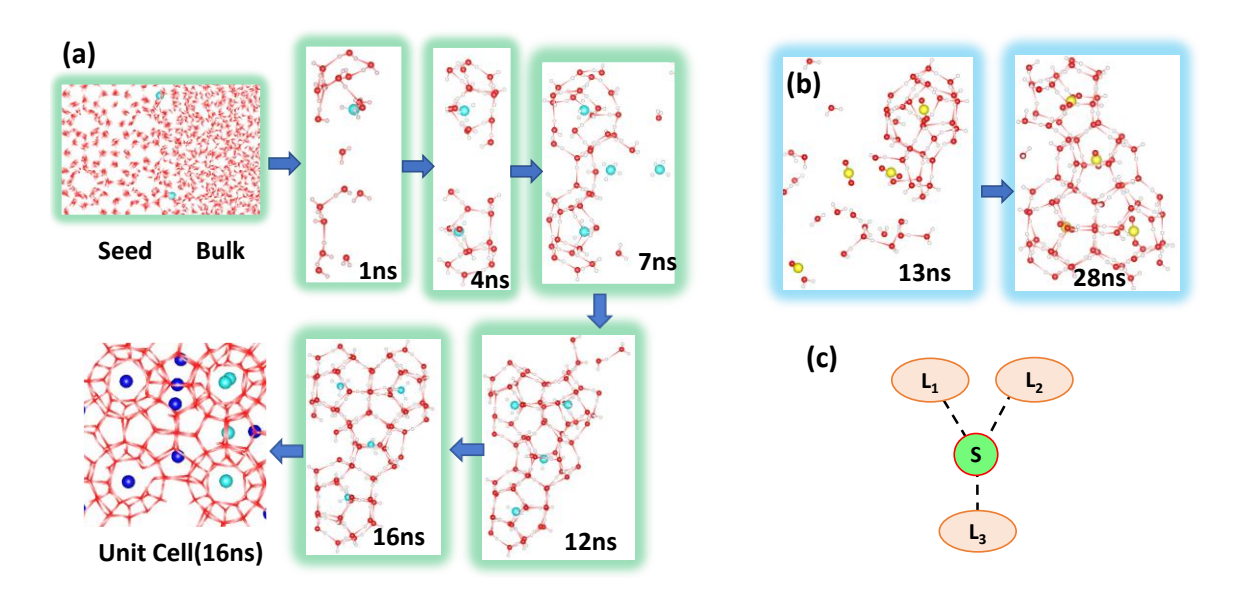


Figure 2.6: Snapshots from trajectories of (a) pure CH_4 system at different simulation times, $t^* = 1$ ns, 4ns, 7ns, 12ns and 16ns; (b) pure CO_2 system at 13ns and 28ns and (c) schematic of 4-caged, Y-shaped growth synthon $(L_1L_2L_3S)$ where L_1 , L_2 and L_3 are three large cages and S is the small cage. Here t^* is considered from the beginning of simulation (NVT at 250K, Simulation Details). Here white, red, cyan, green and yellow spheres represent H, O, $C(CH_4)$, Ar and $C(CO_2)$ atoms.

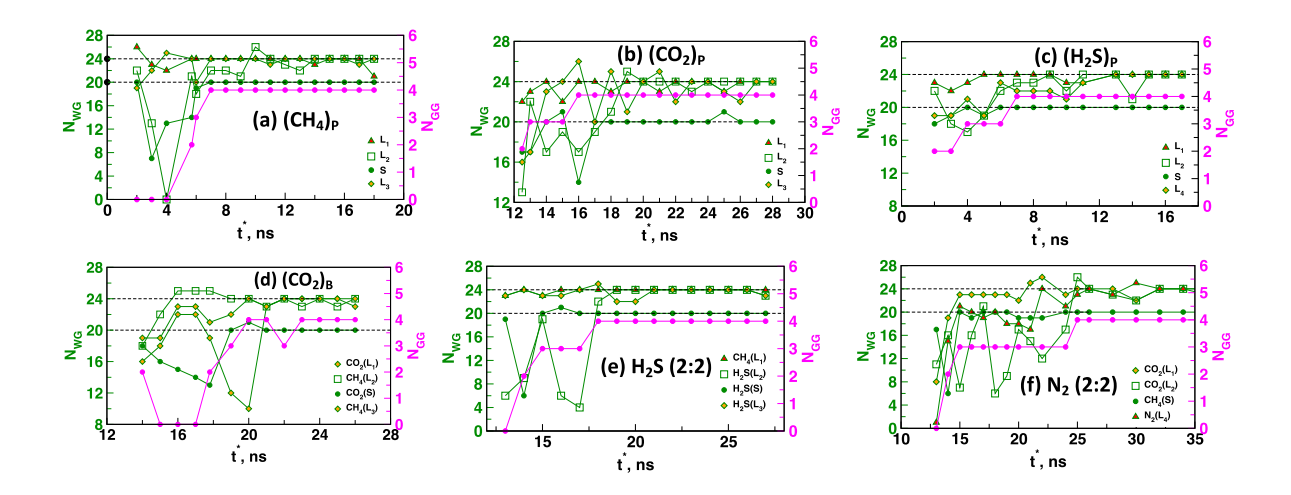


Figure 2.7: Number of water molecules (N_{GW}) around a gas species in a growth synthon and number of gas species (N_{GG}) in growth synthon within a distance of 8 Å as a function of t^* in (a) (CH_4)_P, (b) (CO_2)_P, (c) (H_2S)_P, (d) (CO_2)_B, (e) $H_2S(2:2)$ and (f) $N_2(2:2)$ systems.

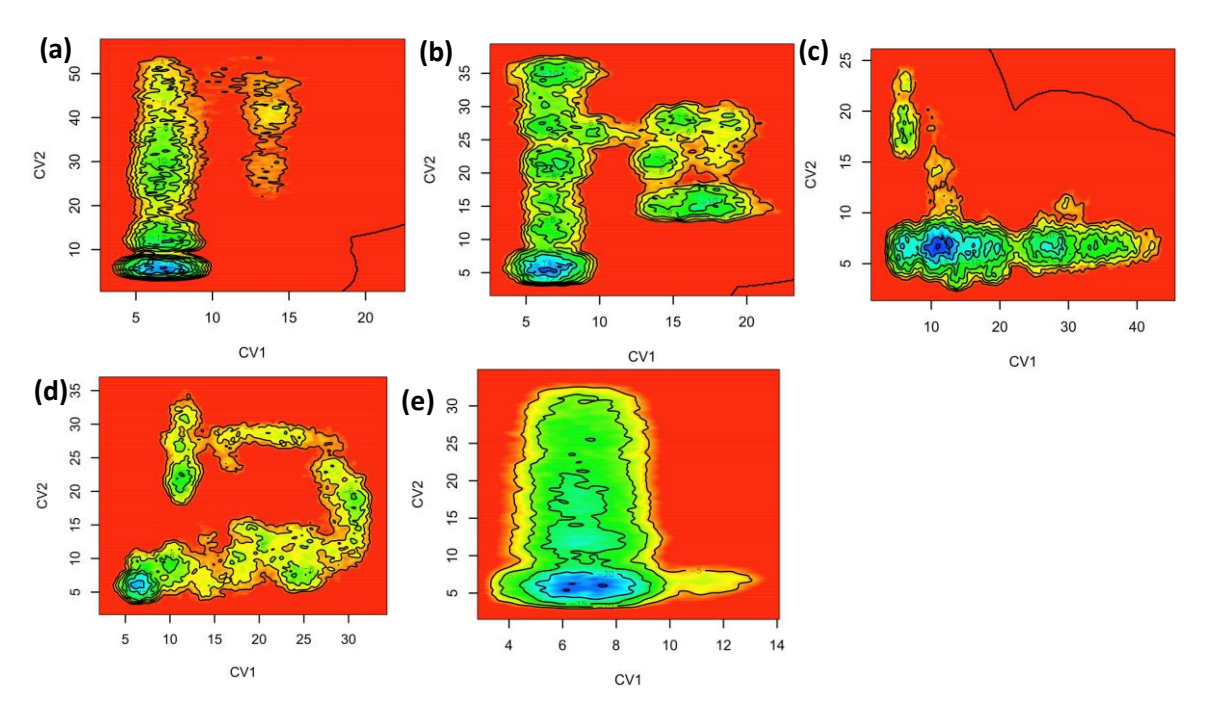


Figure 2.8: (a-e) Free energy profiles of pure methane, pure H₂S, pure CO₂, bulk CO₂ and H₂S(2:2) as a function of two collective variables; CV1 (distance between gases in SL dual cages) and CV2 (distance between gases in LL dual cages).

Figure 2.8 reports the free energy profiles for SLDC and LLDC as a function of both the collective variables (CV1; distance between the gases in SL dual cages and CV2; distance between the gases in LL dual cages of a growth synthon) in different systems. The FE minimum

is observed when CV1 and CV2 are between 6-8 Å and is consistent with the typical gas-gas inter-cage distance observed in sI hydrate ⁵⁹.

Selective sequestration of CO_2 over CH_4 in hydrate cages was assessed as selectivity (ΔS) for CO_2 over CH_4 in the first hydrate layer besides the interface as shown in Eq. 2.3 where N is the number of total cages occupied by a gas.

$$\Delta S = \frac{(N_{CO_2} - N_{CH_4})100}{N_{tot}}$$
 Eq. (2.3)

Figure 2.9 shows that $\Delta S > 60\%$ in all the third gas systems when the conc. of third gas was high as compared to $\Delta S = 42\%$ in bulk CO₂ system. The ΔS is good for H₂S(3:1) and CO(3:1) systems. However, with increase in conc. of third polyatomic gases, the ΔS is poor in respective systems (H₂S(2:2) and CO(2:2)) which is consistent with reports of poor CO2 sequestration with increase in conc. of flue gas in a system ^{12-13,44}. Interestingly, N₂ shows poor ΔS at both low and high conc. of N₂ unlike H₂S and CO and is consistent with the earlier reports ^{12-13,44}.

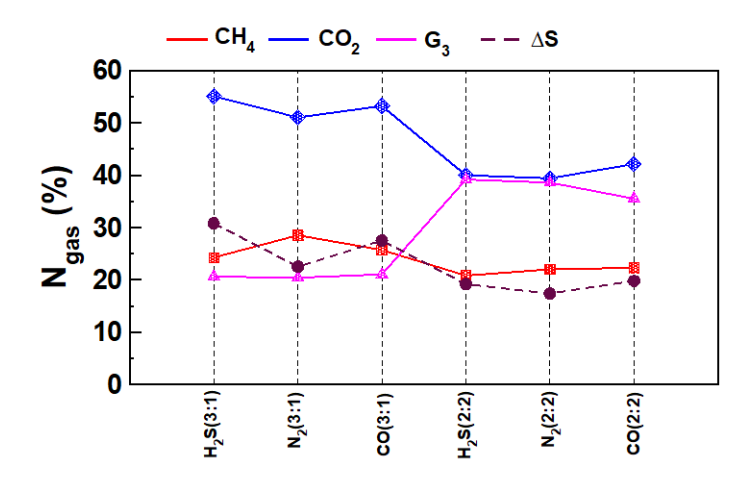


Figure 2.9: Percentage of different gases, N_{gas} (methane, carbon dioxide and third gas, $G_3 = H_2S$, N_2 and CO) in the hydrate cages in different systems; also shown is selectivity (ΔS , %) for CO_2 as difference in N_{CO2} and N_{CH4} in different polyatomic system.

Conclusions

The present work highlights the effect of polyatomic gases (flue gases) on CH₄-CO₂ exchange in NGHs using molecular dynamics simulations at 250K and 15MPa. There is formation of Y-shaped (LLSL) growth synthon during sI hydrate formation in heterogeneous medium and growth synthon formation is governed by the dual cages where LL and SL (L-large, S-small) cages lead to the formation.

References

- 1. Sloan E. D. Jr Fundamental principles and applications of natural gas hydrates. *Nature* **2003**,426, 353-359.
- 2. Boswell R. and Collett T. S. Current perspectives on gas hydrate resources. *Energy Environ. Sci.* 2011, 4, 1206–1215.
- 3. Sloan E. D. Jr Physical and chemical properties of gas hydrates and application to world margin stability and climatic change. Gas Hydrates: Relevance to World Margin Stability and Climate Change. Geological Society, London, Special Publications **2014**, 137, 31-50
- 4. Yang M.; Fu Z.; Zhao Y., Jiang L.; Zhao J. and Song Y. Effect of depressurization pressure on methane recovery from hydrate-gas-water bearing sediments," *Fuel* **2016**, 166, 419–426.
- 5. Wang, Y.; Lang, X.; Fan, S.; Wang, S.; Yu, C.; Li, G. Review on enhanced technology of natural gas hydrate recovery by carbon dioxide replacement. Energy&Fuels, 2021, 46(5), 3659-3674.
- 6. Wu, G.; Tian, L.; Chen, D., Niu, M.; Ji, H. CO₂ and CH₄ Hydrates: Replacement or Cogrowth? *J. Phys. Chem. C* **2019**, 123, 13401–13409, DOI: 10.1021/acs.jpcc.9b00579
- 7. He, Z.; Gupta, K. M.; Linga, P.; Jiang, J. Molecular Insights into the Nucleation and Growth of CH₄ and CO₂ Mixed Hydrates from Microsecond Simulations. *J. Phys. Chem. C* **2016**, 120, 25225–25236.

- 8. Doman, P.; Alavi, S.; Woo, T. K. Free energies of carbon dioxide sequestration and methane recovery in clathrate hydrates. J. Chem. Phys. **2007**, 127, 124510-124518.
- 9. Park, Y.; Kim, Do-Y.; Lee, Jon-W.; Huh, D-Gee; Park, K-Pil; Lee, J.; Lee H. Sequestering carbon dioxide into complex structures of naturally occurring gas hydrates. *PNAS* **2006**, 103, 12690-12694.
- 10. Liu, J.; Yan, Y.; Xu, J.; Li, S.; Chen, G.; Zhang, J. Replacement micro-mechanism of CH₄ hydrate by N₂/CO₂ mixture revealed by ab initio studies. *Comput. Mater. Sci.* **2016**, 123, 106-110.
- 11. Zhou, H.; Chen, B.; Wang, S.; Yang, M. CO₂/N₂ mixture sequestration in depleted natural gas hydrate reservoirs. *J. Pet. Sci. Eng.* **2019**, 175, 72–82.
- 12. Bhawangirkar, D. R.; Sangwai, J. S. Insights into Cage Occupancies during Gas Exchange in CH4+CO2 and CH4+N2+CO2 Mixed Hydrate Systems Relevant for Methane Gas Recovery and Carbon Dioxide Sequestration in Hydrate Reservoirs: A Thermodynamic Approach. *Ind. Eng. Chem. Res.* **2019**, 58 (31), 14462–14475.
- 13. Zhang, Y.; Cui, M; Xin, G.; Li, D. Microscopic insights on the effects of flue gas components on CH4-CO2 replacement in natural gas hydrates. J. Nat. Gas Sci. **2023**, 112, 204947-204959.
- 14. Jacobson L. C., Hujo W., and Molinero V., Nucleation pathways of clathrate hydrates: Effect of guest size and solubility. *J. Phys. Chem. B* **2010**, 114, 13796–13807.
- 15. Jacobson, L. C.; Hujo, W. and Molinero, V. Amorphous precursors in the nucleation of clathrate hydrates. J. *Am. Chem. Soc.* **2010**, 132, 11806–11811.
- 16. Zhang Z.; Walsh M. R.; and Guo G. J. Microcanonical molecular simulations of methane hydrate nucleation and growth: Evidence that direct nucleation to sI hydrate is among the multiple nucleation pathways. *Phys. Chem. Chem. Phys.* **2015**, 17, 8870–8876.
- 17. Radhakrishnan, R. and Trout, B. L. A new approach for studying nucleation phenomena using molecular simulations: application to CO₂ hydrate clathrates. *J. Chem. Phys.*, **2002**, 117, 1786–1796.
- 18. He Z.; Linga P. and Jiang J. What are the key factors governing the nucleation of CO₂ hydrate? *Phys. Chem. Chem. Phys.* 2017, 19, 15657-15661.
- 19. Arjun A. and Bolhuis P. G. Molecular understanding of homogeneous nucleation of CO2 hydrates using Transition Path Sampling. *J. Phys. Chem. B* 2021, 125, 338-349.
- 20. Hu W.; Chen C.; Sun J.; Zhang N. Zhao J.; Liu Y.; Ling Z.; Li W.; Liu W. and Song Y. Three-body aggregation of guest molecules as a key step in methane hydrate nucleation and growth. *Commun. Chem.* **2022**, 5, 1-11.

- 21. He Z.; Gupta K. M.; Linga P.; and Jiang J. Molecular Insights into the Nucleation and Growth of CH4 and CO2 Mixed Hydrates from Microsecond Simulations. *J. Phys. Chem. C* **2016**, 120, 25225–25236.
- 22. Baig K.; Kvamme B.; Kuznetsova T. and Bauman J. Impact of Water Film Thickness on Kinetic Rate of Mixed Hydrate Formation During Injection of CO₂ into CH₄ Hydrate. *AIChE J.* **2015**, 61, 3944-3957.
- 23. Liu, J.; Yan, Y.; Liu, H.; Xu, J.; Zhang, J.; Chen, G. Understanding effect of structure and stability on transformation of CH4 hydrate to CO₂ hydrate. *Chem. Phys. Lett.* **2016**, 648, 75–80.
- 24. Tung, Yen-T.; Chen, Li-J.; Chen, Y-Ping.; Lin, S-T. In situ methane recovery and carbon dioxide sequestration in methane hydrates: A molecular dynamics simulation study. *J. Phys. Chem. B* **2011**, 115, 15295–15302.
- 25. Tung, Yen-T.; Chen, Li-J; Chen, Yan-P.; Lin, Shiang-T. The growth of structure I methane hydrate from molecular dynamics simulations. *J. Phys. Chem. B* **2010**, *114*, 10804–10813.
- 26. Bai, D.; Zhang, X.; Chen, G.; Wang, W. Replacement mechanism of methane hydrate with carbon dioxide from micro-second molecular dynamics simulations. *Energy Environ. Sci.* **2012**, 5 (5), 7033–7041.
- 27. Yoon, J.-H.; Kawamura, T.; Yamamoto, Y.; Komai, T. Transformation of Methane Hydrate to Carbon Dioxide Hydrate: In Situ Raman Spectroscopic Observations. J. Phys. Chem. A 2004, 108 (23), 5057–5059.
- 28. Qi, Y.; Ota, M.; Zhang, H. Molecular dynamics simulation of replacement of CH4 in hydrate with CO₂. Energy Convers. Manage. 2011, 52 (7), 2682–2687.
- 29. Circone, S.; Stern, L. A.; Kirby, S. H.; Durham, W. B.; Chakoumakos, B. C.; Rawn, C. J.; Rondinone, A. J.; Ishii, Y. CO₂ Hydrate: Synthesis, Composition, Structure, Dissociation Behavior, and a Comparison to Structure I CH4 Hydrate. *J. Phys. Chem. B* **2003**, 107, 5529-5539.
- 30. Moon, C.; Taylor, P. C.; Rodger, P. M. Molecular dynamics study of gas hydrate formation. *J. Am. Chem. Soc.* **2003**, 125, 4706-4707.
- 31. Plimpton, S. Fast parallel algorithms for short-Range Molecular Dynamics. *Soft Matter*, 1995, 14, 1–19.
- 32. Abascal, J. L. F.; Vega, C. A general purpose model for the condensed phases of water: TIP4P/2005. *J. Chem. Phys.* **2005**, 123, 234505.

- 33. Conde, M. M.; Vega, C. Determining the three-phase coexistence line in methane hydrates using computer simulations. *J. Chem. Phys.* **2010**, 133, 064507.
- 34. Liang S. and Kusalik P. G. Exploring nucleation of H₂S hydrates. *Chem. Sci.* 2011, 2,1286–1292.
- 35. Jorgensen W. L.; Maxwell D. S. and Tirado-Rives J. Development and testing of the OPLS all-atom force field on conformational energetics and properties of organic liquids. *J. Am. Chem. Soc.* **1996**, 118, 11225–11236.
- 36. Cygan R. T.; Romanov V. N.; and Myshakin E. M. Molecular simulation of carbon dioxide capture by montmorillonite using an accurate and flexible force field. *J. Phys. Chem. C* 2012, 116, 13079–13091.
- 37. Somasundaram T.; Panhuis M. in het; Lynden-Bell R. M. and Patterson C. H. A simulation study of the kinetics of passage of CO2 and N2 through the liquid/vapor interface of water. *J. Chem. Phys.* **1999**, 111, 2190–2199.
- ^{38.} Martín-Calvo A.; Lahoz-Martín F. D., and Calero S. Understanding carbon monoxide capture using metal-organic frameworks. J. *Phys. Chem. C* **2012**, 116, 6655–6663.
- ³⁹ Huang P. H. Molecular dynamics investigation of separation of hydrogen sulfide from acidic gas mixtures inside metal-doped graphite micropores. *Phys. Chem. Chem. Phys.* **2015**, 17, 22686–22698.
- 40. Walsh, M. R.; Koh, C. A.; Sloan, E. D.; Sum, A. K.; Wu, D. T. Microsecond simulations of spontaneous methane hydrate nucleation and growth. *Science*, **2009**, 326, 1095-1098.
- 41. Evans D. J. and Holian B. L. The Nose-Hoover Thermostat. *J. Chem. Phys.* **1985**, 83, 4069-4074.
- 42. Sarupria, S.; Debenedetti, P. G. Homogeneous nucleation of methane hydrate in microsecond molecular simulations. *J. Phys. Chem. Lett.* **2012**, 3, 2942–2947.
- 43. Matsui, H.; Jia, J.; Tsuji, T.; Liang, Y.; Masuda, Y. Microsecond simulation study on the replacement of methane inmethane hydrate by carbon dioxide, nitrogen, and carbon dioxidenitrogen mixtures. *Fuel*, **2020**, 263, 116640.
- 44. Sun, Y.-H.; Li, S.-L.; Zhang, G.-B.; Guo, W.; Zhu, Y.-H. Hydrate Phase Equilibrium of CH4+N2+CO2 Gas Mixtures and Cage Occupancy Behaviors. *Ind. Eng. Chem. Res.* **2017**, 56 (28), 8133–8142.
- 45. Tribell, G. A.; Bonomi, M.; Branduardi, D.; Camilloni, C. and Bussi, G. PLUMED2: New feathers of an old bird. *Comput. Phys. Commun.* **2014**, 185, 604.

- 46. Bussi, G. and Laio, A. Using metadynamics to explore complex free-energy landscapes. *Nat. Rev. Phys.* **2020**, 2, 200-212.
- 47. Trapl, D. and Spiwok, V. Analysis of the Results of Metadynamics Simulations by metadynminer and metadynminer3d. *R. Journal*, **2022**, 14, 46-58.
- 48. Mahmoudinobar, F. and Dias, C. L. GRADE: A code to determine clathrate hydrate structures. *Comput. Phys. Commun* **2019**, 244, 385-391.
- 49. Momma, K. and Izumi, F. VESTA 3 for three-dimensional visualization of crystal, volumetric and morphology data. *J. Appl. Crystallogr.* 2011, 44, 1272-1276.
- 50. Humphrey, W.; Dalke, A. and Schulten, K. VMD Visual Molecular Dynamics. *J. Mol. Graph.* **1996**, 14, 33-38.
- 51. Cladek, B. R.; Everett, S. M.; McDonnell, M. T.; Tucker, M. G.; Keffer, D. J.; Rawn, C. J. Guest–Host Interactions in Mixed CH4–CO2 Hydrates: Insights from Molecular Dynamics Simulations. *J. Phys. Chem. C* **2018**, 122, 19575-19583.
- 52. Kirchner, M. T.; Boese, R.; Billups, W. E.; Norman, L. R. Gas hydrate single-crystal structure analyses. *J. Am. Chem. Soc.* **2004**, 126, 9407-9412.

Chapter 3

Role of Monatomic Gases in CO₂-CH₄ Exchange in NGHs

Introduction

Natural Gas Hydrates (NGHs) are potential candidates with dual-purpose that could provide methane as clean energy and simultaneously sequestrate carbon dioxide 1-3. Conventional techniques like depressurization and steam technology have limited-scale applications due to potential hazards of geological catastrophes ⁴. Hence, several other alternatives have been proposed to extract methane from NGHs; adding chemical additives (hydrate promoters) to enhance methane extraction, replacement of CH₄ in NGHs with CO₂ by injecting CO₂ as gas or emulsion during extraction process ⁴⁻⁷. However, one of the major challenges in this process is the formation of CH₄-CO₂ mixed hydrates that reduces the rate of methane recovery ⁵. Recently, flue gases like N2 and H2S along-with CO2 have shown promising enhancement in CH₄-CO₂ exchange in NGHs ⁸⁻¹³. However, exchange of CH₄-CO₂ in NGHs is dependent on the concentration of flue gases; high concentration of N₂ can destabilize the hydrates and cage occupancy by CO₂ reduces at high concentration of H₂S and SO₂. The theoretical studies could provide microscopic insights into the factors that control hydrate growth unlike experiments that currently have spatiotemporal restrictions to explore nucleation mechanisms. The hydrate nucleation in homogeneous medium has been theoretically proposed to occur either through formation of labile water-gas clusters; amorphous water-gas aggregates; local ordering of gas

and water molecules due to thermal fluctuations ¹⁴⁻²⁰. On the other hand, hydrate nucleation in *heterogeneous medium* has been reported to occur either through the direct exchange of methane and carbon dioxide in hydrate cages or melting of methane cages due to the heat released from the exothermic formation of CO₂ hydrates ^{6, 21-22}.

Commercially, methane-carbon dioxide exchange process is a heterogeneous process and the formation of hydrate layer besides the interface slows down the recovery of methane, thus, multiphase recovery of methane has been proposed as an alternative to enhance the rate of methane extraction ^{5, 23-28}. Noble gas hydrates are known to exist at very high pressures and low temperatures as sII hydrates; thus, noble gases could be also be explored as potential gas candidates along-with CO₂ during MCE process ⁴⁵⁻⁴⁷. In this work, we explore the role of monatomic (noble) gases Ar, Kr and Xe) in the formation of first hydrate layer beside the interface in heterogeneous medium during MCE process and effect of these gases on CO₂ sequestration using molecular dynamics simulation techniques and DFT calculations and to the best of our knowledge no such comparison studies are reported till date.

Computational Details

We chose the following systems: *third gas systems* (G₃) with sI hydrate seed and mixture of CO_2 and G_3 (Ne/Ar/Kr/Xe) in bulk; where two concentrations of G_3 were studied: $CO_2(3)$: $G_3(1)$ (*low*) and $CO_2(2)$: $G_3(2)$ (*high*) except Xe (only low conc. system) ^{12,29}.

MODEL SYSTEM: The model system consisted of sI hydrate seed $(5x5x3 \text{ supercell})^{59}$ in the center of the simulation box with randomly placed supersaturated solution of gases in water (equivalent to $5 \times 5 \times 1.5$ of sI hydrate) on either side of the seed along the z-axis. The number

of water and gas molecules in each bulk region were taken equivalent to 5x5x1.5 of sI hydrate where 1720 water molecules and 300 gas molecules were randomly placed in each bulk region. The supersaturation in the bulk region was obtained by replacing 5 H₂O molecules with 5 gas molecules in bulk regions. The relaxed systems of $CO_2:G_3(3:1)$ systems were chosen as the initial configurations for $CO_2:G_3(2:2)$ systems where relevant number of CO_2 molecules were replaced by G_3 as reported in Table 3.1. Hereon, all third gas systems are referred as $G_3(3:1)$ for $CO_2(3):G_3(1)$ and $G_3(2:2)$ for $CO_2(2):G_3(2)$ as CO_2 is the common gas in all these systems.

SIMULATION DETAILS: All the molecular dynamics (MD) simulations were performed using LAMMPS package ³⁰ and all-atom forcefields were chosen for all the species; water (TIP4P-2005) ³²⁻³³, CH₄ and Ne (OPLS-AA) ³⁵, CO₂ ³⁶ and (Ar, Kr and Xe) ³⁷. A timestep of 1fs and three-dimensional periodic boundary conditions was chosen in all the systems. We chose cutoff distance of 12Å and 10Å for the van der Waals and electrostatic interactions. In G₃(3:1) systems, NVT simulations were performed for 2ns at 250K followed by 10ns of NVT simulations at 300K to generate a uniform interface between bulk phase and hydrate seed ^{24,29-30}. Finally, all the systems were simulated for 60ns (80ns for larger Ar(2.5:1.5) system) using NPT simulations at 250K and 15MPa (noble gases form clathrates at very high pressures and low temperature and CO₂ hydrate are stable in this T and P range) ^{18,29,37}. The relaxation times for Nose-Hoover thermostat and barostat were chosen as 0.06ps and 2ps respectively ³⁸.

ANALYSIS: The velocities were stored every 2fs for initial 1.5ns of NPT simulation run for the calculation of velocity autocorrelation function. The free energy calculations on MD data were performed in PLUMED2 (LAMMPS) using the configuration 1ns prior to formation of growth synthon as the initial configuration ⁴⁸⁻⁴⁹. The restraint metadynamics was employed by constraining the dihedral angle between the four gas species of the growth synthon (details in

Results and Discussions section) to 180° with a force constant between 50 kcal/mol to 200 kcal/mol in different systems. The width and height of Gaussians were chosen as 0.25kcal/mol and 0.50kcal/mol respectively. The Gaussians were deposited at every 100fs and data was analyzed using metadynminer package ⁵⁰. The last configuration of NPT simulation was used to calculate the total and CO₂ selectivities. The first hydrate layers (left and right side of interface) were chosen as 12Å along the z-axis from the interface (which is equivalent to unit cell dimension of sI hydrate). The cage analysis was done using GRADE code, where hydrogen bond distance between oxygens of hydrogen-bonded ordered water molecules in a cage is taken less than or equal to 3.0Å and guest is included in a cage if distance between center of mass of guest and center of cage in less than or equal to 2.0 Å and gases are assigned to small (5¹² type cages) or large (5¹²6² type cages) ⁵¹. All the snapshots were generated using VESTA or VMD software ⁵²⁻⁵³.

DFT Free Energy Calculations We performed two sets of zero-point corrected DFT free energies calculations in the gas phase; (i) *single cage* with a gas species in the center of a small or large sI hydrate cage (ii) *dual cages* with small-large or large-large cages of sI hydrate. All DFT calculations were performed as single-point energy calculations in Gaussian 09 package using B3LYP functional with cc-pVDZ basis set for all atoms except cc-pVDZ-pp basis set for Xe ⁴²⁻⁴⁴. There are imaginary frequencies in different systems as cages were not optimized which is expected as many of the gas species (noble gases, N_2 and CO) are reported to form sII hydrates at very high pressure and low temperatures ⁴⁵⁻⁴⁷. We did not observe cages of s-II hydrates in any system during MD simulations so DFT calculations were performed only with sI cages. The DFT free energy, ΔG in all the systems is calculated as ($\Delta G = G_{G+C} - G_G - G_C$) where G_{G+C} is the DFT zero-point corrected free energy of gas in a small or large (SC /

LC) or in large-large or small-large dual cages (LLDC or SLDC), G_G and G_C are the zero-point corrected free energy of gas and empty cage / cages respectively.

Table 3.1: Box dimensions and number of molecules/atoms in different systems where G_3 is the flue or noble gas, G_3 = H_2S , N_2 , CO, Ne, Ar, Kr and Xe; here $G_3(3:1)$ and $G_3(2:2)$ represent ($CO_2:G_3$) in ratios of (3:1) and (2:2) respectively.

Systems	Box Dimensions (ų)	N _{H2O}	N сн4	N _{CO2}	N _G 3
G ₃ (3:1) G ₃ (2:2) Ar(2.5:1.5)* Ar(2.35:1.65)	58.1 x 58.1 x 69.72	6890	600	458 306 382 358	152 304 228 252

^{*} Large system size for Ar(2.5:1.5) has box dimensions of 58.1 x 58.1 x 92.96 Å 3 ; where N_{H2O} = 5740, N_{CO2} = 632 and N_{Ar} = 378

Results and Discussions

Table 3.2: Number of methane molecules diffused in the bulk phase at end of NVT simulations at 300K due to melting of hydrate cages during the formation of interface.

System	N _{CH4}
Ne (3:1)	169
Ar(3:1)	171
Kr(3:1)	155
Xe(3:1)	128
Ne (1:1)	153
Ar(1:1)	154
Kr(1:1)	147
CO ₂ :Ar(2.35:1.65)	147
CO ₂ :Ar(2.5:1.5)	150
CO ₂ :Ar(2.5:1.5) (Large system)	158

We observed melting of hydrate seed layer besides the interface during NVT simulations at 300K with diffusion of $\geq 80\%$ methane molecules in third gas systems as reported in Table 3.2.

However, there was no further melting of the inner layers of the seed during the NPT simulations at 250K which is consistent with the earlier reports that the formation of hydrate layer besides the interface blocks the access to the inner hydrate layers though we observed diffusion of few gases into the hydrate seed in some (Ne, Ar and Kr) systems as shown in Figure 3.1 ²⁶⁻²⁸.

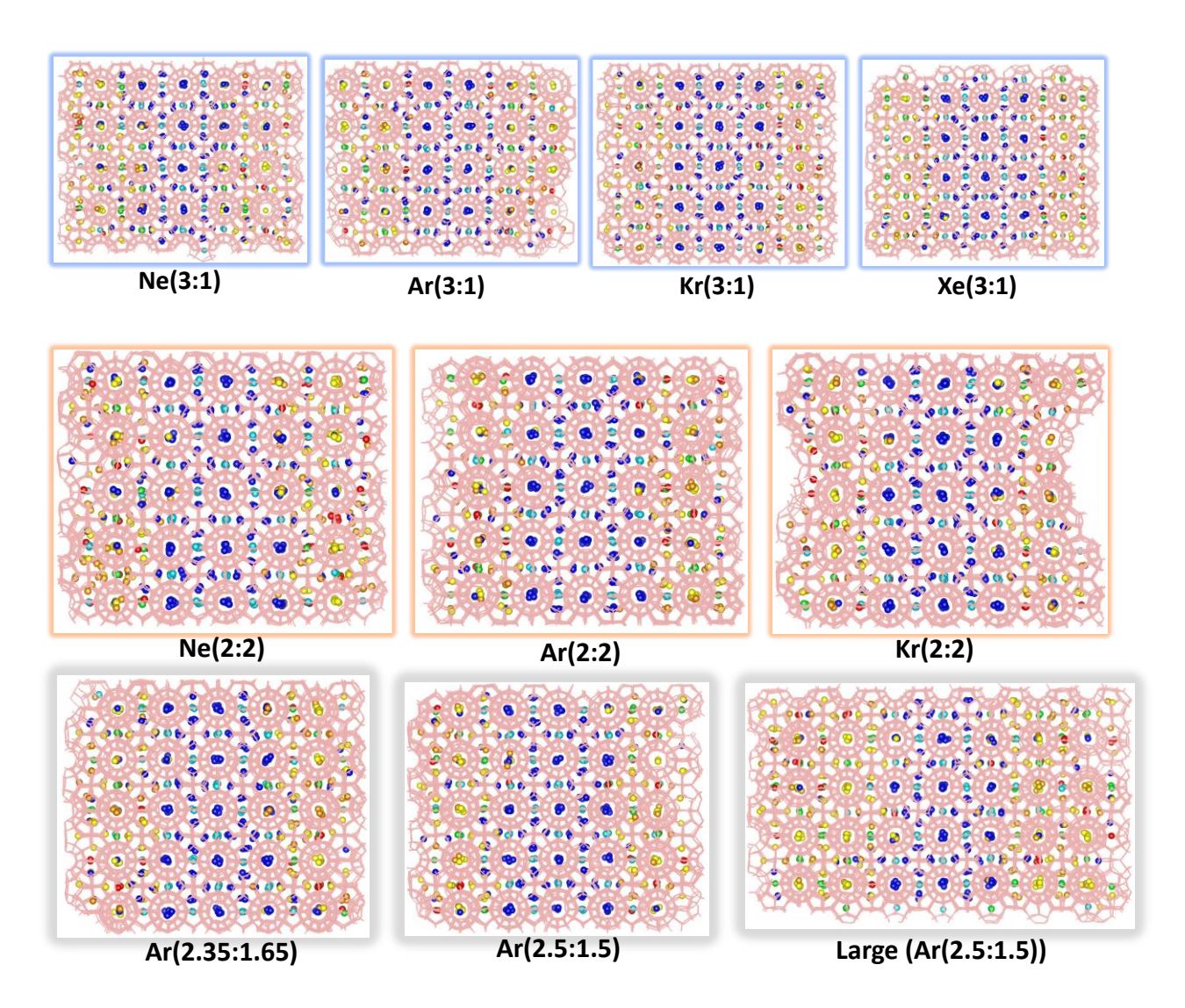


Figure 3.1: Snapshots of z-axis view of the trajectories of final configurations (60ns, NPT simulation) in different systems; the center of mass of all the gases are shown in the trajectories based on type of cage occupied; cyan (methane in SC), blue (methane in LC), green (carbon dioxide in SC), yellow (carbon dioxide in LC), red (H₂S in SC of pure H₂S system or third gas in SC in third gas systems) and orange (H₂S in LC of pure H₂S system or third gas in LC in third gas systems).

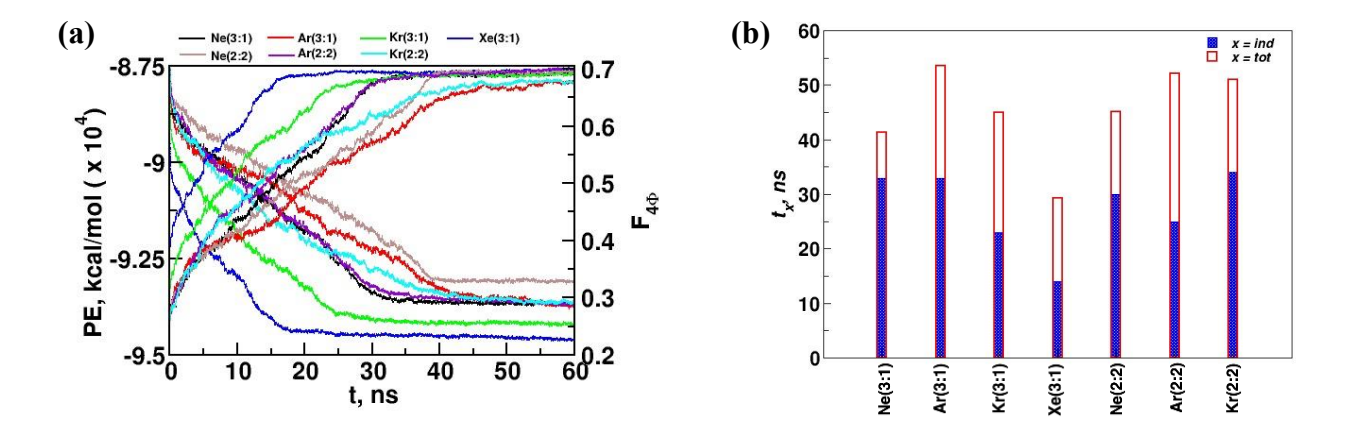


Figure 3.2: (a) Potential energy and F4 order parameter of full system as a function of time for systems with monatomic gases as third gas (Ne, Ar, Kr and Xe) at 250K and 15 MPa, where third gas systems have two conc. of CO_2 : $G_3(3:1)$ and CO_2 : $G_3(2:2)$ referred here as $G_3(3:1)$ and $G_3(2:2)$; (b) average induction time (t_{ind}) for the formation of first hydrate layer near interface (and) total time (t_{tot}) for hydrate growth in different systems. The observed trend for t_{ind} is $Xe(3:1) < Kr(3:1) \approx Ar(2:2) < Ne(3:1) < Ar(3:1) < Ne(2:2) < Kr (2:2)$ and trend for t_{tot} is $Xe(3:1) < Ne(3:1) \approx Ne(2:2) < Ar(3:1) < Ar(2:2) < Kr(2:2)$.

Figure 3.2a show the growth of hydrate in different systems as a time plot of potential energy (PE) and F4 order parameter (OP) ³⁷. F4 OP can quantitatively differentiate water in bulk water (-0.04), ice (0.4) and hydrate phase (0.70) and can be calculated as shown in Eq 3.1 ³⁷

$$F4 = \frac{1}{N} \sum_{i=1}^{N} \cos 3 \, \emptyset_i$$
 Eq (3.1)

where, \emptyset represents the torsion angle between two near-by oxygen atoms of water molecules within cutoff of 3.5Å and outermost hydrogen of both water molecules. There is a gradual decrease in PE and increase in F4 OP till former reached minimum and latter reached a value between 0.68-0.70 that indicated complete hydrate formation in all the systems within 60ns (80ns for L(Ar(2.5:1.5))system) and as expected hydrate growth in heterogeneous medium is faster than induction time for methane hydrate nucleation in homogeneous medium $(0.1 \mu s)^{15,39}$. Interestingly, though most of the flue and noble gases form s-II hydrates in pure forms but they form sI hydrates in the presence of sI hydrate seed $^{24,45-47}$. In general, heterogeneous nucleation could occur simultaneously from several nucleation sites, thus, we chose time for the formation

of first hydrate layers besides the interface as the induction time for hydrate growth. Figure 3.2b reports the average induction time (t_{ind}) and total time (t_{tot}) for hydrate formation in different systems. Among the monatomic gas systems, Xe(3:1) is the fastest $(t_{ind} = 14\text{ns})$ growing system and Ar(3:1) is the slowest growing system. These trends are also visible in slow change in slope of PE and OP for these systems in Figure 3.2a. Ar(2:2) showed short t_{ind} but longer t_{tot} and vice-versa was observed for Ne(2:2) system. The velocity autocorrelation function provides insights into the dynamics of particles with respect to their environment and is calculated as

$$C_v(t) = \frac{1}{N} \sum_{i=1}^{N} \frac{\langle v_i(t).v_i(0) \rangle}{\langle v_i(0).v_i(0) \rangle}$$
 Eq. (3.2)

where $v_i(0)$ and $v_i(t)$ are velocities of particle at time t = 0 and t as shown in Eq. 3.2. Figure 3.3 shows that VACF plot of a gas is independent of the concentration of gas in a system (3:1 or 2:2 system) and depends only on the type of gas species. Xe showed a larger cage effect, thus, expected lower diffusivity than CH₄ (Chapter 2) but first hydrate layer formation in Xe(3:1) system is similar to pure CH₄ system (Chapter 2). The noble gases like Ne and Ar are lighter gases but hydrate growth is slower in their systems than Xe systems. These anomalies are hard to answer based on diffusivity or size of the gas species.

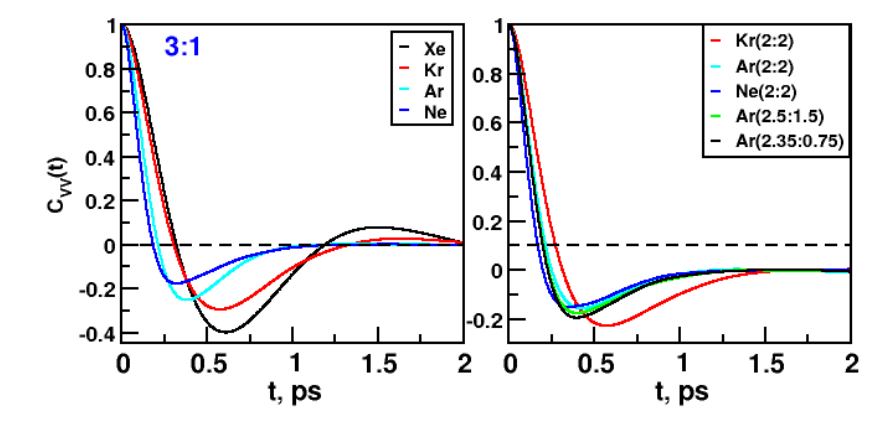


Figure 3.3: Velocity autocorrelation function (vacf) plots of systems with CO₂ and third gases (Xe, Kr, Ar and Ne) in 3:1 and 2:2 ratios and also shown are vacf for Ar(2.5:1.5) and Ar(2.35:0.75) systems.

Figure 3.4 shows the time plot of number of SCs and LCs formed by different gas species in a system during NPT simulations. The preferential occupation of a cage by a gas in a third gas systems is evident only after t > 10ns though it's observed at t > 1ns in Xe(3:1) system. Ne(d=3.08Å) is the smallest noble gas and forms unstable SCs in *low conc.* system but Ne dominates the LCs in *high conc.* system which is due to double occupancy of LCs by Ne as shown in Figure 3.5. The size of Xe (d=4.32Å) is similar to CH₄ but it dominates over CH₄ to occupy cages in Xe(3:1) system. On the other hand, Kr (d=4.04 Å) is smaller than CH₄ but it competes with CH₄ to occupy cages at *low conc.* and competes with both CO₂ and CH₄ to occupy cages at *high conc* similar to flue gas systems. Interestingly, Ar occupies the least number of cages at *low conc.* but dominates over CH₄ and competes with CO₂ to occupy cages at *high conc.* and size of Ar (3.76Å) is smaller than both CO₂ (5.12Å) and CH₄. Thus, the hydrate formation in heterogeneous medium could not be understood only on the basis of size of a gas.

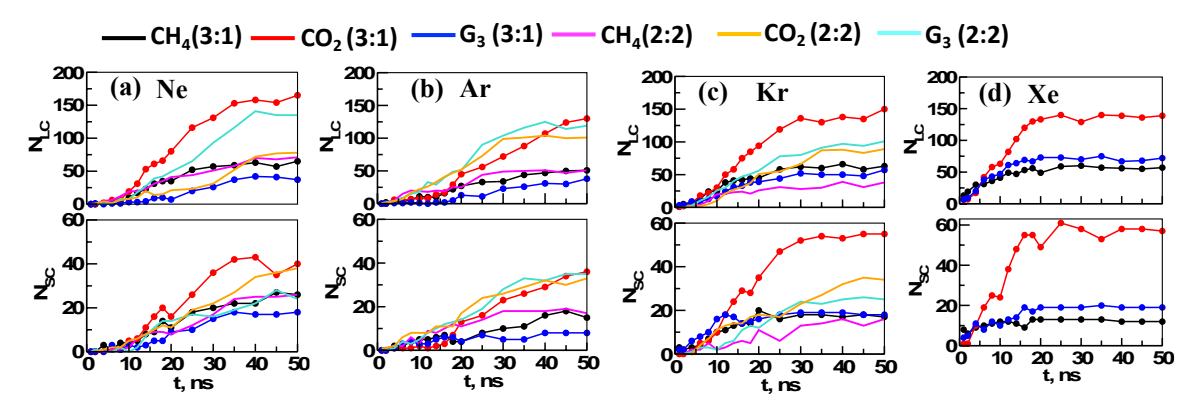


Figure 3.4: Number of gas species (methane, carbon dioxide and third gas) in small (N_{SC}) and large (N_{LC}) cages as a function of time during the simulation at 250K and 15MPa in third gas systems where third gas is ;(a) Ne, (b) Ar, (c) Kr and (d) Xe at low concentration CO_2 : $G_3(3:1)$ and high concentrations CO_2 : $G_3(2:2)$ referred here as $G_3(3:1)$ and $G_3(2:2)$ systems.

We elucidated the mechanism of hydrate formation based on the simulation trajectories during the total simulation time, t^* . There is formation of stable, dual cages occupied by particular gas

species that eventually leads to the formation of four-caged, Y-shaped growth synthon similar to polyatomic gas systems (Chapter 2) as shown in Figure 3.6. The growth synthon consists of one large-large dual cage (LLDC) and three small-large dual cages (SLDC) and leads to the growth of unit cell. The formation of GS in most of the systems occurs mainly *via* the four steps by formation of (i) a L cage initially (ii) LL dual cage (iii) LLS cluster and (iv) LLSL cluster.

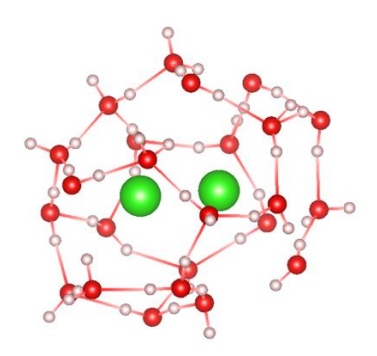


Figure 3.5: Snapshot of double occupancy of Ne atoms (green sphere) in large cage of hydrate (observed both in Ne(3:1) and Ne(2:2) systems).

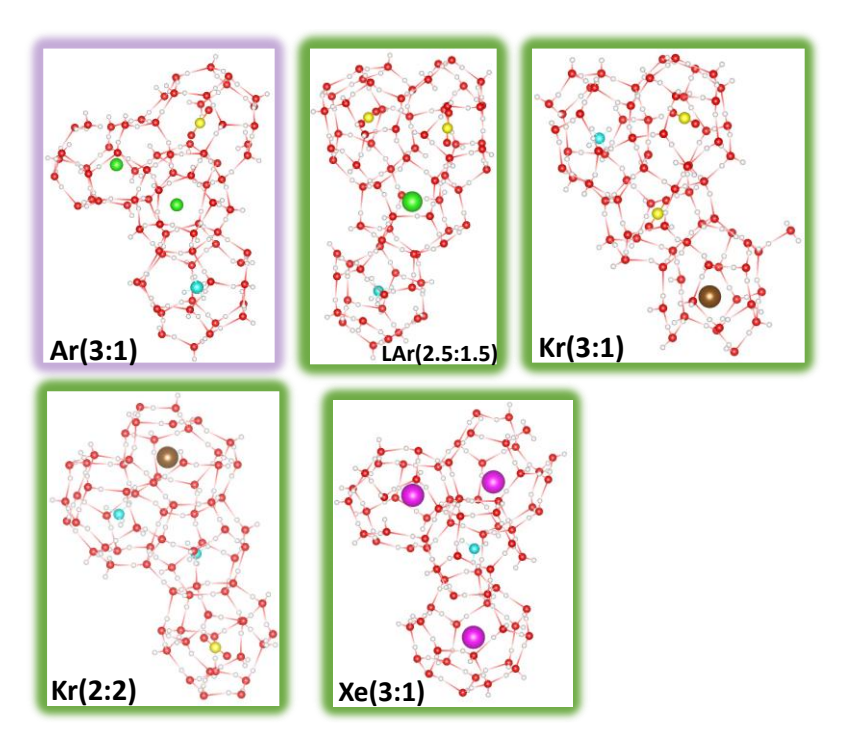


Figure 3.6: Snapshots of growth synthon in different systems. Here, green, yellow, cyan, brown, magenta, red and white spheres represent Ar, C(CO₂), C(CH₄), Kr, Xe, O and H atoms respectively and GS similar to bulk CO₂ (Chapter 2) was also observed in all the systems.

In a sI hydrate, SC and LC are formed by 20 and 24 water molecules respectively with an intermolecular distance of 6-8Å between the gas species ^{1,55}. The formation of GS was further quantified by calculating two coordination numbers; water-guest, N_{WG} (N_{GW} is 20 and 24 for SC and LC in a sI hydrate) and guest-guest, N_{GG} (N_{GG}=4 in a GS, where two gas species are within distance of 8Å) as a function of time (t^* where time from beginning of simulations (NVT, 250K) is considered) as shown in Figure 3.7. The cut-off distance between center of cage and center-of-mass of gas species was chosen as 5.8Å and 5.0Å for a gas to belong to a large and small cage respectively. We observed "memory effect" in Ar(2:2) system where four-atom Ar cluster was observed initially that dissociates and later these atoms occupy cages of the GS as reported in Figure 3.6a. Thus, thermal fluctuations lead to the formation of ordered cages though no amorphous cages or labile clusters that contribute to growth synthon are observed during heterogeneous nucleation of hydrates $^{15-20}$. In Ar(2:2) system, initially N_{GG} is 4 at $t^* =$ 12.3ns though only one LC is formed (N_{GW}=23) but Ar cluster breaks and N_{GG} decreases to 2 at $t^* = 13.2$ ns where two Ar atoms move away from the cluster and two of the Ar atoms form two LCs and eventually, GS with all the four cages and N_{GG} of 4 is formed at 22ns. Similar memory effect was observed in Kr(3:1) system where two gas species were within distance of 8Å at 12.2ns and later move away and there is formation of three-gas species cluster at 14.4ns as shown in Figure 3.6c. There is initial formation of dual large-large cage in all the systems during the formation of growth synthon as can be seen the value of N_{WG} for two of the cages is greater than 22 in the beginning of formation of growth synthon.

Figure 3.8 reports the free energy profiles for SLDC and LLDC as a function of both the collective variables (CV1; distance between the gases in SL dual cages and CV2; distance between the gases in LL dual cages of a growth synthon) in different systems. The FE minimum

is observed when CV1 and CV2 are between 6-8 Å which is consistent with the typical gas-gas intercage distance observed in a sI hydrate ⁵⁹. However, for Kr(2:2) system, minimum in FE was observed for CV1 around 10 Å which suggests that SL cages in this system are distorted unlike sI hydrate dual cages. We also estimated the stability of different gases in dual cages of sI hydrate by calculating the DFT free energy (ΔG_{DC} , kcal/mol) in dual cages of sI hydrates for different orientations of gas species (orientations chosen are reported in Figure 3.9) where we included both polyatomic (Chapter 2) and monatomic gases in the calculations. The DFT free energies in Figure 3.10a can be grouped into three regions; R-I that favours sI hydrate cages $(\Delta G_{DC} < 0)$, R-II with less favourable sI cages $(0 < \Delta G_{DC} < 5 \text{ kcal/mol})$ and R-III that does not favour sI cages ($\Delta G_{DC} > 5$ kcal/mol). The ΔG_{DC} of SLDC and LLDC of H₂S with H₂S, CH₄, CO₂ and LLDC of pure CH₄ belong to region R-I and thus, CH₄ and H₂S can form pure sI hydrates though H₂S is larger than CH₄, similarly H₂S can form sI hydrates with CH₄ and CO₂. In region R-II, the ΔG_{DC} of SLDC of pure CH₄ and LLDC of CH₄-CO₂ are similar and in region R-III ΔG_{DC} of LLDC CO₂-CO₂ is similar to SLDC of CH₄-CO₂. Thus, regions R-II and R-III favour mixed CH₄-CO₂ hydrates. The third gases (G₃) like Kr, N₂, CO and Ne also form G₃-G₃ dual cages or G₃-CH₄ and G₃-CO₂ dual cages in regions R-II and R-III, thus, these gases would reduce CO_2 sequestration over CH_4 ^{8,10}. There is a large difference in ΔG_{DC} of LLDC (*R-II*) and SLDC (*R-III*) for CO₂-CO₂ as SLDC of CO₂-CO₂ is energetically unfavourable ¹⁰. Thus, gases that show ΔG_{DC} of LLDC in region *R-III* could facilitate the formation of SLDC of CO₂-CO₂ and enhance CO₂ sequestration (Kr-CO₂, Ar-Ar and Ar-CO₂). The trends in free energies in present work (without bulk water) are in qualitative agreement with earlier reports of DFT calculations of N₂ where N₂ prefer SCs and N₂-CH₄ free energies are more favourable then N₂- CO_2 ¹⁰. If the difference between the ΔG_{DC} of SLDC and LLDC of pure (e.g. Xe-Xe and Ar-Ar) or mixed (e.g. LLDC of N2-N2 and SLDC of N2-CO2) gas combinations is small, these

gases could form GS though at low conc. if in region R-I/R-II or they could form cages at high conc. after the initial dual cage formation by gases in R-I and R-II.

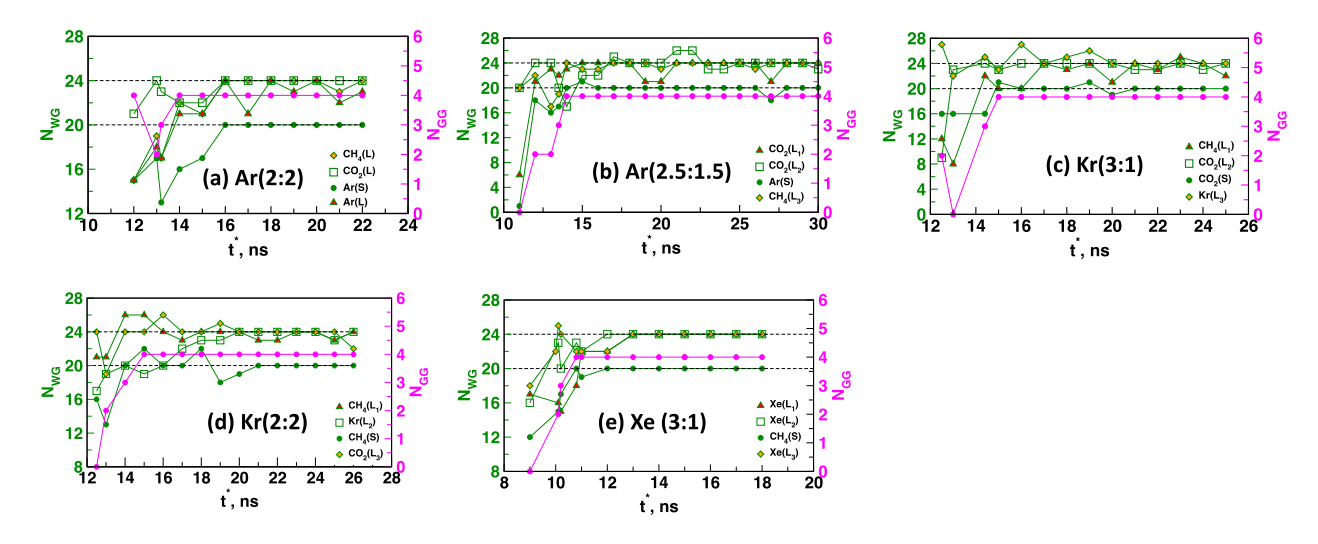


Figure 3.7: Number of water molecules ($N_{\rm GW}$) around a gas species in a growth synthon and number of gas species ($N_{\rm GG}$) in growth synthon within a distance of 8 Å as a function of t^* . Here t^* is considered from the beginning of simulation (2ns NVT at 250K (t^* =2ns) + 10ns NVT at 300K (t^* =12ns) and 60ns of NPT (t^* =72ns) at 250K and 15MPa).

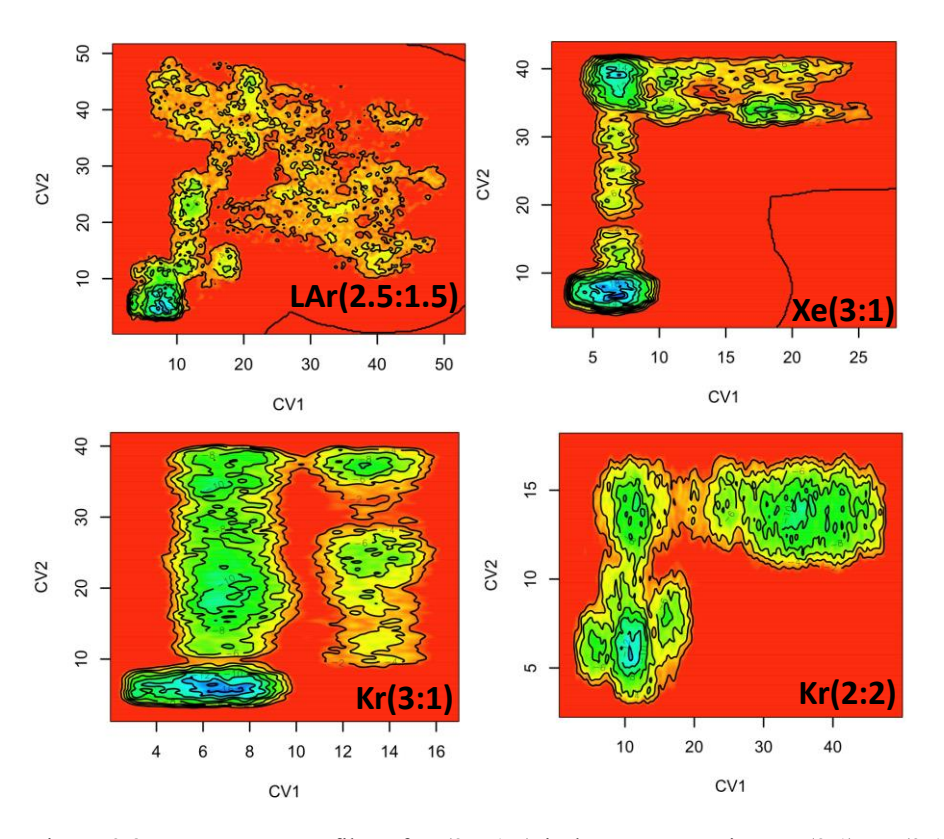


Figure 3.8: Free energy profiles of Ar(2.5:1.5) in large system size, Xe(3:1), Kr(3:1) and Kr(2:2) systems as a function of two collective variables; CV1 (distance between gases in SL dual cages) and CV2 (distance between gases in LL dual cages).

Selective sequestration of CO_2 over CH_4 in hydrate cages was assessed as selectivity (ΔS) for CO_2 over CH_4 in the first hydrate layer besides the interface as shown in Eq. 3.3 where N is the number of total cages occupied by a gas.

$$\Delta S = \frac{(N_{CO_2} - N_{CH_4})100}{N_{tot}}$$
 Eq. (3.3)

Figure 3.9b shows that $N_{CO_2} > 60\%$ in all the third gas systems as compared to 70% in bulk CO₂ system (Chapter 2) due to the presence of monatomic gases along-with CO₂ in bulk phase in these systems. The largest and the least number of CO₂ molecules encapsulated in the cages of first layers were observed in Ne(3:1) and Kr(2:2) systems respectively. There is gradual decrease in N_{CO_2} with increase in size of monatomic gas species and vice versa trend is observed for N_{G_3} . The number of methane molecules encapsulated in cages of first layer are low only for Ar based systems with high conc. of Ar (2.5:1.5, 2.35:1.65 and 2:2) and Kr(2:2) systems. As a result, CO₂ selectivity is better in Ar based systems with the highest selectivity in Ar(2.5:1.5) system. The number of SCs and LCs occupied by gases in Ar based systems can be compared in Figures 3.4b and 3.9(c-d) where CO₂ occupies maximum number of LCs in all the Ar systems except Ar(2:2) system where Ar occupies the maximum number of LCs. On the other hand, Ar occupancy in SCs in different systems increase as (3:1) < (2.5:1.5) < (2.35:1.65)< (2:2) as a results optimum CO₂ sequestration was observed in Ar(2.5:1.5) system. Further, we looked into system size effect for Ar(2.5:1.5) system by simulating double the simulation size system along z-axis and shows ΔS = 41.6% which is higher than original Ar(2.5:1.5) (ΔS = 30.6%) system and further studies are required to explore CO₂ selectivity as a function of system size.

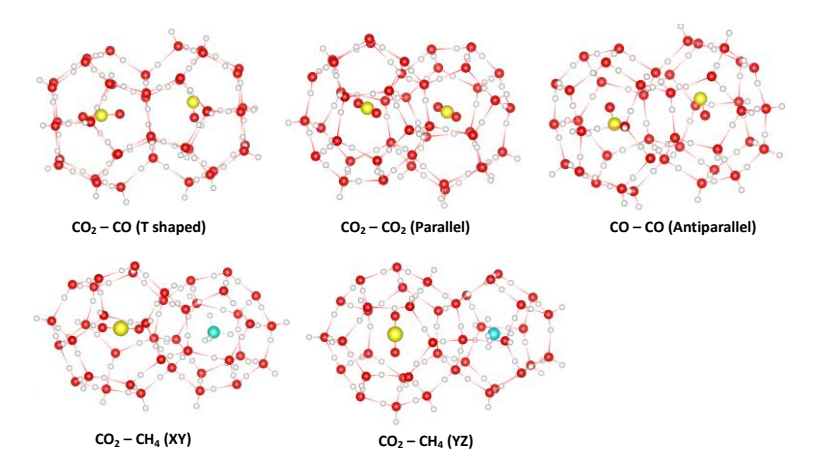


Figure 3.9: Different orientations chosen for gas species in dual cages for DFT free energy calculations.

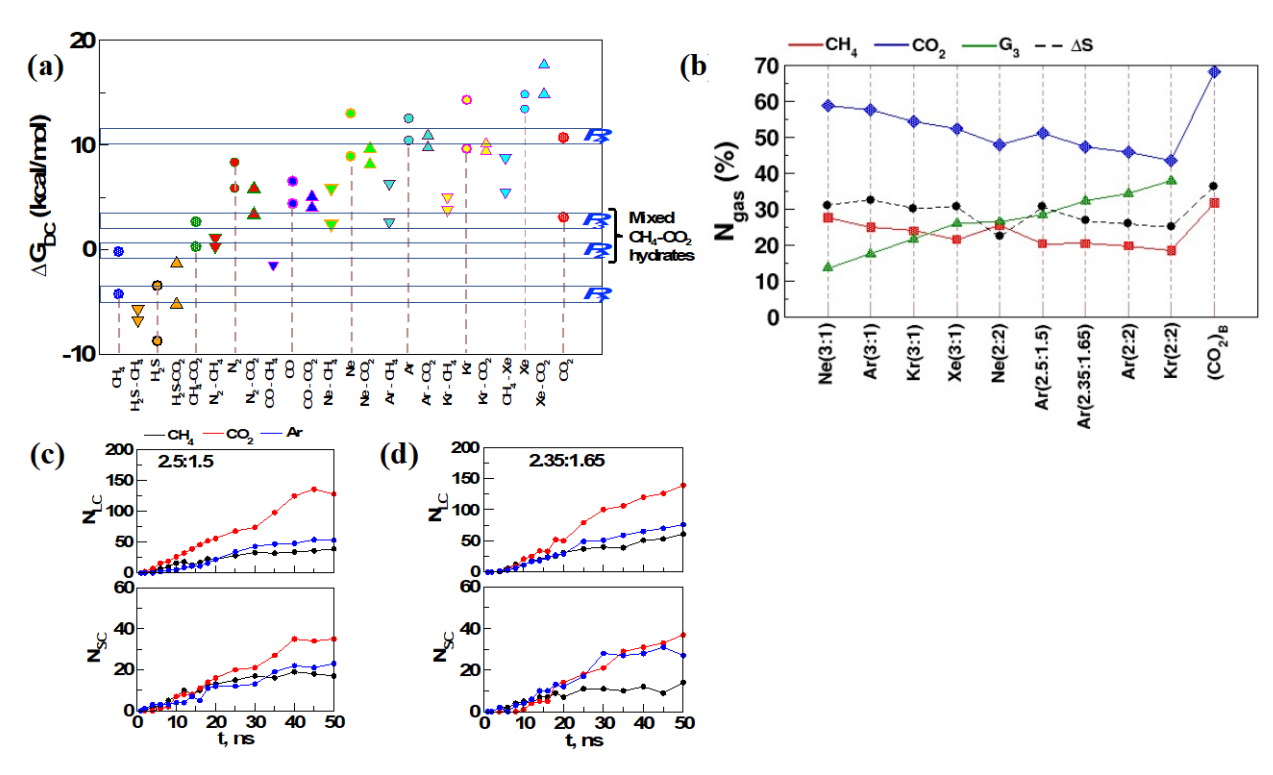


Figure 3.10: (a) Zero-point corrected DFT free energy (ΔG_{DC} , kcal/mol) for different combinations (gas-gas, gas-CH₄ and gas-CO₂ where gas can be CH₄, CO₂ or third gas (H₂S, N₂, CO, Ne, Ar, Kr and Xe) of gas species in LL and SL dual cages. The ΔG_{DC} of LL dual cages is lower than ΔG_{DC} in SL cages for all the gas combinations except for Ne-CO₂, Kr-CO₂ and Xe-CO₂ where ΔG_{DC} of SL favourable then ΔG_{DC} of LL cages (b) Percentage of different gases, N_{gas} (methane, carbon dioxide and third gas, G₃ – Ne, Ar, Kr and Xe) in the hydrate cages in different systems; also shown is selectivity (ΔS ,%) for CO₂ as difference in N_{CO2} and N_{CH4} and (c-d) number of gas molecules (methane, carbon dioxide and third gas) in small and large cages of Ar based systems for CO₂: Ar ratios of (2.5:1.5) and (2.35:1.65) where black symbols represent data for large system size, CO₂:Ar(2.5:1.5) system.

Conclusions

We have elucidated the factors that govern CH₄-CO₂ exchange in NGHs in the presence of monatomic gases by performing molecular dynamics simulations at 250K and 15MPa. The formation of sI hydrates in heterogeneous medium is governed by dual cages where LL and SL (L-large, S-small) cages lead to the formation of Y-shaped (LLSL) growth synthon similar to polyatomic gas systems. If a third gas (N₂, H₂S, CO, Ne, Kr and Xe) forms energetically favourable dual cages with both CH₄ and CO₂ then mixed CH₄-CO₂ hydrates are formed in the system that reduces CO₂ sequestration. However, if the conc. of third gas (N₂, H₂S, Ar, Kr and CO) is high and it forms favourable dual cages with itself and CO₂ then it competes with CO₂ to occupy the cages and reduces CO₂ sequestration. An ideal third gas candidate to enhance selective CO₂ sequestration is a gas species that (i) shows large difference in SLDC and LLDC with CH₄ (ii) forms SLDC and LLDC with less free energy difference with itself or CO₂ in a range similar to free energy of SL dual cages of CO₂. Argon meets conditions (i) and (ii), thus, shows good selective CO₂ sequestration at different concentrations and the highest CO₂ selectivity is observed for $CO_2(2.5)$:Ar(1.5) system. Most of the noble (monatomic in present study) gases form pure sII hydrates with large dissociation pressures but earlier reports of methane-carbon dioxide exchange with CO2 and N2 showed that N2 as a third gas forms sI hydrates with CO₂ and CH₄ with lower hydrate dissociation pressure ²⁴.

References

- 1. Sloan E. D. Jr Fundamental principles and applications of natural gas hydrates. *Nature* **2003**,426, 353-359.
- 2. Boswell R. and Collett T. S. Current perspectives on gas hydrate resources. *Energy Environ. Sci.* **2011**, 4, 1206–1215.

- 3. Sloan E. D. Jr Physical and chemical properties of gas hydrates and application to world margin stability and climatic change. Gas Hydrates: Relevance to World Margin Stability and Climate Change. Geological Society, London, Special Publications **2014**, 137, 31-50
- 4. Yang M.; Fu Z.; Zhao Y., Jiang L.; Zhao J. and Song Y. Effect of depressurization pressure on methane recovery from hydrate-gas-water bearing sediments," *Fuel* **2016**, 166, 419–426.
- 5. Wang, Y.; Lang, X.; Fan, S.; Wang, S.; Yu, C.; Li, G. Review on enhanced technology of natural gas hydrate recovery by carbon dioxide replacement. Energy&Fuels, **2021**, 46(5), 3659-3674.
- 6. Wu, G.; Tian, L.; Chen, D., Niu, M.; Ji, H. CO₂ and CH₄ Hydrates: Replacement or Cogrowth? *J. Phys. Chem. C* **2019**, 123, 13401–13409.
- 7. He, Z.; Gupta, K. M.; Linga, P.; Jiang, J. Molecular Insights into the Nucleation and Growth of CH₄ and CO₂ Mixed Hydrates from Microsecond Simulations. *J. Phys. Chem. C* **2016**, 120, 25225–25236.
- 8. Doman, P.; Alavi, S.; Woo, T. K. Free energies of carbon dioxide sequestration and methane recovery in clathrate hydrates. J. Chem. Phys. **2007**, 127, 124510-124518.
- 9. Park, Y.; Kim, Do-Y.; Lee, Jon-W.; Huh, D-Gee; Park, K-Pil; Lee, J.; Lee H. Sequestering carbon dioxide into complex structures of naturally occurring gas hydrates. *PNAS* **2006**, 103, 12690-12694.
- 10. Liu, J.; Yan, Y.; Xu, J.; Li, S.; Chen, G.; Zhang, J. Replacement micro-mechanism of CH4 hydrate by N₂/CO₂ mixture revealed by ab initio studies. *Comput. Mater. Sci.* **2016**, 123, 106-110.
- 11. Zhou, H.; Chen, B.; Wang, S.; Yang, M. CO₂/N₂ mixture sequestration in depleted natural gas hydrate reservoirs. *J. Pet. Sci. Eng.* **2019**, 175, 72–82.
- 12. Bhawangirkar, D. R.; Sangwai, J. S. Insights into Cage Occupancies during Gas Exchange in CH4+CO2 and CH4+N2+CO2 Mixed Hydrate Systems Relevant for Methane Gas Recovery and Carbon Dioxide Sequestration in Hydrate Reservoirs: A Thermodynamic Approach. *Ind. Eng. Chem. Res.* **2019**, 58 (31), 14462–14475.
- 13. Zhang, Y.; Cui, M; Xin, G.; Li, D. Microscopic insights on the effects of flue gas components on CH4-CO2 replacement in natural gas hydrates. J. Nat. Gas Sci. 2023, 112, 204947-204959.
- ¹⁴ Jacobson L. C., Hujo W., and Molinero V., Nucleation pathways of clathrate hydrates: Effect of guest size and solubility. *J. Phys. Chem. B* **2010**, 114, 13796–13807.

- 15. Jacobson, L. C.; Hujo, W. and Molinero, V. Amorphous precursors in the nucleation of clathrate hydrates. J. *Am. Chem. Soc.* **2010**, 132, 11806–11811.
- 16. Zhang Z.; Walsh M. R.; and Guo G. J. Microcanonical molecular simulations of methane hydrate nucleation and growth: Evidence that direct nucleation to sI hydrate is among the multiple nucleation pathways. *Phys. Chem. Chem. Phys.* **2015**, 17, 8870–8876.
- 17. Radhakrishnan, R. and Trout, B. L. A new approach for studying nucleation phenomena using molecular simulations: application to CO₂ hydrate clathrates. *J. Chem. Phys.*, **2002**, 117, 1786–1796.
- 18. He Z.; Linga P. and Jiang J. What are the key factors governing the nucleation of CO₂ hydrate? *Phys. Chem. Chem. Phys.* 2017, 19, 15657-15661.
- 19. Arjun A. and Bolhuis P. G. Molecular understanding of homogeneous nucleation of CO2 hydrates using Transition Path Sampling. *J. Phys. Chem. B* 2021, 125, 338-349.
- 20. Hu W.; Chen C.; Sun J.; Zhang N. Zhao J.; Liu Y.; Ling Z.; Li W.; Liu W. and Song Y. Three-body aggregation of guest molecules as a key step in methane hydrate nucleation and growth. *Commun. Chem.* **2022**, 5, 1-11.
- 21. He Z.; Gupta K. M.; Linga P.; and Jiang J. Molecular Insights into the Nucleation and Growth of CH4 and CO2 Mixed Hydrates from Microsecond Simulations. *J. Phys. Chem. C* **2016**, 120, 25225–25236.
- 22. Baig K.; Kvamme B.; Kuznetsova T. and Bauman J. Impact of Water Film Thickness on Kinetic Rate of Mixed Hydrate Formation During Injection of CO₂ into CH₄ Hydrate. *AIChE J.* **2015**, 61, 3944-3957.
- 23. Liu, J.; Yan, Y.; Liu, H.; Xu, J.; Zhang, J.; Chen, G. Understanding effect of structure and stability on transformation of CH₄ hydrate to CO₂ hydrate. *Chem. Phys. Lett.* **2016**, 648, 75–80.
- 24. Tung, Yen-T.; Chen, Li-J.; Chen, Y-Ping.; Lin, S-T. In situ methane recovery and carbon dioxide sequestration in methane hydrates: A molecular dynamics simulation study. *J. Phys. Chem. B* **2011**, 115, 15295–15302.
- 25. Tung, Yen-T.; Chen, Li-J; Chen, Yan-P.; Lin, Shiang-T. The growth of structure I methane hydrate from molecular dynamics simulations. *J. Phys. Chem. B* **2010**, *114*, 10804–10813.
- 26. Bai, D.; Zhang, X.; Chen, G.; Wang, W. Replacement mechanism of methane hydrate with carbon dioxide from micro-second molecular dynamics simulations. *Energy Environ. Sci.* **2012**, 5 (5), 7033–7041.

- 27. Yoon, J.-H.; Kawamura, T.; Yamamoto, Y.; Komai, T. Transformation of Methane Hydrate to Carbon Dioxide Hydrate: In Situ Raman Spectroscopic Observations. J. Phys. Chem. A **2004**, 108 (23), 5057–5059.
- 28. Qi, Y.; Ota, M.; Zhang, H. Molecular dynamics simulation of replacement of CH4 in hydrate with CO₂. Energy Convers. Manage. **2011**, 52 (7), 2682–2687.
- 29. Circone, S.; Stern, L. A.; Kirby, S. H.; Durham, W. B.; Chakoumakos, B. C.; Rawn, C. J.; Rondinone, A. J.; Ishii, Y. CO₂ Hydrate: Synthesis, Composition, Structure, Dissociation Behavior, and a Comparison to Structure I CH4 Hydrate. *J. Phys. Chem. B* 2003, 107, 5529-5539.
- 30. Moon, C.; Taylor, P. C.; Rodger, P. M. Molecular dynamics study of gas hydrate formation. *J. Am. Chem. Soc.* **2003**, 125, 4706-4707.
- 31. Plimpton, S. Fast parallel algorithms for short-Range Molecular Dynamics. *Soft Matter*, **1995**, 14, 1–19.
- 32. Abascal, J. L. F.; Vega, C. A general purpose model for the condensed phases of water: TIP4P/2005. *J. Chem. Phys.* **2005**, 123, 234505.
- 33. Conde, M. M.; Vega, C. Determining the three-phase coexistence line in methane hydrates using computer simulations. *J. Chem. Phys.* **2010**, 133, 064507.
- ³⁴· Jorgensen W. L.; Maxwell D. S. and Tirado-Rives J. Development and testing of the OPLS all-atom force field on conformational energetics and properties of organic liquids. *J. Am. Chem. Soc.* **1996**, 118, 11225–11236.
- 35. Cygan R. T.; Romanov V. N.; and Myshakin E. M. Molecular simulation of carbon dioxide capture by montmorillonite using an accurate and flexible force field. *J. Phys. Chem. C* 2012, 116, 13079–13091.
- 36. Yerlet L. and Weis J. J. Perturbation theory for the thermodynamic properties of simple liquids. *Mol. Phys.* **1972**, 24, 1013–1024.
- 37. Walsh, M. R.; Koh, C. A.; Sloan, E. D.; Sum, A. K.; Wu, D. T. Microsecond simulations of spontaneous methane hydrate nucleation and growth. *Science*, **2009**, 326, 1095-1098.
- 38. Evans D. J. and Holian B. L. The Nose-Hoover Thermostat. *J. Chem. Phys.* **1985**, 83, 4069-4074.
- 39. Sarupria, S.; Debenedetti, P. G. Homogeneous nucleation of methane hydrate in microsecond molecular simulations. *J. Phys. Chem. Lett.* **2012**, 3, 2942–2947.

- 40. Matsui, H.; Jia, J.; Tsuji, T.; Liang, Y.; Masuda, Y. Microsecond simulation study on the replacement of methane inmethane hydrate by carbon dioxide, nitrogen, and carbon dioxidenitrogen mixtures. *Fuel*, **2020**, 263, 116640.
- 41. Sun, Y.-H.; Li, S.-L.; Zhang, G.-B.; Guo, W.; Zhu, Y.-H. Hydrate Phase Equilibrium of CH₄+N₂+CO₂ Gas Mixtures and Cage Occupancy Behaviors. *Ind. Eng. Chem. Res.* **2017**, 56 (28), 8133–8142.
- 42. Gaussian 09, Frisch, M. J.; Trucks, G. W.; Schlegel, H. B.; Scuseria, G. E.; Robb, M. A.; Cheeseman, J. R.; Scalmani, G.; Barone, V.; Mennucci, B.; Petersson, G. A.; Nakatsuji, H.; Caricato, M.; Li, X.; Hratchian, H. P.; Izmaylov, A. F.; Bloino, J.; Zheng, G.; Sonnenberg, J. L.; Hada, M.; Ehara, M.; Toyota, K.; Fukuda, R.; Hasegawa, J.; Ishida, M.; Nakajima, T.; Honda, Y.; Kitao, O.; Nakai, H.; Vreven, T.; Montgomery, J. A., Jr.; Peralta, J. E.; Ogliaro, F.; Bearpark, M.; Heyd, J. J.; Brothers, E.; Kudin, K. N.; Staroverov, V. N.; Kobayashi, R.; Normand, J.; Raghavachari, K.; Rendell, A.; Burant, J. C.; Iyengar, S. S.; Tomasi, J.; Cossi, M.; Rega, N.; Millam, J. M.; Klene, M.; Knox, J. E.; Cross, J. B.; Bakken, V.; Adamo, C.; Jaramillo, J.; Gomperts, R.; Stratmann, R. E.; Yazyev, O.; Austin, A. J.; Cammi, R.; Pomelli, C.; Ochterski, J. W.; Martin, R. L.; Morokuma, K.; Zakrzewski, V. G.; Voth, G. A.; Salvador, P.; Dannenberg, J. J.; Dapprich, S.; Daniels, A. D.; Farkas, Ö.; Foresman, J. B.; Ortiz, J. V.; Cioslowski, J.; Fox, D. J. Gaussian, Inc., Wallingford CT, 2009.
- 43. Woon, D. E. and Dunning, Jr. Gaussian basis sets for use in correlated molecular calculations. V. Core-valence basis sets for boron through neon. *J. Chem. Phys.* **1995**, 103, 4572-4585.
- 44. Hill, J. G. and Peterson, K. A. Gaussian basis sets for use in correlated molecular calculations. XI. Pseudopotential-based and all-electron relativistic basis sets for alkali metal (K-Fr) and alkaline earth(Ca-Ra) elements. *J. Chem. Phys.* **2017**, 147, 244106.
- 45. Sugahara, K.; Sugahara, T. and Ohgaki, K. Thermodynamic and Raman Spectroscopic Studies of Xe and Kr Hydrates. *J. Chem. Eng.* **2005**, 50, 274-277.
- 46. Davidson, D. W.; Desando, M. A.; Gough, S. R.; Handa, Y. P.; Ratcliffe, C. I.; Ripmeester, J. A. and Tse, J. S. A clathrate hydrate of carbon monoxide. *Nature* **1987**, 328, 418-419.
- 47. Dyadin, Y. A.; Larionov, E. G.; Aladko, E. Ya.; Manakov, A. Yu.; Zhurko, F. V.; Mikina, T. V.; Komarov, V. Yu and Grachev, E. V. Clathrate formation in water-noble gas (Hydrogen) systems at high pressures. *J. Struct. Chem.* 1999, 40, 790-795.
- 48. Tribell, G. A.; Bonomi, M.; Branduardi, D.; Camilloni, C. and Bussi, G. PLUMED2: New feathers of an old bird. *Comput. Phys. Commun.* **2014**, 185, 604.

- 49. Bussi, G. and Laio, A. Using metadynamics to explore complex free-energy landscapes. *Nat. Rev. Phys.* **2020**, 2, 200-212.
- 50. Trapl, D. and Spiwok, V. Analysis of the Results of Metadynamics Simulations by metadynminer and metadynminer3d. *R. Journal*, **2022**, 14, 46-58.
- 51. Mahmoudinobar, F. and Dias, C. L. GRADE: A code to determine clathrate hydrate structures. *Comput. Phys. Commun.* **2019**, 244, 385-391.
- 52. Momma, K. and Izumi, F. VESTA 3 for three-dimensional visualization of crystal, volumetric and morphology data. *J. Appl. Crystallogr.* **2011**, 44, 1272-1276.
- 53. Humphrey, W.; Dalke, A. and Schulten, K. VMD Visual Molecular Dynamics. *J. Mol. Graph.* **1996**, 14, 33-38.
- 54. Cladek, B. R.; Everett, S. M.; McDonnell, M. T.; Tucker, M. G.; Keffer, D. J.; Rawn, C. J. Guest–Host Interactions in Mixed CH4–CO2 Hydrates: Insights from Molecular Dynamics Simulations. *J. Phys. Chem. C* **2018**, 122, 19575-19583.
- 55. Kirchner, M. T.; Boese, R.; Billups, W. E.; Norman, L. R. Gas hydrate single-crystal structure analyses. *J. Am. Chem. Soc.* **2004**, 126, 9407-9412.

Chapter 4

Role of Flue Gases and Noble Gases in CO₂-CH₄ exchange in NGHs

Introduction

Recovery of methane from natural gas hydrates is one of the promising approaches for clean energy to meet the growing demands for energy all over the world. Natural gas hydrates (NGHs) are non-stochiometric crystalline compounds with non-polar gas molecules entrapped inside the hydrogen-bonded water cages and are formed at low temperature and high pressures under sea sediments and in permafrost regions¹⁻³. The sI hydrate is the most abundant NGHs with methane entrapped in its small and large cages as compared to sII and sH hydrates ⁴. The sI hydrates are considered as the potential future clean energy resource with dual-purpose as methane can be recovered during melting of NGHs cages and simultaneously carbon dioxide can be trapped in the newly formed NGHs ². Currently, methane is extracted from NGHs through traditional approaches like heat injection and depressurization at a limited scale to avoid any natural geo-catastrophe or excessive release of methane as greenhouse gas due to large-scale melting of NGHs ⁵⁻⁷. The enthalpy for formation of methane hydrates and carbon dioxide hydrates is very similar as a result large scale exchange of methane with carbon dioxide has practical limitations due to the formation of energetically favourable mixed hydrates of methane and carbon dioxide at the interface of sI hydrates and bulk liquid water. Hence, currently different approaches are being explored at laboratory scale to enhance methanecarbon dioxide exchange in NGHs such as use of hydrate promoters or injection of flue gases along-with CO₂ during extraction of methane from NGHs ^{8-9,13}. Nitrogen is explored mainly as a flue gas along-with carbon dioxide during CH₄-CO₂ exchange in NGHs in swap process where N₂ replaces CH₄ in small cages and CO₂ occupies the large cages of sI hydrates ¹³⁻²⁴. However, there is decrease in sequestration of CO₂ with increase in the concentration of N₂ and maximum methane recovery was obtained with 30-40% of CO₂ in CO₂/N₂ mixture ²⁴. Other

flue gases like SO₂, H₂S, N₂ and NO are also reported along-with CO₂ to enhance CH₄-CO₂ exchange in NGHs but the results show reduction in uptake of CO2 with increase in the concentration of these flue gases ¹⁷. Hydrogen sulfide has been theoretically reported as one of the gases that shows faster rate of hydrate formation than the natural sI-NGHs with methane as the inclusion gas ⁴⁵. The theoretical studies could provide detailed insights into mechanism of hydrate growth as current state of the art of experiments is beyond the spatiotemporal limits of nucleation in hydrates. There are several mechanisms reported for the formation of pure gas hydrates in homogeneous medium; formation of labile clusters of methane and water that leads to cages and nucleation in hydrates, thermal fluctuations leading to formation of ordered cages of water with gas entrapped in them, formation of three-atom gas aggregate and formation of CO₂ amorphous cages (4¹⁰5¹²6²) along-with high concentration of CO₂ molecules around these cages ²⁵⁻³¹. The mechanism of CH₄-CO₂ exchange is currently understood as either a direct exchange of methane and carbon dioxide through hydrate cages or melting of methane cages due to heat released from formation of carbon dioxide cages in sI hydrates ^{10, 32-33}. The atomic level insights into the role of flue gases during CH₄-CO₂ exchange in NGHs in heterogeneous medium is currently reported mainly with N_2 as the flue gas 17,22,24 .

Gas hydrates of noble gases (Ar, Kr and Xe) are known to exist at very high pressure (1.5GPa) and low temperatures and thus, noble gases could be one of the potential third gases like flue gases that could be employed to enhance CH₄-CO₂ in NGHs ⁶³⁻⁶⁶. There are no reports of hydrates of He and Ne which could be due to labile nature of these gases due to very small size (< 3.5Å) as compared to size of the hydrate cages ⁶⁶. One of the challenges during CH₄-CO₂ exchange is the formation of first hydrate layer at the interface that blocks the access to inner layers of hydrate during heterogeneous nucleation ³⁴⁻³⁹. Thus, multiphase recovery of methane has been proposed as one of the alternatives to enhance CH₄-CO₂ exchange in NGHs ². Some of the key challenges in this direction are how to enhance methane release and carbon dioxide sequestration in the first hydrate layer that forms at the interface; what is the role of flue and noble gases during formation of hydrate layer interface and how to select third gas species that could enhance CO₂ sequestration during CH₄-CO₂ exchange in sI-NGHs. In this work, we explore the role of mixture of flue gases (H₂S and N₂) and noble gases (Ne, Ar, Kr and Xe) in the formation of first hydrate layer at the interface during CH₄-CO₂ exchange in sI-NGHs and to our best knowledge there are no such studies reported till date. We report an atomic level insight into factors that control CO₂ sequestration in sI-NGHs in presence of flue and noble gases using molecular dynamics simulation techniques and DFT calculations.

Computational Details

Model Systems We simulated following systems; (i) H₂S based (HG) systems that consisted of four systems where H_2S was chosen as third gas, G_3 and noble gas as fourth gas ($G_4 = Ne$) Ar / Kr / Xe) with ratio of 2:1:1 for CO₂: G₃: G₄ (ii) Kr based (KG) systems that had Kr as third gas and Ar as fourth gas and two systems with ratios of CO₂:G₃:G₄ as 2:1.25:0.75 and 2:0.5:1.5 (iii) a N₂ based system (NG) that had N₂ as G₃ and Ar as G₄ with ratio of 2:1:1 for CO₂:G₃:G₄. The initial configuration for HG systems consisted of a sI hydrate seed (simulation cell of 5x5x3)⁴⁰ in the centre of simulation box and other molecules (H₂O, CO₂, H₂S and a noble gas (Ne / Ar / Kr / Xe) were randomly placed in a ratio of 2:1:1 on either sides of the hydrate seed (equivalent to number of molecules in 5x5x1.5 simulation cell of a sI hydrate) as reported in Table 4.1. All the four systems were simulated in NVT ensemble for 2ns at 250K followed NVT simulations for 10ns at 300K. We generated interface in KG and NG systems similar to HG systems, thus, a system with CO₂ and H₂S in ratio of 3:1 in bulk phases on either sides of a sI hydrate seed (5x5x3) was simulated to generate initial configuration for KG and NG systems. This configuration was simulated in NVT ensemble for 2ns at 250K followed NVT simulations for 10ns at 300K. The final configuration was used to replace the required number of CO₂ and H₂S molecules in bulk phases with the desired ratios of CO₂, third and fourth gases in KG and NG systems respectively as shown in Table 4.1. These systems were further equilibrated for 0.5ns at 250K in NVT ensemble to relax the systems. We also simulated a bulk CO₂ system, (CO₂)_B with only CO₂ in bulk phase and sI hydrate as seed in the centre of box to calculate CO₂ selectivity in absence of flue and noble gases. Hereon, all the systems are referred in terms of ratio of G₃ and G₄ gases as CO₂ is the common gas in all the systems (for e.g. CO₂:N₂:Ar(2:1:1) will be referred as N₂:Ar).

Simulation details All the systems were modelled using all-atom forcefields; water molecules were modelled using TIP4P/2005 forcefield ⁴²⁻⁴⁴; methane and neon were modelled using OPLS-AA forcefield ⁴⁶; forcefield parameters for CO₂ were taken from Cygan *et. al.*⁴⁷, N₂ parameters from Somasundaram *et. al.* ⁴⁸, H₂S parameters from Pie-Hsing Huang and forcefield parameters Ar, Kr and Xe were taken from Loup and Jean ⁴⁹⁻⁵⁰. The Lorentz-Berthelot mixing rule was used to calculate the interaction parameters for cross-interaction terms. All the simulations were performed in LAMMPS package with a simulation timestep of 1fs and Noose-Hoover thermostat and barostat with relaxation times of 0.06ps and 2ps were employed for NVT and NPT simulations ⁵¹⁻⁵². The cut-off distances for van der Waals and electrostatic

interactions were chosen as 12\AA and 10\AA respectively . The periodic boundary conditions were applied in all the directions. All the configurations of different systems were simulated using NPT ensemble for 60ns at 250K and 15MPa^{41} . The data for analysis was stored at every 1ps during the simulation. All the snapshots were generated using VESTA or VMD $^{53-54}$.

CAGE ANALYSIS - GRADE code was used to perform cage analysis where criteria for a cage is that water molecules belong to a cage if cut-off distance is equal to or less than 3.5 Å and distance between guest and centre of mass of the cage is less than 2 Å ⁵⁵. We only considered filled cages for the analysis.

FREE ENERGY(FE) ANALYSIS - The free energy calculations were performed by constraining the dihedral angle between the gas species of a growth synthon to 180° with force constant of 50 kcal/mol using restraint metadynamics with PLUMED2 plugin in LAMMPS free energy data was analysed using METADYNMINER package ⁵⁶⁻⁵⁸. The initial configuration for FE calculations was chosen as configuration 1ns *a prior* to the formation of growth synthon. The width and height of Gaussians were chosen as 0.25 kcal/mol and 0.50kcal/mol respectively and the Gaussians were deposited every 100fs.

Table 4.1: Number of different species and box dimensions in different systems where box dimension in the all systems is $58.1 \times 58.1 \times 69.72 \text{ Å}^3$; half of each of N_{G3} , N_{G4} and N_{CO2} molecules are present in the bulk phases on either side of the seed along z-axis of simulation box. Here seed is sI hydrate.

System	N _{H2O} (Seed+ Bulk)	N CH4	Nco2	$N_{G3} + N_{G4}$
$CO_2:G_3:G_4$ (2:1:1) $G_3=H_2S$; $G_4=Ne$, Ar, Kr and Xe $G_3=N_2$; $G_4=Ar$	3450 + 3440	600	306	152+152
CO ₂ :Kr:Ar (2:1.25:0.75) CO ₂ :Kr:Ar (2:0.5:1.5)			306 306	190+114 76+228
Bulk CO ₂			610	-

Results and Discussions

Interface formation between the bulk phase and hydrate seed occurred during the NVT simulations at 300K in all the systems. Figure 4.1a shows the number of methane molecules

that diffused into the bulk phase due to the melting of hydrate seed layer during the formation of interface. We observed that the maximum number of methane molecules (84%) melted from hydrate seed layer (N_{CH4} = 200, one layer of hydrate seed) in bulk CO₂ system whereas number of diffused methane molecules (< 74%) reduced in presence of third and fourth gases in bulk phase. However, melting of seed is slower in HG systems with Ar, Kr and Xe as noble gases as only 63-67% of CH₄ molecules diffused from the hydrate seed into the bulk phase unlike H₂S:Ne, N₂:Ar and KG systems that have (68-74)% of methane molecules in bulk phase. There was no further melting of inner layers of hydrate seed which is consistent with the earlier reports that only outer layers of hydrate seed melt and further access to the inner layers is blocked due to the formation of hydrate layer near the interface in heterogeneous medium ³⁷-³⁹. The growth of a hydrate can be quantitatively analysed based on order parameters that can differentiate between the water molecules in liquid and hydrate phase. F4 order parameter (OP) can quantitatively differentiate between the water molecules that belong to hydrate, liquid and ice phases as F4 OP value are 0.7, -0.04 and 0.4 in these phases. F4 OP is calculated as an average of $cos(3\emptyset_i)$ over all the water molecules (N) in a system where \emptyset_i is the torsion angle between the farthest hydrogen atoms of two water molecules that are within a distance of 3.5Å as shown in Eq. 4.1^{59} .

$$F4 = \frac{1}{N} \sum_{i=1}^{N} \cos 3 \phi_i$$
 Eq. (4.1)

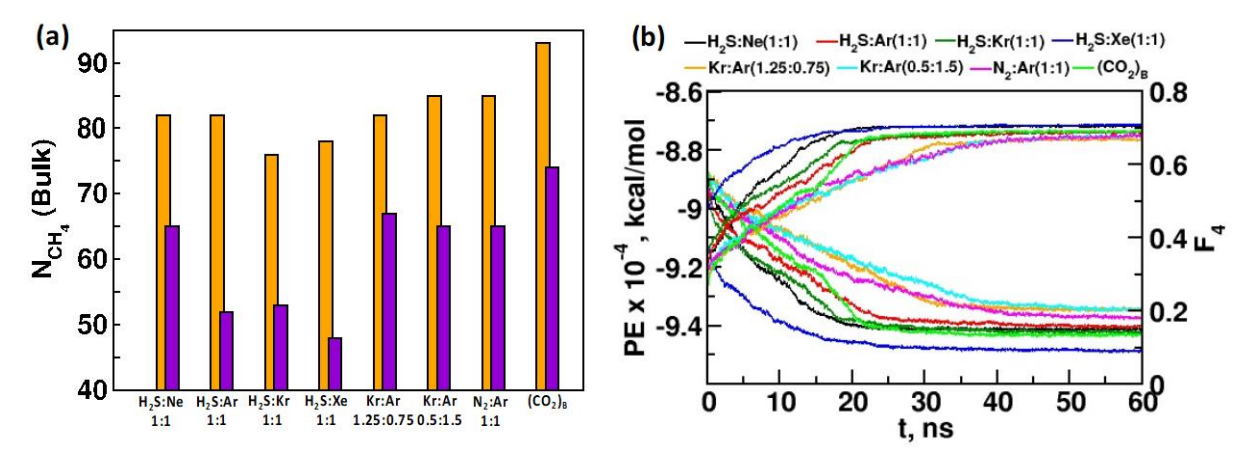


Figure 4.1: (a) Number of methane molecules on left (orange) and right(purple) sides of interface in the bulk phase and (b) potential energy (kcal/mol) and F4 order parameter as a function of time in different systems; H₂S:Ne, H₂S:Ar, H₂S:Kr, H₂S:Kr, H₂S:Xe, Kr(1.25):Ar(0.75), Kr(0.50):Ar(1.50), N₂:Ar and bulk CO₂; (CO₂)_B.

Similarly, change in potential energy of the system can be used to estimate the hydrate growth as the nucleation of gas hydrates in heterogeneous medium can be simulated using brute-force molecular dynamics simulation techniques 59 . Figure 4.1b shows the change in potential energy and F4 OP as a function of time for different systems. The change in potential energy and F4 OP is steep in HG systems and is the slowest for KG systems. The HG systems with different noble gases show trend of decrease in PE and increase in F4 OP as $Xe > Ne \approx Kr > Ar$.

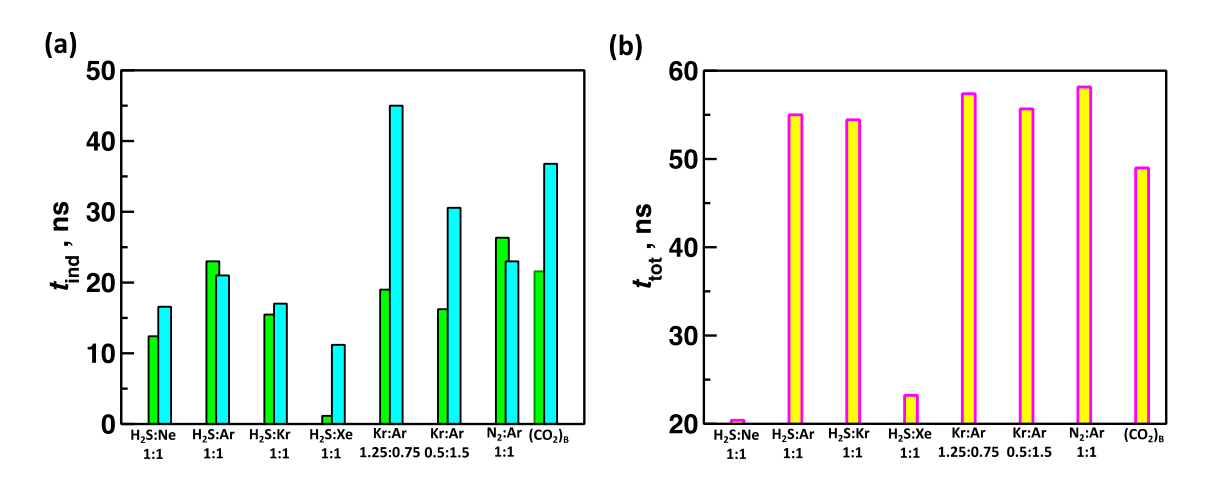


Figure 4.2: (a) Induction time, t_{ind} (ns) for the formation of first layers on left (green) and right (cyan) sides of interface and (b) total time, t_{tot} (ns) for the formation of hydrate in the bulk phase in different systems.

Heterogeneous nucleation could simultaneously initiate from several nucleation sites, thus, we chose formation of first layer besides the interface (along z-axis, 12Å from the interface on either side) as the induction time for the hydrate growth in all the systems. Figure 4.2a shows the induction time (t_{ind}) for first layers on left and right sides of the hydrate seed when value of F4 OP reaches 0.70. The induction time is minimum in H₂S:Xe among all the systems followed by H₂S:Ne and H₂S:Kr systems. The KG and NG systems show the largest induction time and these trends are consistent with the observed trends in change in potential energy and F4 OP in these systems. However, the induction time for the formation of first layer is lower in all the systems with third and fourth gases than bulk CO₂ system with the exception of Kr(1.25):Ar(0.5) system. Among all the systems, we observed only one 6^45^{12} cage in H₂S:Kr system else 5^{12} and 6^25^{12} cages were observed in all systems that suggest that only sI type hydrates were formed in all the systems. Interestingly, time for complete hydrate growth (t_{tot}) in the simulation cell show different trends then t_{ind} in different systems as shown in Figure 4.2b. The hydrate growth completion is the fastest in H₂S:Ne (t_{tot} =21ns) system followed by

 $H_2S:Xe$ (23ns) which is reverse of t_{ind} in these systems. Furthermore, all other systems show slower completion of hydrate growth with $t_{tot} > 55$ ns.

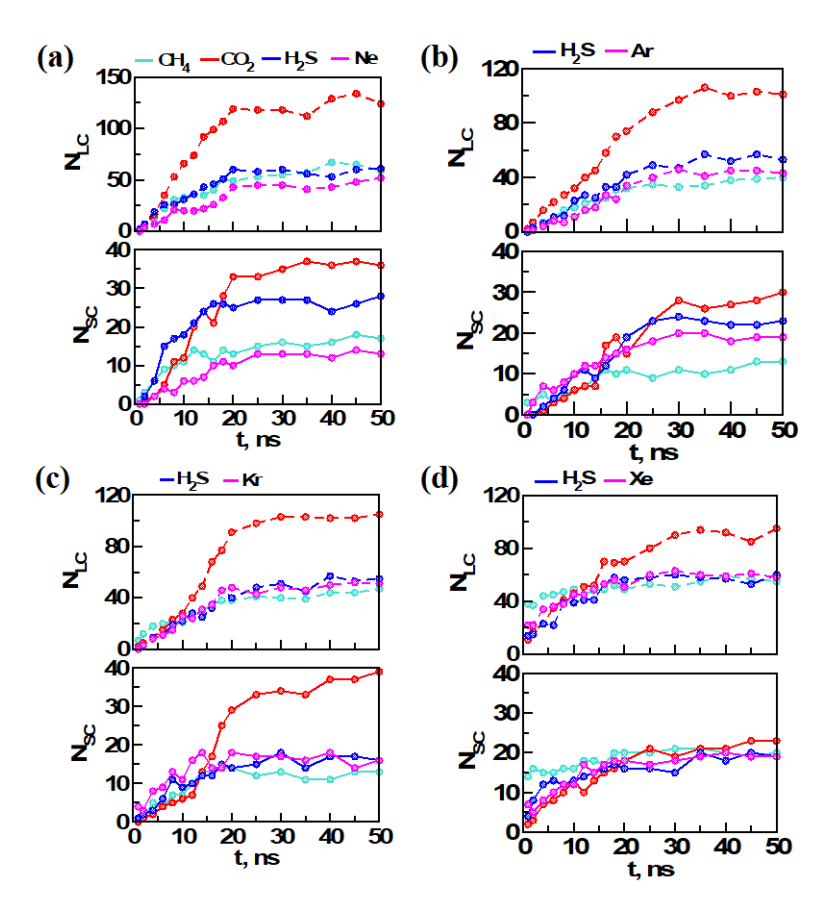


Figure 4.3: (a-d) Time plot of number of small (SC; full line) and large (LC; broken line) cages in HG systems with H_2S as third gas (a) H_2S :Ne, (b) H_2S :Ar, (c) H_2S :Kr and (d) H_2S :Xe.

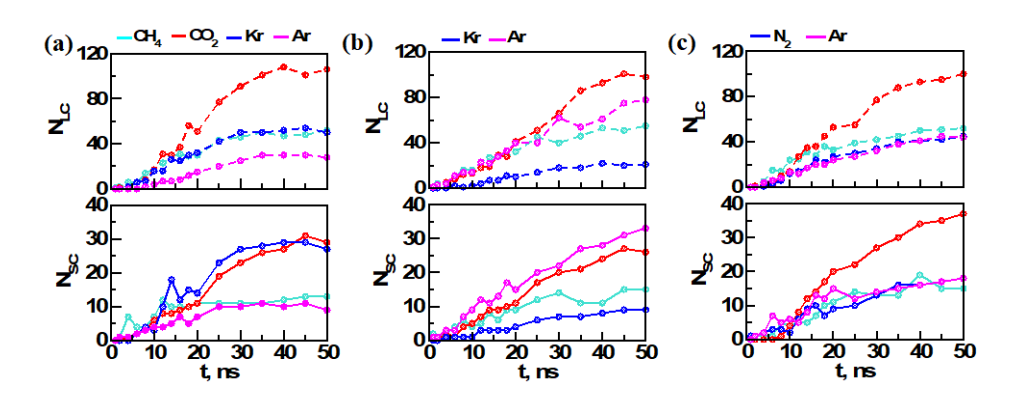


Figure 4.4: (a-c) Time plot of number of small (SC; full line) and large (LC; broken line) cages in KG systems (a) Kr(1.25):Ar(0.75) and (b) Kr(0.50):Ar(1.50); NG system (c) N_2 :Ar system.

Naturally occurring sI hydrates have two small (5^{12}) and six large (6^25^{12}) cages per unit cell. Figures 4.3 and 4.4 report the number of small and large cages (SC and LC) occupied by different gas species as a function of time in different systems. Carbon dioxide molecules occupy maximum number of LC in all the systems which is in agreement with the earlier reports that CO₂ prefers LC of sI hydrates during CH₄-CO₂ exchange ¹⁰⁻¹¹. Interestingly, we observed that after 20ns, CO₂ dominates SC in all the systems (with exception of H₂S:Xe and Kr(1.25):Ar(0.75) systems) which is contrary to the earlier reports that CO₂ prefers only LC in sI hydrates ^{34,37}. Among all the systems, CH₄ occupies minimum number of cages in H₂S:Ar system where the inclusion of different gases in cages of H₂S:Ar system follows the order as CO₂ > H₂S > Ar > CH₄. However, CH₄ inclusion in hydrate cages is different in other Ar-based systems (KG and NG systems) where the other gas is either Kr or N₂ respectively. Thus, both H₂S and Ar could potentially be the right candidates for better extraction of CH₄ during CH₄-CO₂ exchange in sI-NGHs. A small decrease in number of included CH₄ molecules in cages was also observed in H₂S:Kr system. Figure 4.4c shows that in N₂:Ar system, CH₄ competes with N2 and Ar to occupy both SC and LC. Interestingly, in KG systems, both Kr and Ar show concentration dependent occupancy of cages. The cage occupancy follows $CO_2 \approx Kr > CH_4 >$ Ar for SC and $CO_2 > CH_4 \approx Kr > Ar$ for LC respectively in Kr(1.25):Ar(0.75) system. On the other hand, Ar occupies the highest number of both SC and LC with a trend of Ar \approx CO₂ > CH₄ > Kr in Kr(0.5):Ar(1.5) system. Among all the systems, H₂S:Xe system is an exceptional system where all the gas species (CO₂, H₂S, Xe and CH₄) compete to occupy both SC and LC and this could be the reason for the lowest induction time in this system.

Mechanism of hydrate growth in different systems was elucidated by initially assessing the snapshots of configurations at different times, t^* during the simulation; here t^* represents time from the beginning of simulations (NVT, 250K, $t^* = 0$) as formation of cages in some systems (H₂S:Ne, H₂S:Kr and H₂S:Xe) started during the NVT simulations at 300K. The formation of single cages or dual cages was observed in all the systems during the beginning of NPT simulations but most of these cages decay within 1ns of simulation time as discussed in Chapter 2. However, we observed formation of a large cage besides the methane cage of sI hydrate that was stable and eventually there was formation of new large and small cages around this large cage that further leads to a Y-shaped growth synthon (GS) as shown in Figures 4.5-4.7. This is contradictory to the earlier reports of formation of labile gas cages lead to hydrate nuclei ²⁶. The Y-shaped growth synthon is formed by three LC and one SC and is involved in the

formation of hydrate unit cell and was observed at different times in different systems; at t^* =18ns (H₂S:Ne), t^* =25ns (H₂S:Ar), t^* =16ns (H₂S:Kr), t^* =14ns (H₂S:Xe), t^* =19ns for Kr:Ar (1.25:0.75 and 0.50:1.50) and t^* =20ns (N2:Ar). The arms and tail of the Y-shaped growth synthon are formed by the large hydrate cages (L₁, L₂, L₃) and all the larges cages are joined in the middle by a common small cage, S.

Formation of large and small cages in a growth synthon was analysed by calculating time plot of number of water molecules around a gas species (N_{WG}) of a growth synthon along-with number of gas molecules (N_{GG}) that are within distance of 6-8Å and eventually lead to formation of growth synthon as shown in Figures 4.8 and 4.9. There are 24 and 20 water molecules in LC and SC of sI-NGH respectively with gas species in neighbouring cages within a distance of 6-8 Å. Most of the systems show formation of partial dual large cages (LL) in the early stages of growth synthon formation as shown in Figures 4.5a and 4.8a (by two CH₄ molecules at $t^*=11$ ns; L₁L₃) for H₂S:Ne system, Figures 4.5b and 4.8b (by Ar and H₂S at $t^*=12$ ns; L₂L₃) for H₂S:Ar system, Figures 4.6a and 4.8c (by Kr and CH₄ at $t^*=9$ ns; L₁L₃) in $H_2S:Kr$ system, Figures 4.6b and 4.8d (two CH₄ molecules at $t^*=6ns$; L_2L_3) in $H_2S:Xe$ system, Figures 4.7a and 4.9a (N_2 and CH_4 at $t^*=13$ ns) in N_2 :Ar system, Figures 4.7b and 4.9b (Kr and CH₄ at $t^*= 14$ ns; L₂L₃) in in Kr(1.25):Ar(0.75) system except for Kr(0.50):Ar(1.50) system where small and large (SL₂) dual cages are initially formed at $t^*=12$ ns (Figures 4.7c and 4.9c) by two Ar atoms. Later, there is local ordering of water molecules around the LL dual cage that leads to formation of S cage in-and L₁L₂S cluster. This local ordering of water gas molecules is consistent with the earlier reports in CO₂ hydrate systems ²⁸. Finally, there is formation of a large cage near LLS aggregate that leads to a Y-shaped growth synthon. However, in case of Kr(0.50):Ar(1.50) system, there is formation of L cage after the initial formation of SL₂ dual cage that also leads to L₁L₂S type cluster that eventually forms Y-shaped GS with the formation of the fourth cage (L cage).

The thermodynamic stability of the cages that form a growth synthon was assessed by calculating the free energy (FE) of dual cages (SL and LL) as a function of two collective variables; CV1 and CV2 where CV1 is the distance between guests of LL dual cage and CV2 is distance between guests of SL cage in a growth synthon. Figures 4.10 and 4.11 show free energy profiles of dual cages as a function of collective variables CV1 and CV2 for a growth

synthon in different system. The energetically favourable regions are around 8Å for both CV1 and CV2 in all the systems except for a wider range of distance (5-8)Å for CV1 in H₂S:Ar system and for CV2 in Kr(0.5): Ar(1.5) system that suggests that Ar is more labile in these cages. The free energy of LL and SL cages that form growth synthon are similar in most of the systems; N_2 :Ar system has the lowest FE among all the systems where $FE_{L_{CO_2}L_{N_2}} =$ $FE_{S_{CO_2}L_{CH_4}} = -39 \text{ kcal/mol}$; $H_2S:Xe$ system shows the next most favourable FE with $FE_{L_{Xe}L_{CH_4}} = FE_{S_{Xe}L_{CH_4}} = -32 \ \textit{kcal/mol}; \\ (FE_{L_{CH_4}L_{CH_4}} = FE_{S_{H_2}SL_{CH_4}}) \ \text{in H}_2S: Ne \ system, in H}_2S: Ne \ sys$ $H_2S: Kr \ and \ (FE_{L_{Kr}L_{Kr}} = \ FE_{S_{Kr}L_{CH_4}}) \ in \ Kr (1.25): Ar (0.75) \ systems. \ However \ FE_{S_{Ar}L_{Ar}} \ \ is \ more$ in Kr(0.5):Ar(1.5)system $FE_{L_{Ar}L_{Ar}}$ favourable than and similarly, $FE_{L_{CO_2}L_{H_2S}}$ is more favorable than $FE_{S_{Ar}L_{Ar}}$ by 2kcal/mol in H_2S :Ar system and in both the systems broader free energy minima is observed in less favourable dual cages which is consistent with free energy profile results in Figures 4.10 and 4.11.

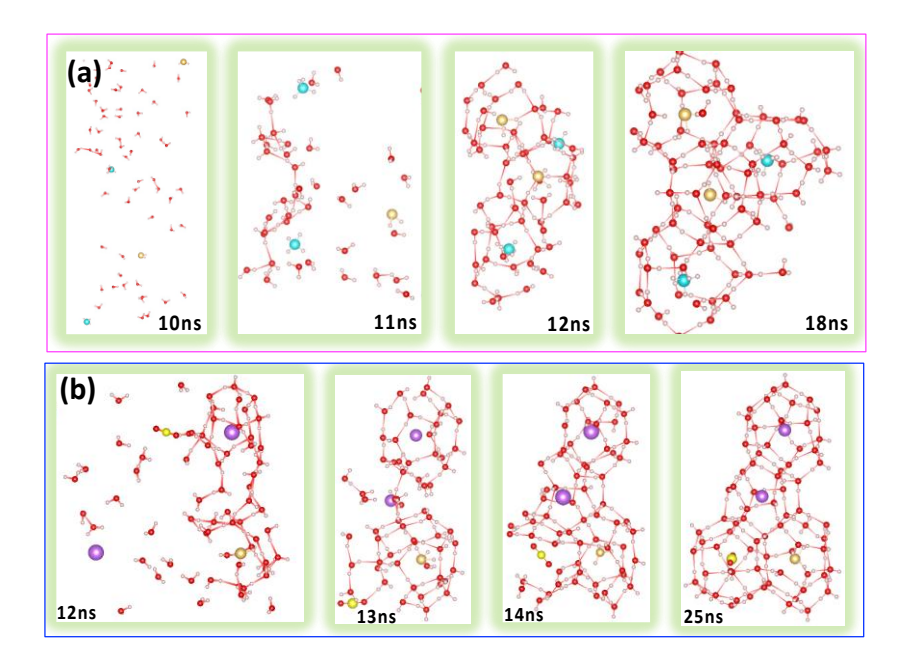


Figure 4.5: Snapshots of trajectories at different times (t^*) for (a) H₂S:Ne and (b) H₂S:Ar during the formation of a growth synthons. Here t^* is the simulation time from beginning of the simulation where total $t^* = 72$ ns (2ns NVT at 250K + 10ns NVT at 300K + 60ns NPT at 250K). The red, cream, cyan, mustard, yellow and purple spheres represent oxygen, hydrogen, carbon in methane, sulfur, carbon in carbon dioxide and argon respectively.

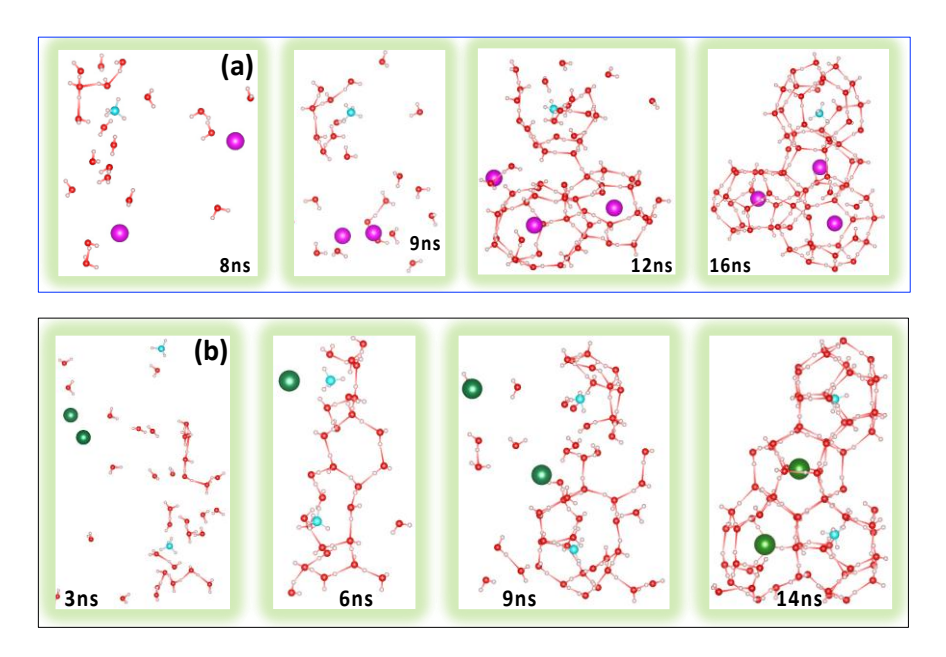


Figure 4.6: Snapshots of trajectories at different times (t^*) for (a) H₂S:Kr and (b) H₂S:Xe during the formation of a growth synthons. Here t^* is the simulation time from beginning of the simulation where total $t^* = 72$ ns (2ns NVT at 250K + 10ns NVT at 300K + 60ns NPT at 250K). The red, cream, cyan, green and magenta spheres represent oxygen, hydrogen, carbon in methane, xenon and krypton respectively.

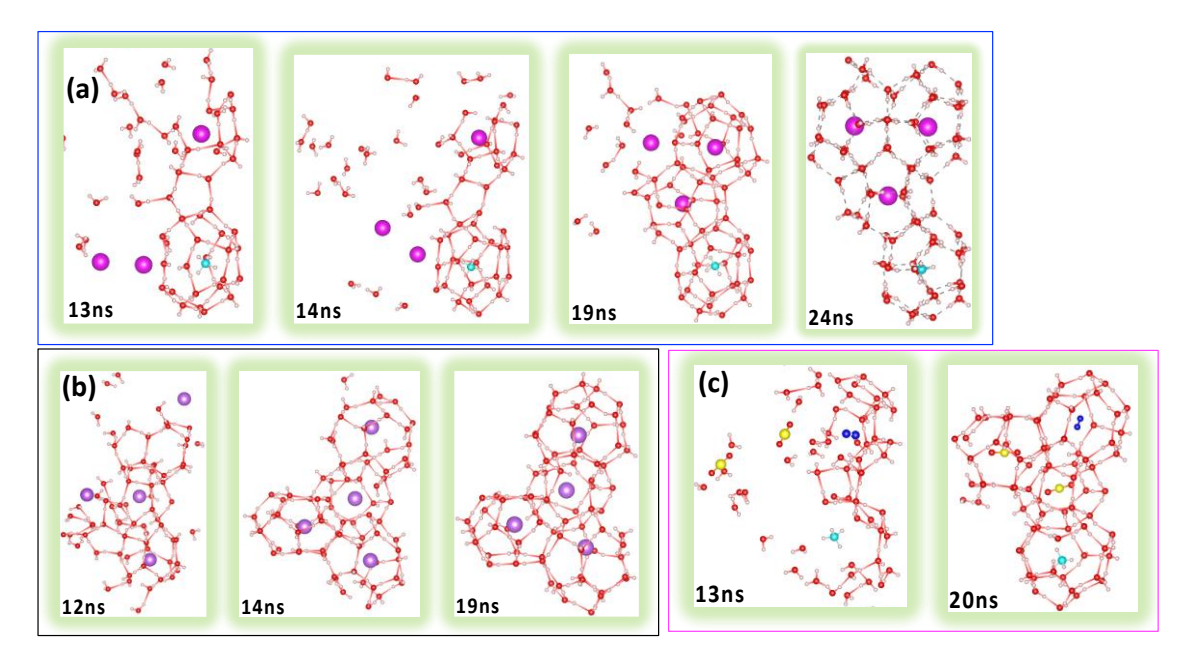


Figure 4.7: Snapshots of trajectories at different times (t^*) for (a) Kr(1.25):Ar(0.75), (b) Kr(0.50):Ar(1.50) and (c) N₂:Ar during the formation of a growth synthons. Here t^* is the simulation time from beginning of the simulation where total $t^* = 72$ ns (2ns NVT at 250K + 10ns NVT at 300K + 60ns NPT at 250K). The red, cream, cyan, blue, magenta, yellow and purple spheres represent oxygen, hydrogen, carbon in methane, nitrogen, krypton, carbon in carbon dioxide and argon respectively.

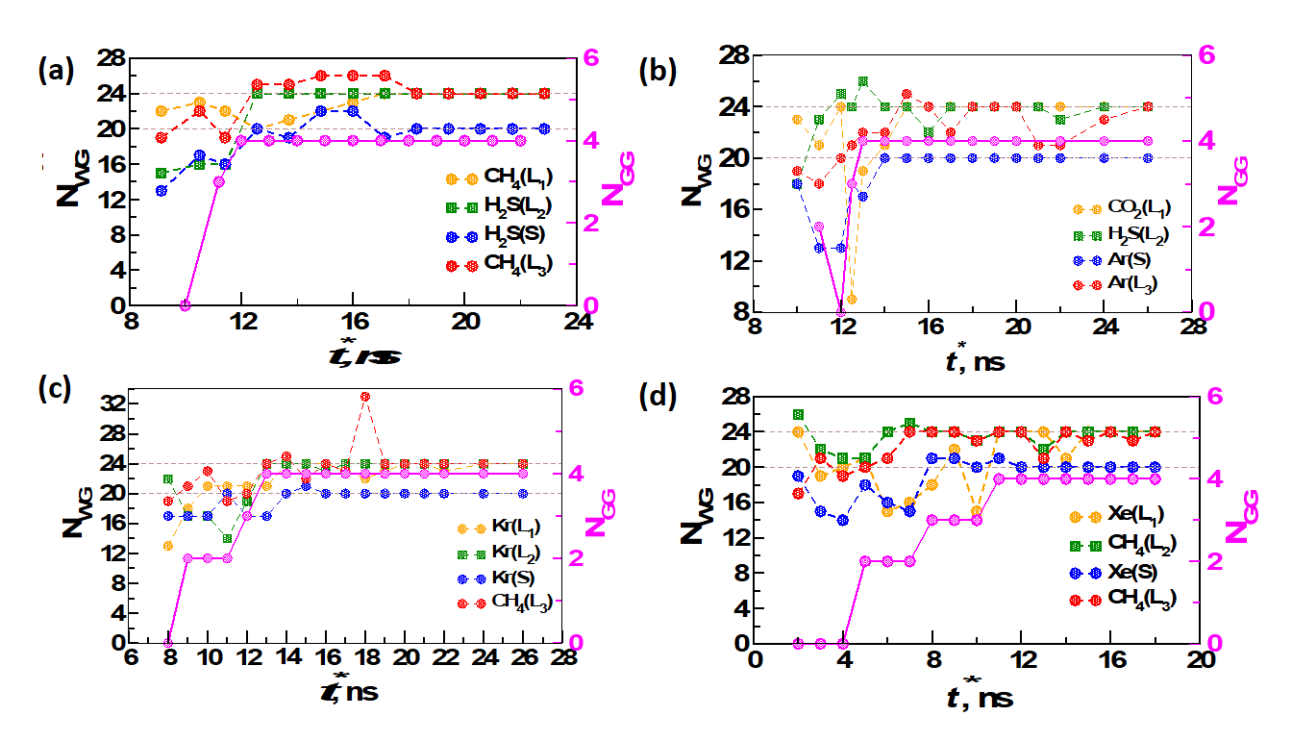


Figure 4.8: Time plot of number of water molecules around a gas species (N_{WG}) and number of gas species (N_{GG}) withing distance of 8Å where gas species belong to a growth synthon in different systems; (a) $H_2S:Ne$, (b) $H_2S:Ar$, (c) $H_2S:Kr$ and (d) $H_2S:Xe$.

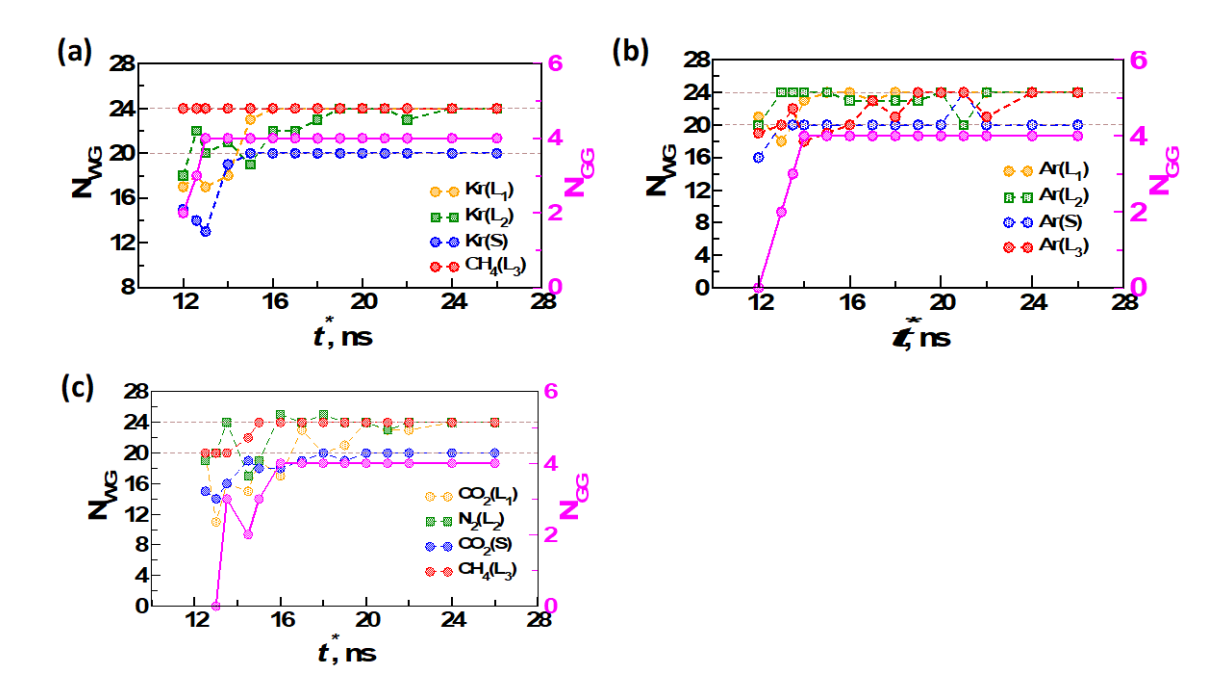


Figure 4.9: Time plot of number of water molecules around a gas species (N_{WG}) and number of gas species (N_{GG}) withing distance of 8\AA where gas species belong to a growth synthon in different systems (a) Kr(1.25):Ar(0.75), (b) Kr(0.50):Ar(1.50) and (c) N_2 :Ar.

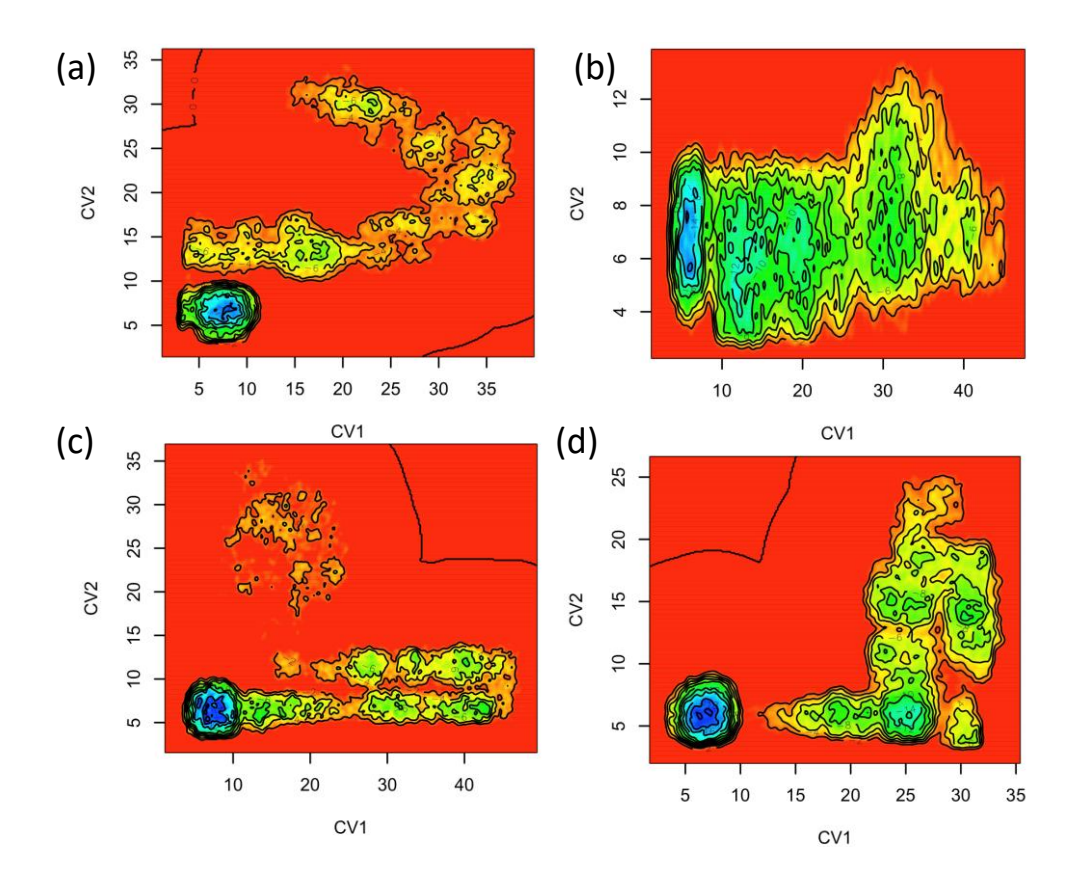


Figure 4.10: Free energy profile (kcal/mol) of dual cages in different systems as a function of two collective variable CV1 and CV2 where CVI and CV2 are distance between the guests in large-large and small-large dual cages.

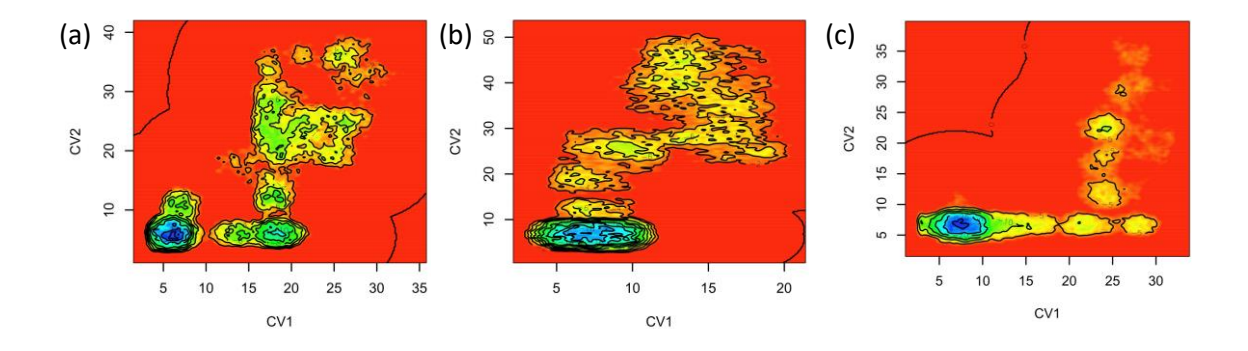


Figure 4.11: Free energy profile (kcal/mol) of dual cages in different systems as a function of two collective variable CV1 and CV2 where CVI and CV2 are distance between the guests in large-large and small-large dual cages.

Selective encapsulation of CO_2 over CH_4 in different systems was evaluated by calculating the percentage difference in number of ordered cages (based on GRADE code) formed by CO_2 and CH_4 respectively and represented as CO_2 selectivity (ΔS_C) as shown in Eqs. 4.2 and 4.3.

Similarly, total selectivity, ΔS_T of cages occupied by CO₂, third and fourth gases as compared to CH₄ was calculated as shown in Eq 4.4.

$$S_{gas}$$
 (%) = $\binom{N_{gas}}{N_{tot}}$ 100 Eq. (4.2)

$$\Delta S_C$$
 (%) = $S_{CO_2} - S_{CH_4}$ Eq. (4.3)

$$\Delta S_T$$
 (%) = $S_{CO_2 + G_3 + G_4} - S_{CH_4}$ Eq. (4.4)

Figures 4.12(a-b) report number of gas species encapsulated in cages (N_{gas}) and selectivities $(\Delta S_C \text{ and } \Delta S_T)$ for ordered cages in the first layer formed beside the interface in different systems. Among HG systems, N_{CH_4} is minimum for Ar system and is maximum for Xe system. The encapsulated number of CO₂ molecules (N_{CO_2}) decreases with increase in the size of noble gas in a system. N_{CO_2} is maximum for Ne but N_{CH_4} is also high as a result CO₂ selectivity (ΔS_C) is low for H₂S:Ne system. Interestingly, both N_{CO_2} and N_{COH_4} are similar in H₂S:Xe system, as a result ΔS_C is minimum in this system. Among all Ar based systems, ΔS_C decreases as H₂S:Ar < Kr(1.25):Ar(0.75) < Kr(0.5):Ar(1.5). This trend can be understood in terms of number of third and fourth gases that are included in cages in different systems. In HG systems, inclusion of third gas, G₃ (H₂S) decreases with increase in size of noble (fourth, G₄) gas. However, reverse trend is observed for inclusion of fourth gas and thus, minimum uptake of both third and fourth gases is observed only in H₂S:Ar system followed by H₂S:Kr system. The inclusion of CO2 is low in NG and KG systems than HG systems (except for H2S:Xe system). In KG systems, third (Kr) and fourth (Ar) gases show reverse trends for cage occupation where Ar occupies large number of cages when conc. of Ar is high in the system (Kr(0.5):Ar(1.5)). As a result, total selectivity, ΔS_T is high in KG systems as G₃ and G₄ occupy more cages than CO₂ that results in low value of ΔS_C . Similarly, in HG systems with Kr and Xe as G₄ gases, ΔS_T is high but ΔS_C is low as more number of G₄ gases occupy cages than CO₂. This is consistent with earlier reports where flue gases showed higher cage encapsulation than CO2 during CH4-CO2 exchange in NGHs ¹⁷⁻¹⁸. The inclusion of both N₂ and Ar in cages is less than CO₂ but CH₄ inclusion is high in N₂:Ar system that reduces both ΔS_C and ΔS_T in this system. H₂S:Ar system is the only system where inclusion of CH₄, Ar and H₂S are low but inclusion of CO₂ is high due to which both ΔS_C and ΔS_T are high in this system. This could be due to fast growth of hydrate in H₂S:Ar system due to faster formation of energetically favourable H₂S dual cages which gives kinetic control for cage occupancy by gases at lower conc. except for CO₂ (high conc.).

However, in KG systems, the hydrate growth is slow, thus, thermodynamically favourable Ar-Ar along-with $Ar-CO_2$ dominate the system with time when conc. of Ar is high in Kr(0.5):Ar(1.5) system.

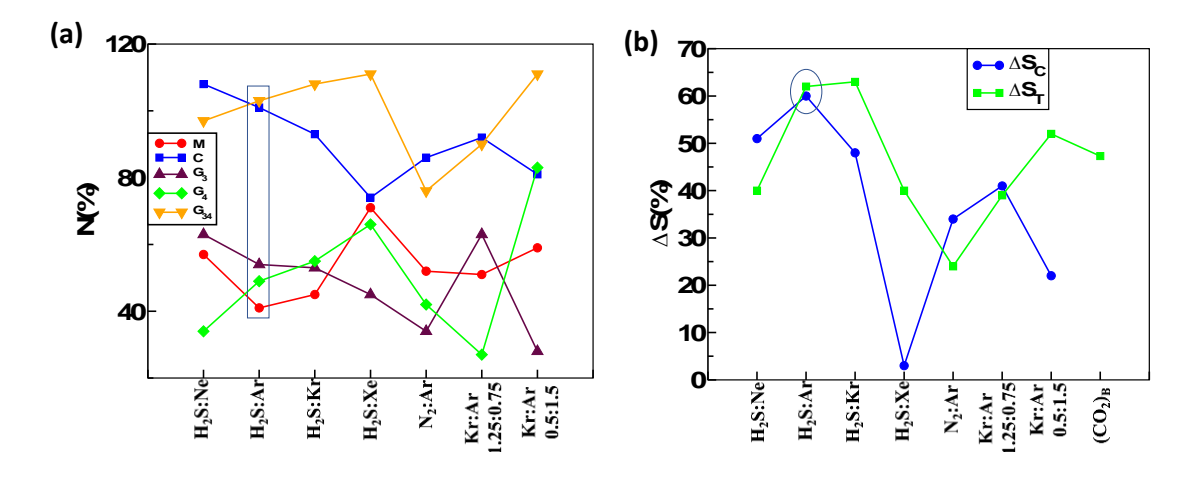


Figure 4.12: (a) Percentage of number of ordered cages (N) formed by methane (M), carbon dioxide (C), sum of third, G_3 , fourth gases, G_4 and G_{34} is the sum of third and fourth gases (b) CO_2 selectivity, ΔS_C and total selectivity, ΔS_T in the first layers formed beside the interface in different systems.

Conclusions

The present work shows that noble gases along-with flue gases can affect the exchange of methane and carbon dioxide in sI natural gas hydrates and could be one of the potential approaches to enhance selectivity for carbon dioxide over methane in sI hydrates. CO₂:H₂S:Ar (2:1:1) system shows the best selectivity for CO₂ over CH₄ in formation of hydrate cages. The formation of dual cages (large-large, LL and small-large, SL) play a crucial in the formation of Y-shaped (formed by four cages; LLSL) growth synthon that initiates unit cell growth. The SL and LL dual cages for Ar-Ar and Ar-CO₂ have small difference in DFT free energies unlike large difference in DFT free energies for Ar-CH₄ combination that leads to better, kinetically-driven CO₂ selectivity in H₂S:Ar system then thermodynamically dominance of Ar over CO₂ to occupy cages in Kr(0.5):Ar(1.5) system. Thus, concentration and choice of mixture of flue and noble gases is crucial in the CO₂ selectivity during CH₄-CO₂ exchange in sI-NGHs. Further studies are required in this direction to understand the role of concentration of Ar and H₂S as a

function of temperature, pressure and hydrate promoter in CO₂ selectivity during CH₄-CO₂ exchange in sI-NGHs.

References

- 1. Sloan, E. D. Fundamental Principles and Applications of Natural Gas Hydrates. Nature **2003**, 426, 353–363.
- Sloan E. D. Jr Physical and chemical properties of gas hydrates and application to world margin stability and climatic change. Gas Hydrates: Relevance to World Margin Stability and Climate Change. Geological Society, London, Special Publications 2014, 137, 31-50.
- 3. Boswell R. and Collett T. S. Current perspectives on gas hydrate resources. *Energy Environ. Sci.* 2011, 4, 1206–1215.
- Sloan E. D. Jr Physical and chemical properties of gas hydrates and application to world margin stability and climatic change. Gas Hydrates: Relevance to World Margin Stability and Climate Change. Geological Society, London, Special Publications 2014, 137, 31-50
- 5. Mu, L.; Solms, N. v. Experimental Study on Methane Production from Hydrate-Bearing Sandstone by Flue Gas Swapping. *Energy Fuels* **2018**, 32, 8167–8174.
- McGuire, P. L. Recovery of Gas from Hydrate Deposits Using Conventional Technology, 1982 SPE/DOE Unconventional Gas Recovery Symposium, Pittsburgh, PA. May 16-18, SPE 10832.
- 7. Yang, M.; Fu, Z.; Zhao, Y.; Jiang, L.; Zhao, K.; Song, Y. Effect of depressurization pressure on methane recovery from hydrate–gas–water bearing sediments. *Fuel* **2016**, 166, 419–426.
- 8. Li, G.; Li, X.-S.; Tang, L.-G.; Zhang, Y. Experimental Investigation of Production Behaviour of Methane Hydrate under Ethylene Glycol Injection in Unconsolidated Sediment. *Energy & Fuels* **2007**, 21, 6, 3389.
- 9. Lee, B. R.; Koh, C. A.; Sum, A. K. Quantitative measurement and mechanisms for CH4 production from hydrates with the injection of liquid CO2. *Phys. Chem. Chem. Phys.* **2014**, 16, 14922
- 10. Wu, G.; Tian, L.; Chen, D., Niu, M.; Ji, H. CO₂ and CH₄ Hydrates: Replacement or Cogrowth? *J. Phys. Chem. C* **2019**, 123, 13401–13409.

- 11. He, Z.; Gupta, K. M.; Linga, P.; Jiang, J. Molecular Insights into the Nucleation and Growth of CH₄ and CO₂ Mixed Hydrates from Microsecond Simulations. *J. Phys. Chem. C* **2016**, 120, 25225–25236.
- 12. Doman, P.; Alavi, S.; Woo, T. K. Free energies of carbon dioxide sequestration and methane recovery in clathrate hydrates. J. Chem. Phys. **2007**, 127, 124510-124518.
- 13. Park, Y.; Kim, Do-Y.; Lee, Jon-W.; Huh, D-Gee; Park, K-Pil; Lee, J.; Lee H. Sequestering carbon dioxide into complex structures of naturally occurring gas hydrates. *PNAS* **2006**, 103, 12690-12694.
- Liu, J.; Yan, Y.; Xu, J.; Li, S.; Chen, G.; Zhang, J. Replacement micro-mechanism of CH4 hydrate by N₂/CO₂ mixture revealed by ab initio studies. *Comput. Mater. Sci.* 2016, 123, 106-110.
- 15. Zhou, H.; Chen, B.; Wang, S.; Yang, M. CO₂/N₂ mixture sequestration in depleted natural gas hydrate reservoirs. *J. Pet. Sci. Eng.* **2019**, 175, 72–82.
- 16. Bhawangirkar, D. R.; Sangwai, J. S. Insights into Cage Occupancies during Gas Exchange in CH4+CO2 and CH4+N2+CO2 Mixed Hydrate Systems Relevant for Methane Gas Recovery and Carbon Dioxide Sequestration in Hydrate Reservoirs: A Thermodynamic Approach. *Ind. Eng. Chem. Res.* 2019, 58 (31), 14462–14475.
- 17. Zhang, Y.; Cui, M.; Xin, G.; Li, D. Microscopic insights on the effects of flue gas components on CH4–CO2 replacement in natural gas hydrate. *Gas Sci. Eng.* **2023**, 112, 204947.
- 18. Cha, M.; Shin, K.; Lee, H.; Moudrakovski, I. L.; Ripmeester, J. A.; Seo, Y. Kinetics of Methane Hydrate Replacement with Carbon Dioxide and Nitrogen Gas Mixture Using in Situ NMR Spectroscopy. *Environ. Sci. Technol.* **2015**, 49, 1964–1971.
- 19. Tupsakhare, S. S.; Castaldi, M. J. Efficiency enhancements in methane recovery from natural gas hydrates using injection of CO2/N2 gas mixture simulating in-situ combustion. *Applied Energy* **2019**,236, 825–836.
- 20. Zhou, X.; Liang, D.; Liang, S.; Yi, L.; Lin, F. Recovering CH4 from Natural Gas Hydrates with the Injection of CO2-N2 Gas Mixtures. *Energy Fuels* **2015**, 29, 1099-1106.
- 21. Yasue, M.; Masuda, Y.; Liang, Y.; Estimation of Methane Recovery Efficiency from Methane Hydrate by the N2–CO2 Gas Mixture Injection Method. *Energy Fuels* **2020**, 34, 5236–5250.

- 22. Song, W.; Sun, X.; Zhou, G.; Huang, W.; Lu, G.; Wu. C. Molecular Dynamics Simulation Study of N2/CO2 Displacement Process of Methane Hydrate. *Chemistry Select* **2020**, 5, 13936 13950.
- 23. Kvamme, B. Thermodynamic Limitations of the CO2/N2 Mixture Injected into CH4 Hydrate in the Ignik Sikumi Field Trial. *J. Chem. Eng. Data* **2016**, 61, 1280–1295.
- 24. Matsui, H.; Jia, J.; Tsuji, T.; Liang, Y.; Masuda, Y. Microsecond simulation study on the replacement of methane in methane hydrate by carbon dioxide, nitrogen, and carbon dioxide–nitrogen mixtures. *Fuel* **2020**,263, 116640.
- 25. Jacobson L. C., Hujo W., and Molinero V., Nucleation pathways of clathrate hydrates: Effect of guest size and solubility. *J. Phys. Chem. B* **2010**, 114, 13796–13807.
- 26. Jacobson, L. C.; Hujo, W. and Molinero, V. Amorphous precursors in the nucleation of clathrate hydrates. J. *Am. Chem. Soc.* **2010**, 132, 11806–11811.
- 27. Zhang Z.; Walsh M. R.; and Guo G. J. Microcanonical molecular simulations of methane hydrate nucleation and growth: Evidence that direct nucleation to sI hydrate is among the multiple nucleation pathways. *Phys. Chem. Chem. Phys.* 2015, 17, 8870–8876.
- 28. Radhakrishnan, R. and Trout, B. L. A new approach for studying nucleation phenomena using molecular simulations: application to CO₂ hydrate clathrates. *J. Chem. Phys.*, **2002**, 117, 1786–1796.
- 29. He Z.; Linga P. and Jiang J. What are the key factors governing the nucleation of CO₂ hydrate? *Phys. Chem. Chem. Phys.* 2017, 19, 15657-15661.
- 30. Arjun A. and Bolhuis P. G. Molecular understanding of homogeneous nucleation of CO2 hydrates using Transition Path Sampling. *J. Phys. Chem. B* 2021, 125, 338-349.
- 31. Hu W.; Chen C.; Sun J.; Zhang N. Zhao J.; Liu Y.; Ling Z.; Li W.; Liu W. and Song Y. Three-body aggregation of guest molecules as a key step in methane hydrate nucleation and growth. *Commun. Chem.* **2022**, *5*, 1-11.
- 32. He Z.; Gupta K. M.; Linga P.; and Jiang J. Molecular Insights into the Nucleation and Growth of CH4 and CO2 Mixed Hydrates from Microsecond Simulations. *J. Phys. Chem. C* **2016**, 120, 25225–25236.
- 33. Baig K.; Kvamme B.; Kuznetsova T. and Bauman J. Impact of Water Film Thickness on Kinetic Rate of Mixed Hydrate Formation During Injection of CO₂ into CH₄ Hydrate. *AIChE J.* **2015**, 61, 3944-3957.

- 34. Liu, J.; Yan, Y.; Liu, H.; Xu, J.; Zhang, J.; Chen, G. Understanding effect of structure and stability on transformation of CH₄ hydrate to CO₂ hydrate. *Chem. Phys. Lett.* **2016**, 648, 75–80.
- 35. Tung, Yen-T.; Chen, Li-J.; Chen, Y-Ping.; Lin, S-T. In situ methane recovery and carbon dioxide sequestration in methane hydrates: A molecular dynamics simulation study. *J. Phys. Chem. B* **2011**, 115, 15295–15302.
- 36. Tung, Yen-T.; Chen, Li-J; Chen, Yan-P.; Lin, Shiang-T. The growth of structure I methane hydrate from molecular dynamics simulations. *J. Phys. Chem. B* **2010**, *114*, 10804–10813.
- 37. Bai, D.; Zhang, X.; Chen, G.; Wang, W. Replacement mechanism of methane hydrate with carbon dioxide from micro-second molecular dynamics simulations. *Energy Environ. Sci.* **2012**, 5 (5), 7033–7041.
- 38. Yoon, J.-H.; Kawamura, T.; Yamamoto, Y.; Komai, T. Transformation of Methane Hydrate to Carbon Dioxide Hydrate: In Situ Raman Spectroscopic Observations. J. Phys. Chem. A 2004, 108 (23), 5057–5059.
- 39. Qi, Y.; Ota, M.; Zhang, H. Molecular dynamics simulation of replacement of CH4 in hydrate with CO₂. Energy Convers. Manage. 2011, 52 (7), 2682–2687.
- 40. Kirchner, M. T.; Boese, R.; Billups, W. E.; Norman, L. R. Gas hydrate single-crystal structure analyses. *J. Am. Chem. Soc.* **2004**, 126, 9407-9412, DOI: https://doi.org/10.1021/ja049247c
- 41. Circone, S.; Stern, L. A.; Kirby, S. H.; Durham, W. B.; Chakoumakos, B. C.; Rawn, C. J.; Rondinone, A. J.; Ishii, Y. CO2 Hydrate: Synthesis, Composition, Structure, Dissociation Behavior, and a Comparison to Structure I CH4 Hydrate. *J. Phys. Chem. B* 2003, 107, 5529-5539.
- 42. Moon, C.; Taylor, P. C.; Rodger, P. M. Molecular dynamics study of gas hydrate formation. *J. Am. Chem. Soc.* **2003**, 125, 4706-4707.
- 43. Abascal, J. L. F.; Vega, C. A general purpose model for the condensed phases of water: TIP4P/2005. *J. Chem. Phys.* **2005**, 123, 234505.
- 44. Conde, M. M.; Vega, C. Determining the three-phase coexistence line in methane hydrates using computer simulations. *J. Chem. Phys.* **2010**, 133, 064507.
- 45. Liang S. and Kusalik P. G. Exploring nucleation of H₂S hydrates. *Chem. Sci.* 2011, 2,1286–1292.

- 46. Jorgensen W. L.; Maxwell D. S. and Tirado-Rives J. Development and testing of the OPLS all-atom force field on conformational energetics and properties of organic liquids. *J. Am. Chem. Soc.* **1996**, 118, 11225–11236.
- 47. Cygan R. T.; Romanov V. N.; and Myshakin E. M. Molecular simulation of carbon dioxide capture by montmorillonite using an accurate and flexible force field. *J. Phys. Chem. C* **2012**, 116, 13079–13091.
- 48. Somasundaram T.; Panhuis M. in het; Lynden-Bell R. M. and Patterson C. H. A simulation study of the kinetics of passage of CO2 and N2 through the liquid/vapor interface of water. *J. Chem. Phys.* **1999**, 111, 2190–2199.
- 49. Yerlet L. and Weis J. J. Perturbation theory for the thermodynamic properties of simple liquids. *Mol. Phys.* 1972, 24, 1013–1024.
- 50. Huang P. H. Molecular dynamics investigation of separation of hydrogen sulfide from acidic gas mixtures inside metal-doped graphite micropores. *Phys. Chem. Chem. Phys.* **2015**, 17, 22686–22698.
- 51. Plimpton, S. Fast parallel algorithms for short-Range Molecular Dynamics. *Soft Matter*, 1995, 14, 1–19.
- 52. Evans D. J. and Holian B. L. The Nose-Hoover Thermostat. *J. Chem. Phys.* **1985**, 83, 4069-4074.
- 53. Momma, K. and Izumi, F. VESTA 3 for three-dimensional visualization of crystal, volumetric and morphology data. *J. Appl. Crystallogr.* 2011, 44, 1272-1276.
- 54. Humphrey, W.; Dalke, A. and Schulten, K. VMD Visual Molecular Dynamics. *J. Mol. Graph.* **1996**, 14, 33-38.
- 55. Mahmoudinobar, F. and Dias, C. L. GRADE: A code to determine clathrate hydrate structures. *Comput. Phys. Commun* **2019**, 244, 385-391.
- 56. Tribell, G. A.; Bonomi, M.; Branduardi, D.; Camilloni, C. and Bussi, G. PLUMED2: New feathers of an old bird. *Comput. Phys. Commun.* **2014**, 185, 604.
- 57. Bussi, G. and Laio, A. Using metadynamics to explore complex free-energy landscapes. *Nat. Rev. Phys.* **2020**, 2, 200-212.
- 58. Trapl, D. and Spiwok, V. Analysis of the Results of Metadynamics Simulations by metadynminer and metadynminer3d. *R. Journal*, **2022**, 14, 46-58.
- 59. Walsh, M. R.; Koh, C. A.; Sloan, E. D.; Sum, A. K.; Wu, D. T. Microsecond simulations of spontaneous methane hydrate nucleation and growth. *Science*, **2009**, 326, 1095-1098.

- 60. Sarupria, S.; Debenedetti, P. G. Homogeneous nucleation of methane hydrate in microsecond molecular simulations. *J. Phys. Chem. Lett.* **2012**, 3, 2942–2947.
- 61. Matsui, H.; Jia, J.; Tsuji, T.; Liang, Y.; Masuda, Y. Microsecond simulation study on the replacement of methane inmethane hydrate by carbon dioxide, nitrogen, and carbon dioxide-nitrogen mixtures. *Fuel*, **2020**, 263, 116640.
- 62. Sun, Y.-H.; Li, S.-L.; Zhang, G.-B.; Guo, W.; Zhu, Y.-H. Hydrate Phase Equilibrium of CH4+N2+CO2 Gas Mixtures and Cage Occupancy Behaviors. *Ind. Eng. Chem. Res.* **2017**, 56 (28), 8133–8142
- 63. Sugahara, K.; Sugahara, T. and Ohgaki, K. Thermodynamic and Raman Spectroscopic Studies of Xe and Kr Hydrates. *J. Chem. Eng.* **2005**, 50, 274-277.
- 64. Davidson, D. W.; Desando, M. A.; Gough, S. R.; Handa, Y. P.; Ratcliffe, C. I.; Ripmeester, J. A. and Tse, J. S. A clathrate hydrate of carbon monoxide. *Nature* **1987**, 328, 418-419.
- Dyadin, Y. A.; Larionov, E. G.; Aladko, E. Ya.; Manakov, A. Yu.; Zhurko, F. V.; Mikina,
 T. V.; Komarov, V. Yu and Grachev, E. V. Clathrate formation in water-noble gas
 (Hydrogen) systems at high pressures. *J. Struct. Chem.* 1999, 40, 790-795.
- 66. Winckler, G.; Aeschbach-Hertig, W.; Holocher, J.; Kipfer, R., Levin; I., Poss; C., Rehder; G., Schlosser, P.; Suess, E.; Noble gases and radiocarbon in natural gas hydrates, *Geophys. Res. Lett.* 2002, 29(10), 63-1-63-4.

Chapter 5

Role of Hydrate Promoter (EDTA Bisamides) in CO₂-CH₄ Exchange in NGHs in Presence of Monatomic and Polyatomic Gases

Introduction

Currently, fossil fuels are the primary source of energy but are limited resources that also contribute to pollution. The amount of carbon, mainly stored as CH₄ in Natural Gas Hydrate (NGHs) reservoirs is approximately twice the amount of carbon present in fossil fuels all over the worldwide ¹. Thus, NGHs could be potential clean energy resources that could also be potential candidates for sequestration of carbon dioxide. Natural gas hydrates are solid, nonstochiometric crystalline compound in with small gas species entrapped as guest molecules in cages for e.g. gases like CH₄, CO₂, ethane and propane where these gases stabilize the cavities of hydrogen-bonded water molecules of cages through van der Waals interactions. NGHs primarily exists in sea sediments and permafrost regions and form at low temperature and high pressure ²⁻⁴. The safe and efficient recovery of methane from NGHs is a grand challenge. Some of the conventional methods such as depressurization ⁵⁻⁶, heat injection ^{5,7} and hydrate inhibitor techniques ^{5,8} are employed to recover methane from NGHs. The methane recovery occurs by exploiting the hydrate structure via altering the phase equilibria of hydrate reservoirs to high temperature and low pressure. These techniques are based on the principle of hydrate decomposition. Thus, large scale usage of these techniques may affect the strength of gas hydrate reservoirs that could lead to reservoir destruction that could cause geological disasters

CO₂-CH₄ exchange in NGHs is considered as a better alternative over the conventional techniques to recover methane from NGH reservoirs as simultaneous sequestration of CO₂ as hydrates could stabilize the hydrate reservoirs ¹⁰. However, both CO₂ and CH₄ form stable mixed hydrates as compared to pure CH₄ or CO₂ hydrates that reduces the CH₄-CO₂ exchange rate ¹¹⁻¹⁴. The exchange of CO₂ and CH₄ in NGHs is confirmed by several experimental reports ¹⁵⁻²¹, where both CO₂ and CH₄ prefer to form sI hydrate and enthalpy of CO₂ hydrate formation

(-57.98 kcal/mol) is less than enthalpy of CH₄ hydrate formation (-54.49 kcal/mol) ²². The thermodynamic equilibrium curve for CO₂ and CH₄ falls in a narrow region at hydrate forming conditions that reduces the exchange efficiency ²³⁻²⁵. Thus, other approaches like inclusion of flue gases or hydrate promoters along-with CO₂ are being explored to enhance CH₄-CO₂ exchange in NGHs. Nitrogen has been mainly employed as flue gas to enhance CH₄-CO₂ exchange in NGHs ²⁶⁻³⁰. Park et at. had first reported usage of mixture of CO₂ and N₂ (80 mol% + 20 mol%) in CH₄-CO₂ exchange in NGHs where 85% and 92% of methane was recovered in sI and sII hydrates ²⁶. However, a very high conc. of N₂ could collapse the hydrates and thus, injection pressure of CO₂/N₂ is crucial to improve the CO₂ capture efficiency

Hydrate Promotes (HP) are compounds that could enhance formation of hydrates and are divided into two groups; thermodynamic hydrate promotes (THPs) and kinetic hydrate promoters (KHPs)³³. THPs shifts the phase equilibrium curve of hydrate to the right side (i.e., low pressure and high temperature), thus, high concentration of THPs is required for hydrate growth ³³. Tetrahydrofuran (THF) ³⁴, cyclopentane (CP) ³⁵, propane ³⁵ and tetrabutylammonium bromide (TBAB) ³⁶ are some of the widely used THPs for CO₂ and CH₄ hydrates, however, there are other THPs: cyclohexane ³⁷, acetone ³⁸ and methylcyclohexane ³⁷ that are employed to enhance formation of other gas hydrates. THPs usually form the gas hydrates at mild conditions, where, gas molecules as well as hydrate promoter molecules participate in hydrate formation and THF is good example in this direction, it forms sII- hydrate (6⁴5¹²) at ~277.5K and ambient pressure ³⁴. KHPs do not participate itself in cage formation and are employed in low concentration and thus they do not show effect hydrate equilibria curve. KHPs do not participate itself in cage formation ³³ for e.g. surfactants (anionic, cationic, and nonionic) ³⁹, amino acids ⁴⁰, nanoparticles ⁴¹, oxide of metals ⁴² and derivatives of cellulose ⁴³, cyclodextrin ⁴⁴ and starches ⁴⁵. KHPs enhance nucleation process by reducing the induction time and accelerate the hydrate formation process. Sodium dodecyl sulphate (SDS) is one of widely explored and a well-known KHP and theoretical studies have shown that SDS-CO2 interactions are entirely different than SDS-CH₄ interactions ³⁹. CO₂ shows strong interactions with SDS, as a result, CO₂ loses its ability to drive water molecules to form a suitable hydrate cage. However, shape distortion does not occur when SDS interacts with CH₄ due to weak interactions, and drives water molecules to form the cages 46-47. The two main functional group in a hydrate promoter are polar groups (sulfonate, sulfate, hydroxyl, amine, amide, and so on) that interact with water molecules and solubilize the hydrate promoter in water and secondly, alkyl chains of different size and branching. In this work, we report CH₄-CO₂ exchange in NGHs in presence of monatomic and polyatomic gases that show better CO₂ selectivity in NGHs and a KHPs (Ethylenediamine Tetraacetic Acid (EDTA) bisamide) ⁴⁸. The earlier studies on EDTA-bisamide were reported for pure CH4 system where the length of alkyl side-chain effects the CH₄ hydrate formation; short alky chains (n-propyl and isopropyl) promoted CH₄ hydrate formation with prolonged nucleation time and long chain length (butyl and hexyl) showed a transition from promotion to inhibition of hydrate growth. Currently, there are no reports into the role of hydrate promoters on mixture of flue gases and CO₂ for CH₄-CO₂ exchange in NGHs. Hence, in this work, we report role of EDTA-bisamide in CH₄-CO₂ exchange in NGHs in presence of polyatomic (flue) and monatomic (noble). We have chosen n-heptyl alkyl chain as side group in EDTA-bisamide as shown in Figure 5.1.

Computational Details

Model System We chose few systems based on the earlier results (Chapter 2-4) of better CO₂ selectivity [CO₂:Kr(2:2), CO₂:Ar(2.5:1.5) and CO₂:Kr(3:1)] or fast hydrate growth [Xe(3:1)] in these systems and also N_2 ($N_2(2:2)$ and $N_2(3:1)$) for two different concentrations as most of studies are reported with N2 as flue gas for CH4-CO2 exchange in sI-NGHs till date. We also chose Xe and Ar based system, CO₂(3):Xe(0.67):Ar(0.33) as Xe enhances hydrate growth and Ar induces CO₂ selectivity in NGHs (Chapter 3). All the gas selectivity results were compared with bulk CO₂ system, (CO₂)_B. The initial configuration for systems with third gas (except for CO₂:Xe:Ar(3:0.67:0.33) system) were generated from the equilibrated configuration of H₂S(3:1) system (Chapter 2) that was simulated in NVT ensemble for 2ns at 250K and for 10ns at 300K. The H₂S(3:1) system consisted of a 5x5x3 supercell of sI hydrate seed in the centre of simulation box with a bulk phase on either side of seed where bulk phase consisted of water and gas molecules equivalent to 5x5x2.5 supercell of sI hydrate on either side of the hydrate seed. The CO₂ and H₂S molecules were replaced by the desired gas species in the equilibrated configuration of H₂S(3:1) system to generate a system of interest. We included one molecule each of ethylenediamine tetraacetic acid bisamide as hydrate promoter, (HP) in left and right bulk phases. The structure of hydrate promoter is shown in Figure 5.1. The details of system size and number of gas species in each system are reported in Table 5.1. However, CO₂:Xe:Ar(3:0.67:0.33) system was generated by replacing the gas species from equilibrated configuration of CO₂:Xe(3:1) system with HP.

Simulation Details

We chose different forcefields to model the systems; TIP4P/2005 49-50 for water, OPLS-AA for CH₄, hydrate promoter and Ne ⁵¹, parameters from Cyan et al. ⁵² for CO₂, parameters from Somasundaram et. al. for N₂ ⁵³, parameters from Pie-Hsing Huang ⁵⁴ for H₂S and from Loup and Jean for noble gases (Ar, Kr and Xe) 55. All the cross-interaction parameters were generated using Lorentz-Berthelot combination rules. All the simulations were performed in LAMMPS ⁵⁶ and Noose-Hoover thermostat and barostat with relaxation time of 0.06ps and 2ps were chosen ⁵⁶⁻⁵⁹. The cut-off distances for van der Waals and electrostatic interactions were chosen as 12.0Å and 10.0Å. The three-dimensional periodic boundary conditions were applied in all the systems. A time step of 1fs was chosen and data was stored at every 1ps for analysis. The simulation runs were divided into three sets; (i) all the systems except for CO₂:Xe (3:1) and CO₂:Xe:Ar(3:0.67:0.33) systems, were energy minimized by descent algorithm followed by 2ns of NVT at 300K to equilibrate the system; (ii) CO₂:Xe(3:1) system was simulated for 5ns of NVT at 300K due to slow diffusivity of Xe and (iii) CO₂:Xe:Ar(3:0.67:0.33) was generated from equilibrated configuration of CO₂:Xe(3:1) system by energy minimization using descent algorithm. Further, all systems were simulated for 80ns using NPT simulations at 250K and 15MPa.

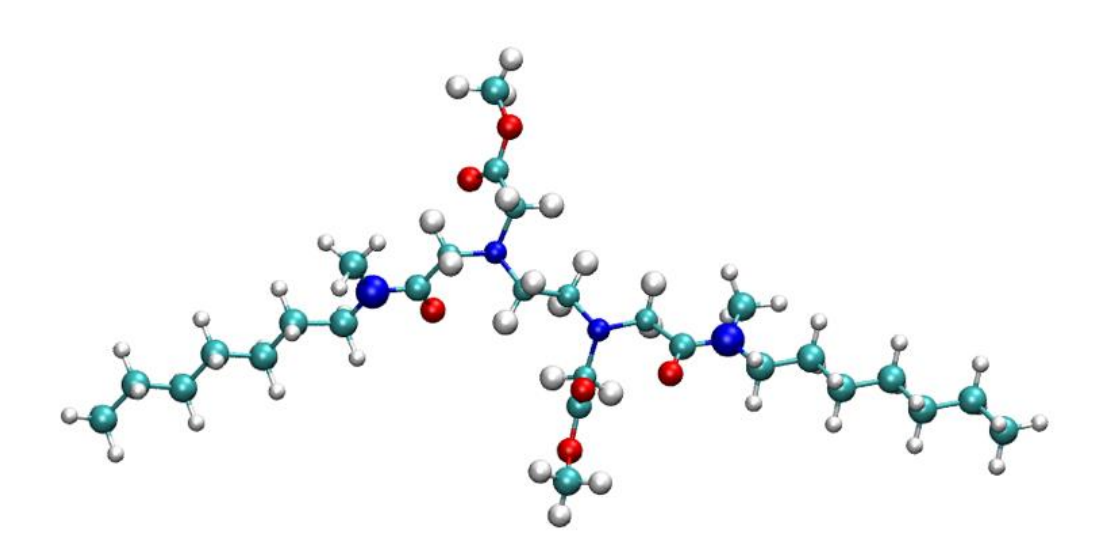


Figure 5.1: Structure of Ethylenediamine tetraacetic acid bisamide, hydrate promoter (HP). Here, cyan, white, blue and red spheres represent carbon, hydrogen, nitrogen and oxygen atoms respectively.

Table 5.1: Number of gas species and box dimensions in different systems.

S. No.	Systems	Box Dimension (ų)	N _{H2O}	N CH4	N _{CO2}	N _{G3}
1	Bulk CO ₂				1010	-
2	CO ₂ :Kr(2:2)				506	504
3	CO ₂ :N ₂ (2:2)				506	504
4	CO ₂ :H ₂ S(2:2)	58.1 x 58.1 x 96.96	9190	600	506	504
5	CO ₂ :Kr(3:1)				758	252
6	CO ₂ :N ₂ (3:1)				758	252
7	CO ₂ :Xe(3:1)				758	252
8	CO ₂ :Ar(2.5:1.5)				632	378
9	CO ₂ :Xe:Ar (3:0.67:0.33)				758	168(Xe) 84 (Ar)

Results and Discussions

Figure 5.2a shows the potential energy (PE) and F4 OP as a function of time in different systems. There is a steep decrease in potential energy and increase in F4 OP for $H_2S(2:2)$ system and F4 OP value reaches 0.7 at 40ns. However, in all other systems F4 OP value is between 0.66 to 0.69 at the end of NPT simulation run (80ns) which could be due to formation of disordered hydrate cages in these systems. Figure 5.2b shows the time for formation of first hydrate layers on either side of the interface in different systems. The trends in PE and F4 OP are consistent with the time taken for formation of first hydrate layer where rate of hydrate growth decreases as $H_2S(2:2) > (CO_2)_B > Kr(3:1) > Kr(2:2) \cong N_2(3:1) > N_2(2:2) \cong$

 $Xe:Ar(3:0.67:0.33) \cong Ar(2.5:1.5) > Xe(3:1)$. Kr and N_2 show reverse trend in hydrate growth as a function of concentration of the respective third gas in the system. Interestingly, Xe(3:1) system was the fastest growing system without hydrate promoter (Chapter 3) and reverse trend is observed in the presence of hydrate promoters.

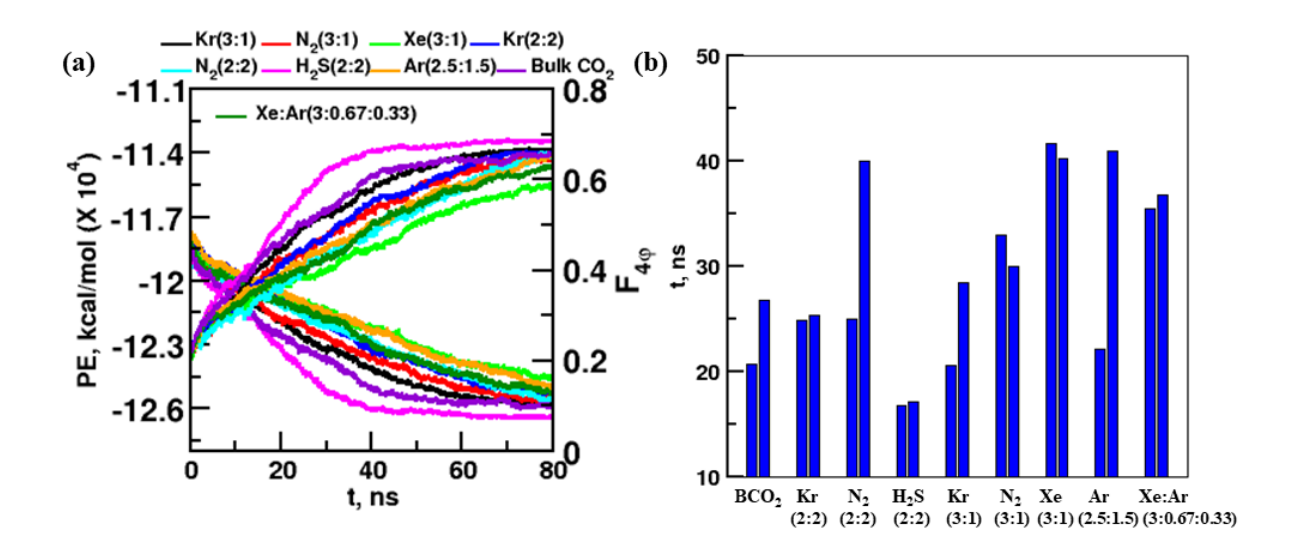


Figure 5.2:(a) Potential Energy and F4 OP as a function of time (b) time for formation of first layer on left and right side of bulk-seed interface in different systems: $(CO_2)_B$ (BCO₂, bulk CO₂), Kr(2:2), $N_2(2:2)$, $N_2(3:1)$, $H_2S(2:2)$, Kr(3:1), Xe(3:1), Xe(0.67):Ar(0.33) and Ar(2.5:1.5).

We observed only 5^{12} and 6^25^{12} type of hydrate cages during hydrate growth in all the systems that confirmed that only sI hydrate formed in all the systems. Figure 5.3, shows the number of small (SC) and large (LC) cages occupied by gas species as a function of time during hydrate growth in different systems. CO_2 dominates SC and LC in all the systems though CO_2 occupancy in cages initiates mainly after 10ns in most of the systems except for $H_2S(2:2)$ and bulk CO_2 where it occurs by 5ns. CO_2 dominates occupancy of both LC and SC in Xe(3:1) system similar to bulk CO_2 system. However, occupancy of SC by CH_4 is slightly lower in Xe(3:1) then bulk CO_2 system. The cage occupancy is dependent on conc. of Kr in Kr(3:1) and Kr(2:2) systems where LC are dominated by CO_2 at low conc of Kr, however, Kr occupies large number of LC along-with CO_2 at high conc of Kr in system respectively. Similar trend is observed in $N_2(3:1)$ and $N_2(2:2)$ systems though occupancy of LC by Kr at high conc. is comparatively less than CO_2 . H_2S and CO_2 compete to occupy small and large cages in $H_2S(2:2)$ system. The SC occupancy is Ar(2.5:1.5) system is $CO_2 > Ar > CH_4$, however, Ar and CH_4 compete to occupy LC and maximum LC are occupied by CO_2 . Interestingly, in

Xe(0.67):Ar(0.33) system, CH4 occupies more number of SC and LC then Xe and Ar as compared to lower occupancy of CH₄ than Xe and Ar in Xe(3:1) and Ar(2.5:1.5) systems.

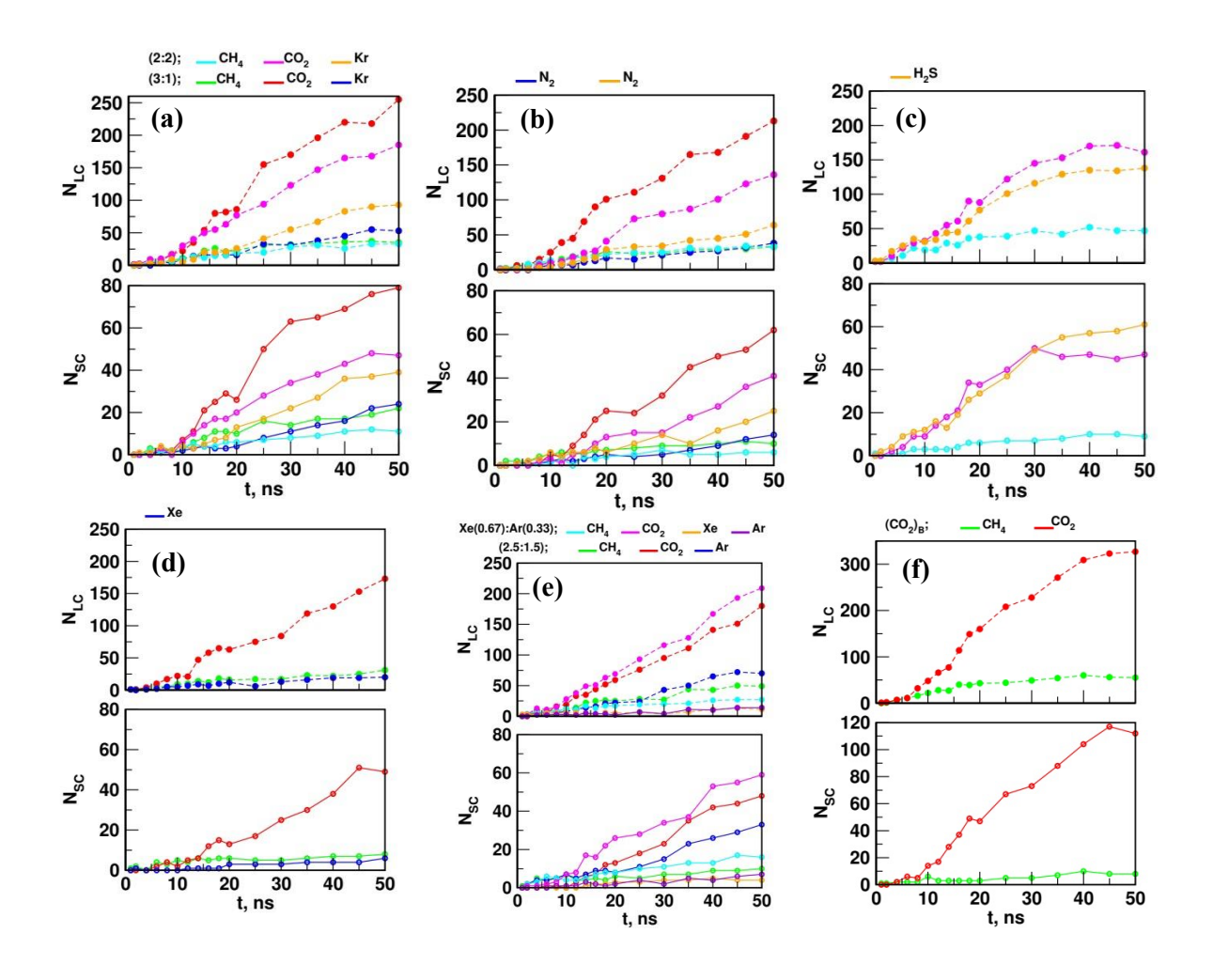


Figure 5.3: Number of small (N_{SC}) and large (N_{LC}) cages as a function of time for different gas species in different systems; (a) Kr(3:1) and Kr(2:2), (b) N_2 (3:1) and N_2 (2:2), (c) H_2 S(2:2), (d) Xe(3:1), (e) Xe(0.67):Ar(0.33) and Ar(2.5:1.5) and (f) (CO₂)_B.

Figure 5.4 and 5.5 show the formation of Y-shaped growth synthon in different system which is similar to results reported in previous Chapters during hydrate formation. Growth synthon (GS) is formed by the combination of three large and one small cages, where two large cages (L_1 and L_2) form the arms, third large(L_3) cage forms the tail and small cage (S) connects the arms and tails in the GS. We also report the number of water molecules around a gas species that form cages in a growth synthon as N_{WG} in Figure 5.6. The number of gas species that form a growth synthon are reported as N_{GG} in Figure 5.6 where any two gas species that belong to cage of growth synthon should be within a distance of 6-8Å. The number of gas species that form GS in Xe(3:1) are at a distance > 8Å till $t^* = 15\text{ns}$ as can be seen in Figures 5.4a and 5.6a.

There is formation of tri-cage [L₁(Xe)L₃(CH₄)S(CH₄)] by 17ns and a 4-caged GS was observed at t^* =27ns. Similarly, formation of a tri-cage cluster [L₁(Kr)L₃(Kr)S(Kr) and L₁(H₂S)L₃(CO₂)S(CO₂)] was observed in Kr(2:2) and H₂S(2:2) systems as shown in Figures 5.4b, 5.5a and 5.6(b-c) at t^* = 14ns and 13.6ns respectively. The GS in these systems were observed at t^* = 24ns and 28ns respectively. The formation of tri-cage cluster in presence of hydrate promoter is contrary to dual-cages (LL or LS) formed in systems without hydrate promoter (Chapters 2-4). However, we observed dual-cages (LL, CO₂ and N₂) at t^* = 13.6ns in N₂(2:2) system though larges cages are partially formed as shown in Figures 5.5b and 5.6d. Similar hydrate growth mechanism is observed in Ar(2.5:1.5) system as shown in Figures 5.5c and 5.6e where there is initial formation of LL dual cages formed by CH₄ molecules. The bulk CO₂ system shows formation of dual LL (CH₄ and CO₂) cages followed by tri-cage cluster leading to a growth synthon as reported in Figures 5.5d and 5.6f.

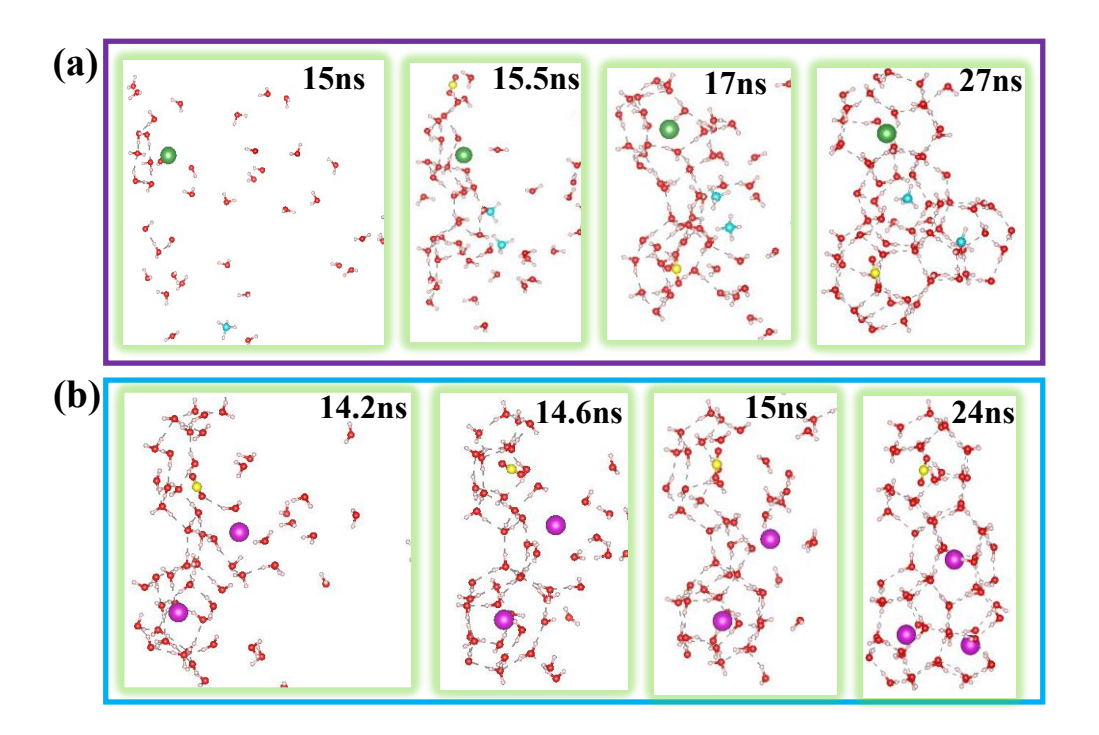


Figure 5.4: Snapshots of MD trajectories during formation of growth synthon in (a) Xe(3:1) at $t^* = 27ns$ and (b) Kr(2:2) at $t^* = 24ns$. The red, white, yellow, cyan, dark green and purple spheres represent oxygen, hydrogen, carbon (CO₂), carbon (CH₄), xenon and krypton atoms respectively.

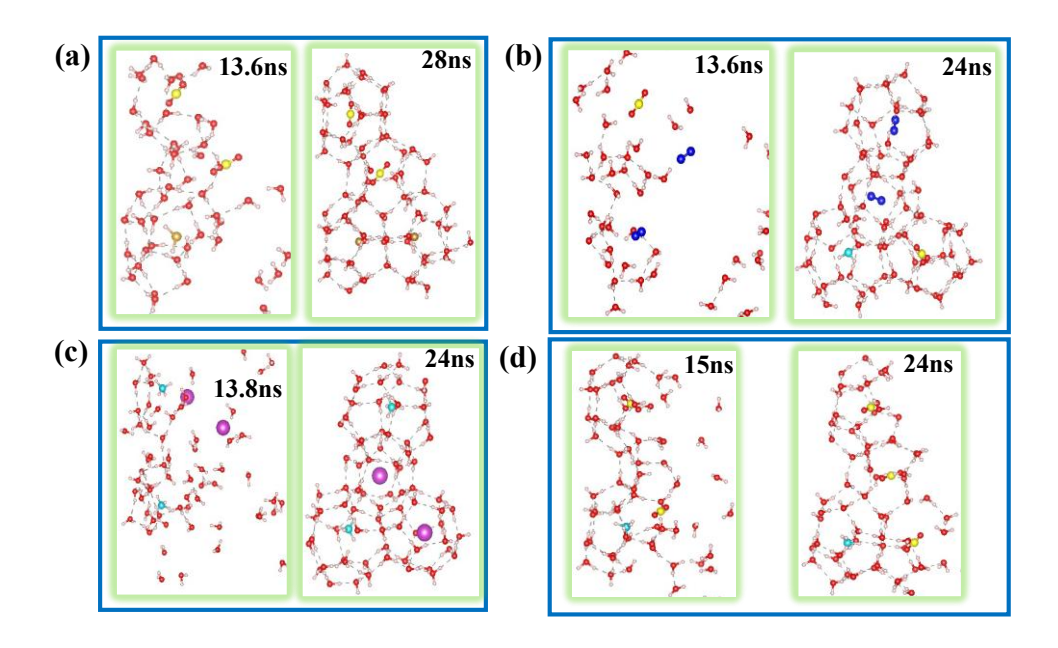


Figure 5.5: Snapshots of MD trajectories during formation of growth synthon in (a) $H_2S(2:2)$ at $t^* = 28$ ns, (b) $N_2(2:2)$ at $t^* = 24$ ns, (c) Ar(2.5:1.5) at $t^* = 24$ ns and (d) $(CO_2)_B$ at $t^* = 24$ ns. The red, white, yellow, cyan, brown, blue and purple spheres represent oxygen, hydrogen, carbon (CO_2) , carbon (CH_4) , sulfur, nitrogen and argon atoms respectively.

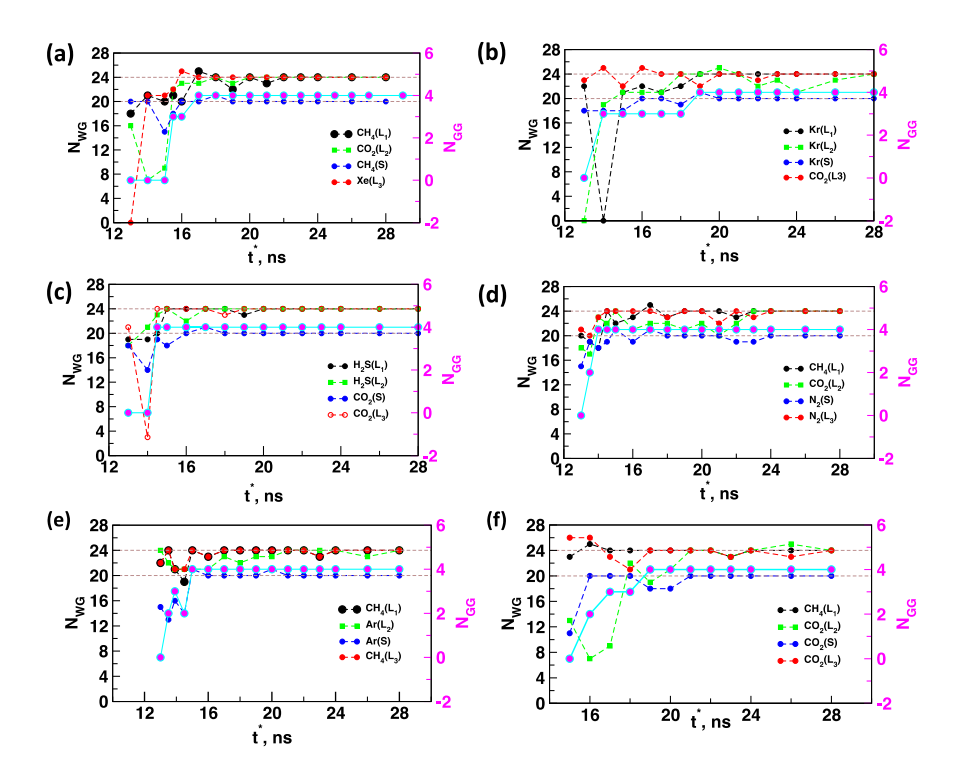


Figure 5.6: Guest-water (N_{GW}) and guest-guest (N_{GG}) coordination number of gas species in a growth synthon as a function of time (t^*) (a) Xe(3:1), (b) Kr(2:2), (c) H₂S(2:2), (d) N₂(2:2), (e) Ar(2.5:1.5) and (f) (CO₂)_B systems. The black, green, blue and red plot represent N_{WG} for large(L_1), large(L_2), small(S) and large(L_3) cages of growth synthon. Cyan and magenta plot represents the N_{GG} coordination number.

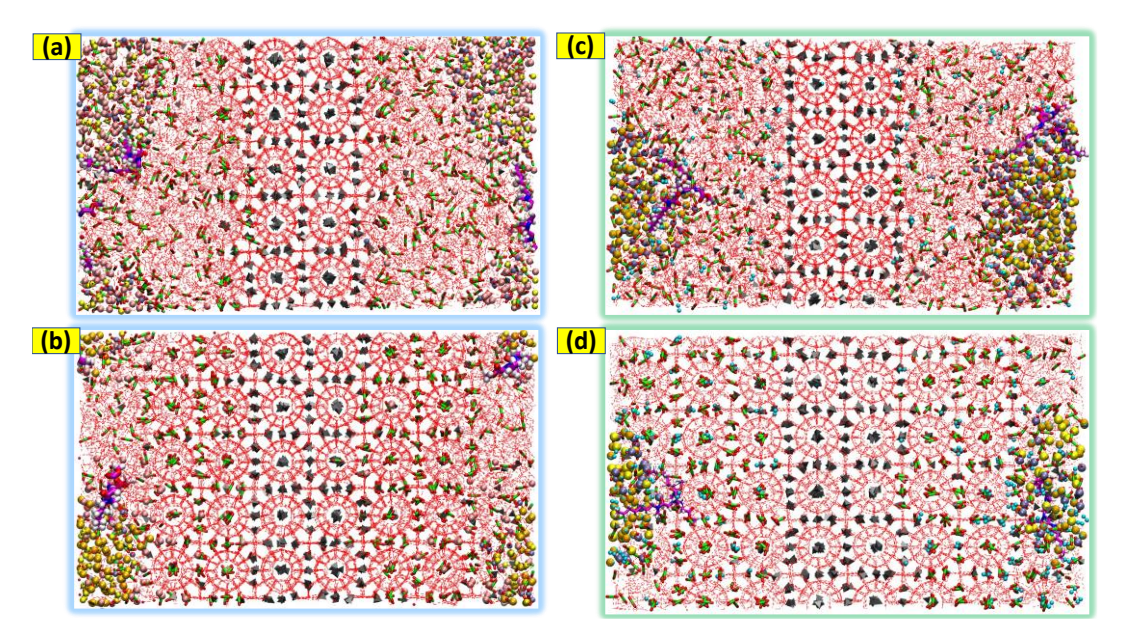


Figure 5.7: Schematic representation of cluster size and hydrate promoter in the system for (a-b) Xe(3:1) at 6ns and 60ns (c-d) N2(3:1) at 1ns and 60ns. Green sphere represents the gas molecules contains in the gas cluster. Rest of molecules are discarded for clear understanding. Cyan, white, red and blue sphere represent the carbon, hydrogen, oxygen and nitrogen of hydrate promoter. Hydrogen bonding and polyhedral representation used for water and methane of system, respectively.

The hydrate promoters preferred to be at the edges of the simulation box in all the systems as shown for reference in Xe(3:1) and $N_2(3:1)$ systems in Figure 5.7. The side groups of HP generated a hydrophobic region in bulk phase that lead to clustering of gas molecules near the HP and was observed during NVT simulations at 300K. In most of the systems, HP was near the gas clusters but in case of Kr(3:1) system, hydrophobic tail of HP interacted with gases in the gas cluster. The hydrate cages start forming when the temperature of simulation was lowered to 250K during NPT simulations and due to concentration gradient, gas species diffuse from the gas hydrates into solution. However, the rate of diffusion of gas species from cluster into the bulk phase varied based on the type of gas species. The gas species were assigned to the cluster based on coordination number of water molecules around the gas species. If the coordination number is 9 for distance between gas species and water being 6.0Å, gas species was assigned to the gas cluster else it belonged to the bulk solution. Figure 5.7 shows the ratio, R of gas species that belong to the gas cluster to gas species in the bulk solution as given in Eq. 5.1.

$$R_{\text{gas in cluster}} = \frac{\text{Number of gas molecules in cluster}}{\text{Number of gas molecules in bulk region}}$$
Eq. (5.1)

Figure 5.8a shows the ratio of all the gas species in a cluster as compared to gases in bulk solution and Figures 5.8(b-d) show R for a gas type (CH₄, CO₂ and G₃). The largest gas cluster was observed in Kr(2:2) system followed by Xe(3:1) system at the beginning of the production run as reported in Figure 5.8a. However, with time, Xe(3:1) system also forms similar-sized cluster and gas clusters are stable in both the systems over a long time. The gas cluster is the smallest in Xe(0.67):Ar(0.33) system followed by H₂S(2:2) system and cluster size in these systems is smaller than (CO₂)_B system. There are different trends in lifetime of clusters and amount of gas species in a cluster if we look at individual gas contribution to gas cluster as shown in Figures 5.8(b-d). CH₄ in gas clusters is retained for a longer time in Xe(3:1), Kr(2:2) and $N_2(3:1)$ systems than any other system which could enhance selectivity of other gases than CH₄ in the cages of first layer besides the interface. CH₄ contribution to gas cluster is least in Xe(0.67):Ar(0.33) system, however, maximum contribution in this system is due to Xe and Ar gases (Figure 5.8b). The contribution of third gas species (also fourth gas, Ar in Xe(0.67):Ar(0.33) system) is shown in Figure 5.8d where H₂S diffuses fastest out of gas cluster in H2S(2:2) system followed by N₂ in N₂(2:2) system. Xe in the gas cluster shows a slower decay than Kr cluster with time in Xe(3:1) and Kr(2:2) systems respectively. CO₂ is the most labile gas in all the systems as could be seen due to small ratio of R_{CO_2} in Figure 5.8c.

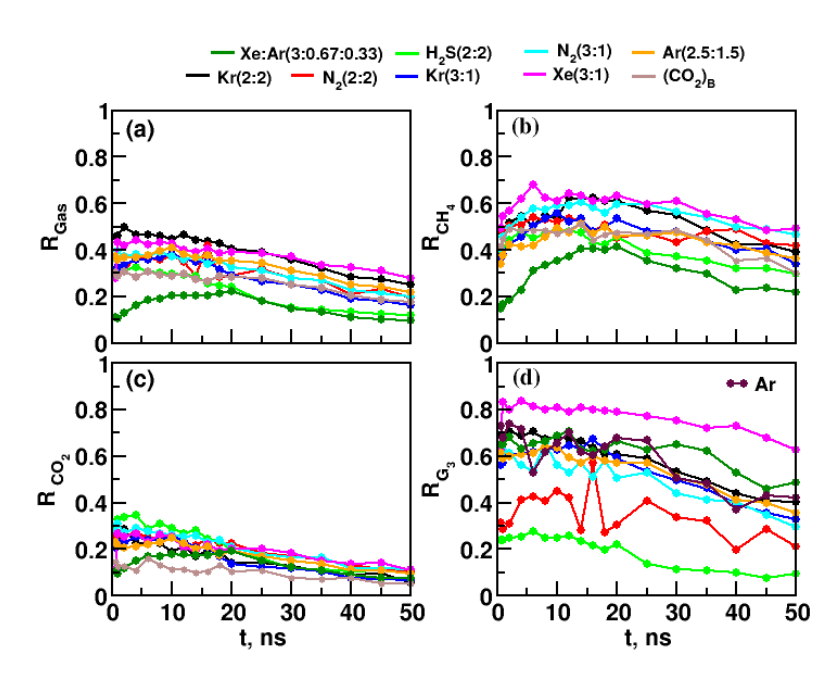


Figure 5.8: Ratio, R (a) all the gas species (b) methane (c) carbon dioxide and (d) third gas (G₃) in a gas cluster as a function of time (t, ns) in different systems.

Figure 5.9-5.11 shows the number of gas species in the simulation box as a function of time in terms of three regions on left (*Region -1*, *Region -2* and *Region -3*) and right (*Region 1*, *Region 2* and *Region 3*) sides of seed (here seed is *Region 0*) where each region is of 12.0Å along z-direction in the simulation box. Figure 5.9 shows that number of CH₄ molecules in different regions for different systems. *Regions -3* and 3 show a greater number of CH₄ molecules with time in all the systems due to the presence of hydrate promoter and gas cluster in these regions. The maximum number of CH₄ molecules in the *Regions 3* and -3 are observed in Xe(3:1) system as shown in Figure 5.9g. Similar scenario was observed in Xe:Ar(3:0.67:0.33) system (Figure 5.9h) but with time few CH₄ molecules diffused from *Regions 3* and -3 into the *Regions 2* and -2. There was diffusion of substantial number of CH₄ molecules between *Regions 2* and 3 with time in Kr(3:1) and N₂(3:1) systems with time as shown in Figure 5.9(e-f). However, high concentration of CH₄ was observed in *Region 1* in H₂S(2:2) system followed by N₂(2:2) and Kr(2:2) systems. Ar(2:5:1.5) system showed higher number of average number of CH₄ molecules in *Regions -1* and *1* than in *Regions -3* and 3. The bulk CO₂ system showed the highest number of CH₄ molecules in *Regions -1* and *1* as reported in Figure 5.9i.

Figure 5.10(a-i) shows the number of CO_2 molecules in different regions as a function of time in different systems. The minimum number of CO_2 molecules in the first layer beside the hydrate seed (*Regions -1* and *1*) were observed in $H_2S(2:2)$ system followed by systems with high conc. of third gas where CO_2 conc. decreases as $Kr(2:2) < Ar(2.5:1.5) < N_2$ (2:2). The highest number of CO_2 molecules in *Regions -1* and *1* were observed for Xe(3:1) system followed by Xe(0.67): $Ar(0.33) < Kr(3:1) < N_2(3:1)$ systems.

Figure 5.11(a-h) shows the 3rd gas distribution in different regions over time for all the systems and Figure 5.11i represent the 4th gas (i.e., Ar) distribution in Xe:Ar(3:0.67:0.33) system only, respectively. At low conentration, in the case of Xe(3:1), Xe:Ar(3:0.67:0.33) system, maximum amount of 3rd gas contains in the 3rd regions over other two regions and least diffusion was observer during simulation. It seems maximum amount of Xe participated in gas cluster fomation that can be seen in Figure 5.9d. N₂(3:1) behave similar to Xe(3:1) system unlike region (-3) showed higher exchange with neighbouring region over time. 3rd gas diffusion between 2nd and 3rd regions was found for Kr(3:1) system. Initially, 3rd gas concentration was high in 3rd regions that diffused with time. Region (3) showed the highest highest exchange with neighbouring region (3) over other sides. The number of third gas

molecules in first layer are higher than in other systems in Kr(2:2), N₂(2:2), H₂S(2:2) systems as shown in Figure 5.11(a-c). This is in contradiction to the observed trend of less number of CO₂ molecules in these systems in Figure 5.10(a-c). Similarly, Xe(3:1), N₂(3:1) and Xe(0.67):Ar(0.33) systems show less conc. of third and fourth gas in *Regions 1* and -1 which is contradictory to CO₂ conc. in these regions of these systems. The number of Xe and Ar atoms are the lowest in *Regions 1* and -1 in Xe(0.67):Ar(0.33) system.

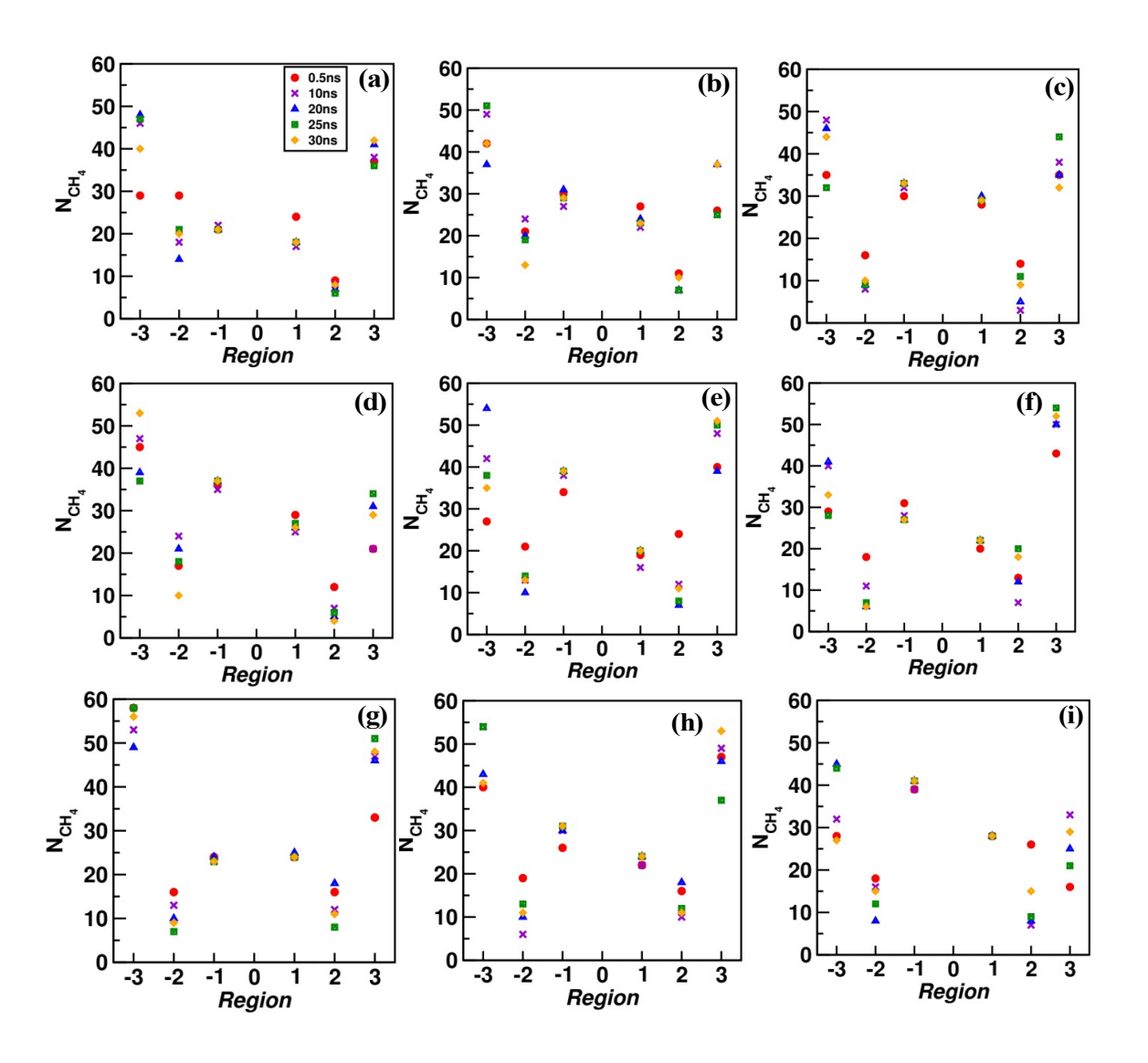


Figure 5.9: Number of CH_4 molecules as a function of time in different regions on left and right side of hydrate seed (region 0) in different systems: (a) Kr(2:2) (b) $N_2(2:2)$ (c) $H_2S(2:2)$ (d) Ar(2.5:1.5) (e) Kr(3:1) (f) $N_2(3:1)$ (g) Xe(3:1) (h) Xe:Ar(3:0.67:0.33) and (i) $Bulk CO_2$.

We calculated the percentage of CO₂ selectivity, S over CH₄ in different systems as shown in Eq (5.2), where N_{gas} is the number of gas molecules of a gas species and N_{total} are the total number of gas molecules in the first hydrate layer formed in bulk phase. Selective sequestration of CO₂ over CH₄ is calculated as CO₂ selectivity, ΔS_{CM} which is difference in selectivity of CO₂ and CH₄ as shown in Eq (5.3). Similarly, total selectivity, ΔS_{TM} is difference in selectivity of CO₂ and third gas, G₃ (except in Xe:Ar (0.67:0.33) system where 4th gas also included) over CH₄ as shown in Eq. (5.4).

$$S_{gas}\% = \left(\frac{N_{gas}}{N_{total}}\right) 100$$
 Eq. (5.2)

$$\Delta S_{CM}(\%) = S_{CO2}(\%) - S_{CH4}(\%)$$
 Eq. (5.3)

$$\Delta S_{TM}(\%) = S_{CO_2+G_3}(\%) - S_{CH4}(\%)$$
 Eq. (5.4)

Figure 5.12(a-b) shows ΔS_{CM} and ΔS_{TM} for ordered and total hydrate cages, respectively in different systems where number of ordered cages are calculated using GRADE code and total cages are calculated based on hydrate layer dimension (i.e., 12.0Å from interface along z-axis) for the first layer. Xe(3:1) showed the highest CO₂ selectivity (ΔS_{CM}) both for ordered (65%) and total (66%) cages. However, Ar(2.5:1.5) shows poor CO₂ selectivity in the presence of the hydrate promoter. This is contradictory to poor CO₂ selectivity observed in Xe(3:1) system and best selectivity observed for Ar(2.5:1.5) system in absence of hydrate promoter (Chapter 4). Similarly, good ΔS_{CM} (61%) was observed in Xe:Ar(3:0.67:0.33) for both ordered and total cages. However, H₂S(2:2) the lowest CO₂ selectivity. All other systems with third gases Kr and N₂ show lower selectivity than Xe(3:1) but higher than Ar(2.5:2.5) system. The selectivity for CO₂ in a system can be compared with bulk CO₂ system only in terms of total selectivity (ΔS_{TM}) as both CO₂ and third gas constitute the gases other than only CO₂ in bulk phase in bulk CO₂ system. The total selectivity for both ordered and total cages is relatively higher in all the systems as compared to CO₂ selectivity. Xe(3:1) system shows good total selectivity both in ordered(74%) and total(73%) cages similar to CO₂ selectivity in this system. Interestingly, Kr(2:2) system also shows large total selectivity for both ordered (74.0%) and total (77%) cages that suggests that Kr along-with CO₂ competes with CH₄ to occupy cages in Kr(2:2) system.

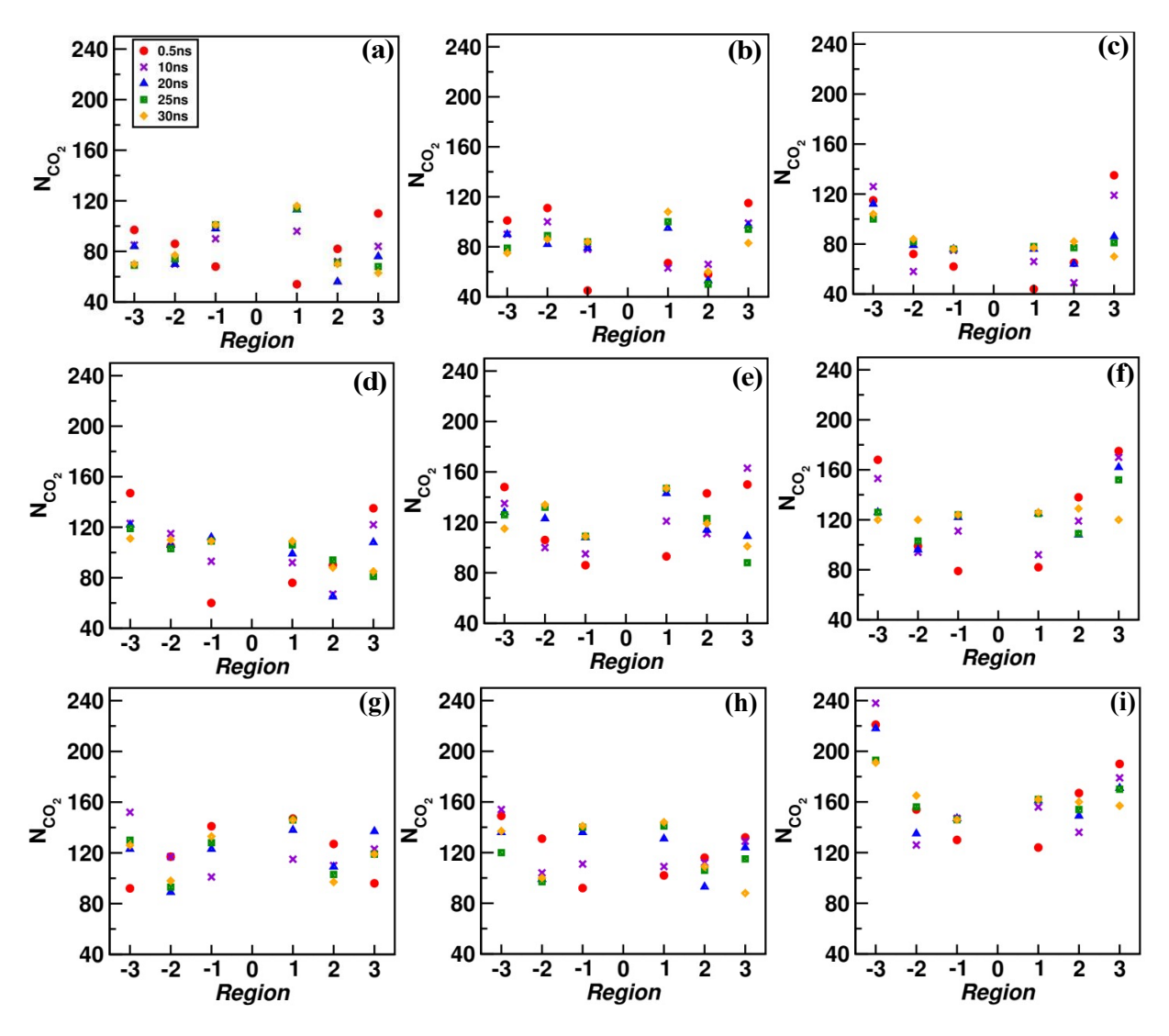


Figure 5.10: Number of CO_2 molecules as a function of time in different regions on left and right side of hydrate seed (region 0) in different systems: (a) Kr(2:2) (b) $N_2(2:2)$ (c) $H_2S(2:2)$ (d) Ar(2.5:1.5) (e) Kr(3:1) (f) $N_2(3:1)$ (g) Xe(3:1) (h) Xe:Ar(3:0.67:0.33) and (i) Bulk CO_2 .

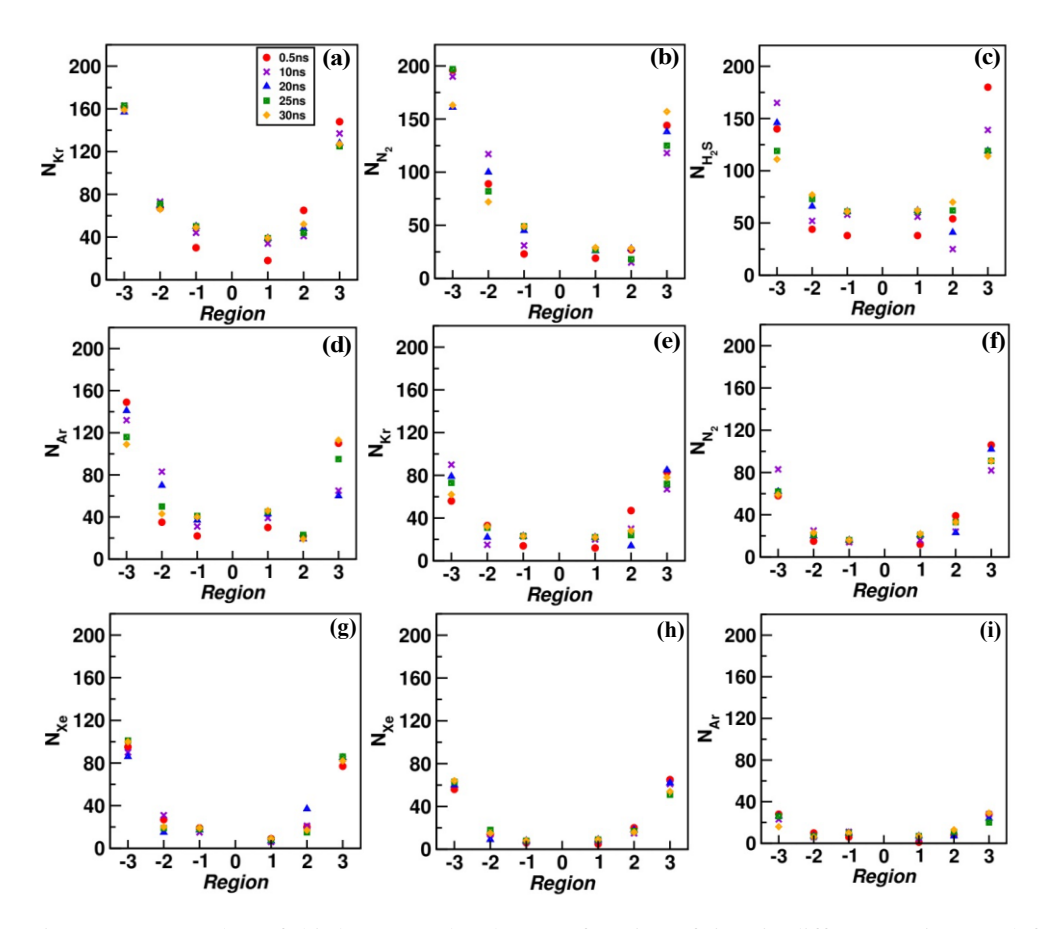


Figure 5.11: Number of third guest molecules as a function of time in different regions on left and right side of hydrate seed (region 0) in different systems: (a) Kr(2:2) (b) $N_2(2:2)$ (c) $H_2S(2:2)$ (d) Ar(2.5:1.5) (e) Kr(3:1) (f) $N_2(3:1)$ (g) Xe(3:1) (h) Xe in Xe:Ar(3:0.67:0.33) and (i) Ar in Xe:Ar(3:0.67:0.33).

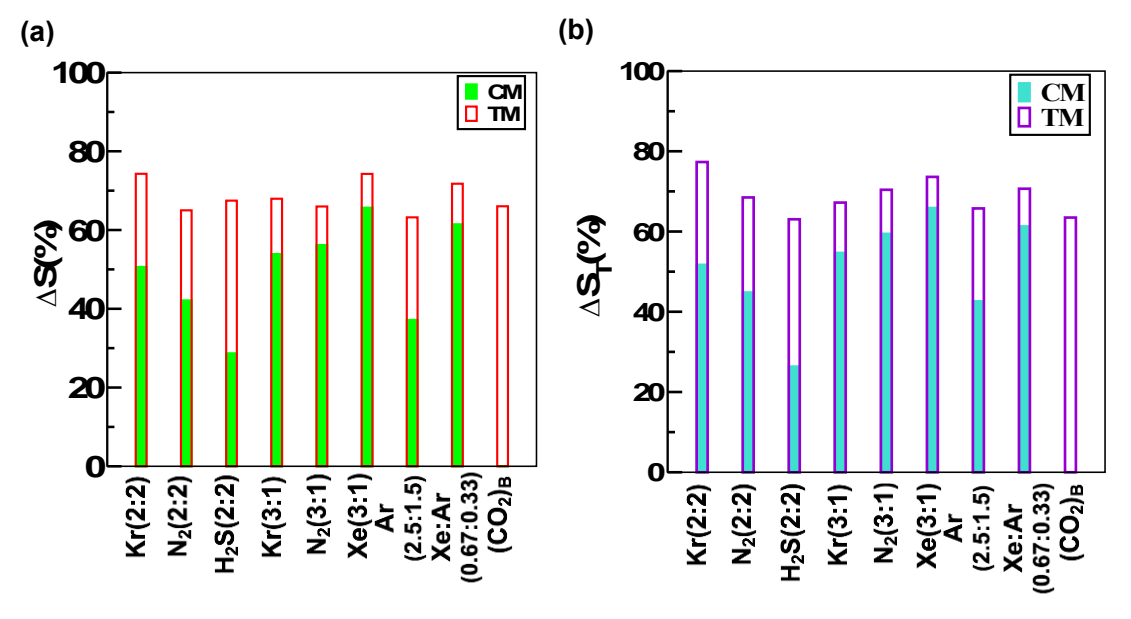


Figure 5.12: Selectivity (ΔS) in (a) Ordered cages (b) Total (Ordered + Disordered cages) hydrate cages in different systems. Here, CM represents selectivity of CO_2 over CH_4 and TM represents selectivity of both CO_2 and third gas (in Xe:Ar (0.67:0.33) system where fourth gas is also included) as compared to CH_4 .

Conclusions

The present work reports the role of hydrate promoter in selective inclusion of CO_2 in sI-NGHs in presence of polyatomic and monatomic third gases. The hydrate growth occurs via growth synthon as was observed in systems without hydrate promoter (Chapters 2-4). However, formation of three-caged aggregate in the initial stages of formation of growth synthon is observed in presence of hydrate growth unlike the dual cages in systems without hydrate promoter. There is formation of gas cluster near the hydrate promoter in all the system. The lifetime of cluster is short in systems with H_2S and N_2 as third gases and lifetime is the largest in Xe(3:1) system. The hydrate formation time reduces in presence of growth synthon in most of the systems as compared to systems without hydrate promoter in Chapter 2 and 3, for e.g. in Kr(2:2) system, t = 25ns in presence of HP and 52ns in absence of HP; in Kr(3:1) system, t = 25ns, in presence of HP and 45ns in absence of HP and in $H_2S(2:2)$ system, t = 16ns in presence of HP and 55ns in absence of HP. Interestingly, though Xe(3:1) shows slow hydrate growth in presence of HP (t = 42ns) as compared to system without HP (t = 28ns) but in current work Xe(3:1) shows highest selectivity for CO_2 among all third gas systems unlike poor CO_2 selectivity of Xe(3:1) system in the absence of hydrate promoter.

References

- 1. Mu, L.; Solms, N. v. Experimental Study on Methane Production from Hydrate-Bearing Sandstone by Flue Gas Swapping. *Energy Fuels* **2018**, 32, 8167–8174.
- 2. Sloan, E. D.; Koh, C. A. Clathrate Hydrates of Natural Gases, 3rd ed.; CRC Press: Boca Raton, FL, **2008**.
- 3. Sloan, E. D. Fundamental Principles and Applications of Natural Gas Hydrates. Nature 2003, 426, 353–363.
- 4. Walsh, M. R.; Beckham, G. T.; Koh, C. A.; Sloan, E. D.; Wu, D. T.; Sum, A. K. Methane Hydrate Nucleation Rates from Molecular Dynamics Simulations: Effects of Aqueous Methane Concentration, Interfacial Curvature, and System Size. *J. Phys. Chem. C* **2011**, 115, 21241–21248.

- 5. Li, X.-S.; Xu, C.-G.; Zhang, Y.; Ruan, X.-K.; Li, G.; Wang, Y. Investigation into gas production from natural gas hydrate: A review. *Applied Energy*, **2016**, 172, 286–322.
- 6. Collett, T. S; Ginsburg, G. D. Gas hydrates in the Messoyakha gas field of the west Siberian basin a re-examination of the geologic evidence. *Int Offshore Polar E* **1997**, 96–103.
- 7. Holder, G. D.; Angert, P. F.; John, V. T.; Yen, S. A Thennodynamic Evaluation of Thennal Recovery of Gas From Hydrates in the Earth. *J Petrol Technol* **1982**, 34,1127–32.
- 8. Sira, J. H.; PatH, S. L.; Kamath, V. A. Study of Hydrate Dissociation by Methanol and Glycol Injection. *Society of Petroleum Engineers Inc.* **1990**, 977,984.
- Qorbani, K.; Kvamme, B.; Kuznetsova, T. Simulation of CO2 Storage into Methane Hydrate Reservoirs, Non-equilibrium thermodynamic Approach. *Energy Procedia*, 2017, 114, 5451 – 5459.
- 10. Zhang, Y.; Cui, M.; Xin, G.; Li, D. Microscopic insights on the effects of flue gas components on CH4 –CO2 replacement in natural gas hydrate. *Gas Science and Engineering* **2023**, 112, 204947.
- Stanwix, P. L.; Rathnayake, N. M.; Obanos, F. P. P. D. O.; Johns, M. L.; Aman, Z. M.;
 May. E. F. Characterising thermally controlled CH4–CO2 hydrate exchange in unconsolidated sediments. *Energy Environ. Sci.* 2018, 11, 1828.
- Cladek, B. R.; Everett, S. M.; McDonnell, M. T.; Kizzire, D. G.; Tucker, M. G.; Keffer, D. J.; Rawn, C. J. Local structure analysis of low-temperature neutron pair distribution function coupled with molecular dynamics simulations of CH4 and CO2 hydrates from 2 to 210 K. *Fuel* 2021, 299, 120908.
- 13. Lee, Y.; Kim, Y.; Lee, J.; Lee, H.; Seo, Y. CH4 recovery and CO2 sequestration using flue gas in natural gas hydrates as revealed by a micro-differential scanning calorimeter. *Applied Energy* **2015**, 150, 120–127.
- 14. Liu, J.; Yan, Y.; Liu, H.; Xu, J.; Zhang, J.; Chen, G.; Understanding effect of structure and stability on transformation of CH4 hydrate to CO 2 hydrate. *Chemical Physics Letters* **2016**, 648, 75–80.
- Ota, M.; Saito, T.; Aida, T.; Watanabe, M.; Sato, Y.; Jr., R. L. S.; Hiroshi Inomata, H. Macro and Microscopic CH4–CO2 Replacement in CH4 Hydrate Under Pressurized CO2. *AIChE Journal* 2007, 53, 10.

- 16. Heeschen, K. U.; Deusner, C.; Spangenberg, E.; Priegnitz, M.; Kossel, E.; Strauch, B.; Bigalke, N.; Luzi-Helbing, M.; Haeckel, M.; Schicks, J. M. Production Method under Surveillance: Laboratory Pilot-Scale Simulation of CH4–CO2 Exchange in a Natural Gas Hydrate Reservoir. *Energy Fuels* 2021, 35, 10641–10658.
- 17. Jadhawar, P.; Yang, J.; Chapoy, A.; Tohidi, B.; Subsurface Carbon Dioxide Sequestration and Storage in Methane Hydrate Reservoirs Combined with Clean Methane Energy Recovery. *Energy Fuels* **2021**, 35, 1567–1579.
- 18. Boswell, R.; Schoderbek, D.; Collett, T. S.; Ohtsuki, S.; White, M; Anderson, B. J. The Ig nik Sikumi Field Experiment, Alaska North Slope: Design, Operations, and Implications for CO2–CH4 Exchange in Gas Hydrate Reservoirs. *Energy Fuels* **2017**, 31, 140–153.
- 19. Chen, Y.; Gao, Y.; Chen, L.; Wang, X.; Liu, K.; Sun, B. Experimental investigation of the behavior of methane gas hydrates during depressurization-assisted CO2 replacement. *Journal of Natural Gas Science and Engineering* **2019**, 61, 284–292.
- Lee, S.; Lee, Y.; Lee, J.; Lee, H.; Seo, Y.; Experimental Verification of Methane–Carbon Dioxide Replacement in Natural Gas Hydrates Using a Differential Scanning Calorimeter. *Environ. Sci. Technol.* 2013, 47, 13184–13190.
- 21. Zhou, X.; Lin, F.; Liang, D.; Multiscale Analysis on CH4-CO2 Swapping Phenomenon Occurred in Hydrates. *J. Phys. Chem. C* **2016**, 120, 25668–25677.
- 22. Goel, N. In situ methane hydrate dissociation with carbon dioxide sequestration: current knowledge and issues. *J Petrol Sci Eng* **2006**, 51, 169–184.
- 23. Horvat, K.; Kerkar, P.; Jones, K.; Mahajan, D. Kinetics of the Formation and Dissociation of Gas Hydrates from CO2-CH4 Mixtures. *Energies* **2012**, *5*, 2248-2262.
- 24. Ndlovu, P.; Babaee, S.; Naidoo, P. Review on CH4-CO2 replacement for CO2 sequestration and CH4/CO2 hydrate formation in porous media. *Fuel* **2022**, 320, 123795.
- 25. Gambelli, A. M.; Presciutti, A.; Rossi, F. Review on the characteristics and advantages related to the use of flue-gas as CO2/N2 mixture for gas hydrate production. Fluid *Phase Equilibria* **2021**, 541, 113077.

- 26. Park, Y.; Kim, D.-Y.; Lee, J.-W.; Huh, D.-G.; Park, K.-P.; Lee, J.; Lee, H. Sequestering carbon dioxide into complex structure of naturally occurring gas hydrates. *PNAS* **2006**, 103, 34, 12690 –12694.
- 27. Cha, M.; Shin, K.; Lee, H.; Moudrakovski, I. L.; Ripmeester, J. A.; Seo, Y. Kinetics of Methane Hydrate Replacement with Carbon Dioxide and Nitrogen Gas Mixture Using in Situ NMR Spectroscopy. *Environ. Sci. Technol.* **2015**, 49, 1964–1971.
- 28. Tupsakhare, S. S.; Castaldi, M. J. Efficiency enhancements in methane recovery from natural gas hydrates using injection of CO2/N2 gas mixture simulating in-situ combustion. *Applied Energy* **2019**,236, 825–836.
- 29. Koh D. Y.; Kang H.; Kim D. O.; Park J.; Cha M.; Lee H. Recovery of methane from gas hydrates intercalated within natural sediments using CO2 and a CO2/N2 gas mixture. *ChemSusChem* **2012**, 5, 1443–1448.
- 30. Zhou, X.; Liang, D.; Liang, S.; Yi, L.; Lin, F. Recovering CH4 from Natural Gas Hydrates with the Injection of CO2-N2 Gas Mixtures. *Energy Fuels* **2015**, 29, 1099-1106.
- 31. Chaturvedi, K. R.; Sinha, A. S. K.; Nair, V. C.; Sharma, T. Enhanced carbon dioxide sequestration by direct injection of flue gas doped with hydrogen into hydrate reservoir: Possibility of natural gas production. *Energy*, **2021** 227, 120521.
- 32. Hassanpouryouzband, A.; Yang, J.; Tohidi, B.; Chuvilin, E.; Istomin, V.; Bukhanov, B.; Cheremisin, A. CO 2 Capture by Injection of Flue Gas or CO2–N2 Mixtures into Hydrate Reservoirs: Dependence of CO2 Capture Efficiency on Gas Hydrate Reservoir Conditions. *Environ. Sci. Technol.* **2018**, 52, 4324–4330.
- 33. Majid, A. A. M.; Worley, J.; Koh, C. A. Thermodynamic and Kinetic Promoters for Gas Hydrate Technological Applications. **Energy Fuels 2021**, 35, 19288–19301.
- 34. de Deugd, R. M.; Jager, M. D.; de Swaan Arons, J. Mixed Hydrates of Methane and Water-Soluble Hydrocarbons Modeling of Empirical Results. A*IChE J.* **2001**, 3, 47, 693–704.
- 35. Khan, M. N.; Peters, C. J.; Koh, C. A. Desalination using gas hydrates: The role of crystal nucleation, growth and Separation. *Desalination* **2009**, 468,114049.

- 36. Arjmandi, M.; Chapoy, A.; Tohidi, B. Equilibrium Data of Hydrogen, Methane, Nitrogen, Carbon Dioxide, and Natural Gas in Semi-Clathrate Hydrates of Tetrabutyl Ammonium Bromide. *J. Chem. Eng. Data* **2007**, *52*, 2153-2158.
- 37. Mohammadi, A. H.; Richon, D. Phase Equilibria of Binary Clathrate Hydrates of Nitrogen+ Cyclopentane/Cyclohexane/Methyl Cyclohexane and Ethane+Cyclopentane/Cyclohexane/Methyl Cyclohexane. *Chemical Engineering Science 2011*, 66, 4936–4940.
- 38. Seo, Y.-T.; Kang, S.-P.; Lee, H. Experimental determination and thermodynamic modeling of methane and nitrogen hydrates in the presence of THF, propylene oxide, 1,4-dioxane and acetone. *Fluid Phase Equilib.* **2001**, 189, 99–110.
- 39. Asadi, F.; Nguyen, N. N.; Nguyen, A. V. Synergistic Effects of Sodium Iodide and Sodium Dodecyl Sulfate at Low Concentrations on Promoting Gas Hydrate Nucleation. *Energy Fuels* **2020**, 34, 9971–9977.
- 40. Bhattacharjee, G.; Choudhary, N.; Kumar, A.; Chakrabarty, S.; Kumar, R. Effect of the Amino Acid L-Histidine on Methane Hydrate Growth Kinetics. *J. Nat. Gas Sci. Eng.* **2016**, 35, 1453–1462.
- 41. Arjang, S.; Manteghian, M.; Mohammadi, A. Effect of Synthesized Silver Nanoparticles in Promoting Methane Hydrate Formation at 4.7 MPa and 5.7 MPa. *Chem. Eng. Res. Des.* **2013**, 91, 1050–1054.
- 42. Liu, G.-Q.; Wang, F.; Luo, S.-J.; Xu, D.-Y.; Guo, R.-B. Enhanced Methane Hydrate Formation with SDS-Coated Fe3O4 Nanoparticles as Promoters. *J. Mol. Liq.* **2017**, 230, 315–321.
- 43. Mohammad-Taheri, M.; Moghaddam, A. Z.; Nazari, K.; Zanjani, N. G. Methane Hydrate Stability in the Presence of Water-Soluble Hydroxyalkyl Cellulose. *J. Nat. Gas Chem.* **2012**, 21, 119–125.
- 44. Asadi, F.; Metaxas, P. J.; Lim, V. W. S.; Nguyen, T. A. H.; Aman, Z. M.; May, E. F.; Nguyen, A. V. Cyclodextrins as Eco-Friendly Nucleation Promoters for Methane Hydrate. *Chem. Eng. J.* **2021**, 417, 127932.
- 45. Fakharian, H.; Ganji, H.; Naderi Far, A.; Kameli, M. Potato Starch as Methane Hydrate Promoter. *Fuel* **2012**, 94, 356–360.
- 46. Albertí, M; Costantini, A.; Laganá, A.; Pirani, F. Are Micelles Needed to Form Methane Hydrates in Sodium Dodecyl Sulfate Solutions? *J. Phys. Chem. B* **2012**, 116, 4220–4227.

- 47. Albertí, M.; Pirani, F.; Laganà, A. Carbon Dioxide Clathrate Hydrates: Selective Role of Intermolecular Interactions and Action of the SDS Catalyst. *J. Phys. Chem. A* **2013**, 117, 6991–7000.
- 48. Pavelyev, R. S.; Gainullin, S. E.; Semenov, M. E.; Zaripova, Y. F.; Yarkovoi, V. V.; Luneva, A. I.; Farhadian, A.; Varfolomeev, M. A. Dual Promotion—Inhibition Effects of Novel Ethylenediaminetetraacetic Acid Bisamides on Methane Hydrate Formation for Gas Storage and Flow Assurance Applications. *Energy Fuels* **2022**, 36, 290–297.
- 49. Abascal, J. L. F.; Vega, C. A general purpose model for the condensed phases of water: TIP4P/2005. *J. Chem. Phys.* 2005, 123, 234505.
- 50. RYCKAERT, J.-P.; CICCOTTI, G.; BERENDSEN, H. J. C. Numerical integration of the Cartesian Equations of Motion of a System with Constraints: Molecular Dynamics of n-Alkanes. *JOURNAL OF COMPUTATIONAL PHYSICS* **1977**, 23, 321-341.
- 51. Jorgensen, W. J.; Maxwell, D. S.; Tirado-Rives. J. Development and Testing of the OPLS All-Atom Force Field on Conformational Energetics and Properties of Organic Liquids. J. Am. Chem. Soc. 1996, 118, 11225-11236.
- 52. Cygan, R. T. Molecular Simulation of Carbon Dioxide Capture by Montmorillonite Using an Accurate and Flexible Force Field. *J. Phys. Chem. C* **2012**, 116, 13079–13091.
- 53. Somasundaram, T.; Panhuis, M. I. H.; Lynden-Bell, R. M.; Patterson, C. H. A simulation study of the kinetics of passage of CO2 and N2 through the liquid/vapor interface of water. *J. Chem. Phys.* **1999**, 111, 2190.
- 54. Huang, P.-H. Molecular dynamics investigation of separation of hydrogen sulfide from acidic gas mixtures inside metal-doped graphite micropores. *Phys. Chem. Chem. Phys.* **2015**, 17, 22686.
- 55. VERLET, L.; WEIS, J.-J. Perturbation theory for the thermodynamic properties of simple liquids. *MOLECULAR PHYSICS*, **1972**, 24, 5, 1013-1024.
- 56. PLIMPTON, S.; Fast Paralled Algorithms for Short-Range Molecular Dynamics. *J OURNAL OF COMPUTATIONAL PHYSICS*, **1995**, 117, 1-19.
- 57. Hoover, W. G. Canonical dynamics: Equilibrium phase-space distributions. *PHYSICAL REVIEW A* **1985**, 31, 3.
- 58. Hoover, W. G. Constant-pressure equations of motion. *PHYSICAL REVIEW A* **1986**, 34, 3.
- 59. MELCHIONNA, S.; CICCOTTI. G.; HOLIAN, B. L. Hoover NPT dynamics for systems varying in shape and size. MOLECULAR PHYSICS **1993**, 78, 3, 533-544.
- 60. Hockney, R. W.; Eastwood, J. W. Computer Simulation Using Particles, Adam Hilger, NY, **1989**.

- 61. Moon, C.; Hawtin, R. W.; Rodger, P. M. Nucleation and control of clathrate hydrates: insights from simulation. *Faraday Discuss.* **2007**, 136, 367–382.
- 62. Rodger, P. M.; Forester, T. R.; Smith, W. Simulations of the methane hydrate / methane gas interface near hydrate forming conditions. *Fluid Phase Fxluilibria* **1996**,116, 326-332.
- 63. Mahmoudinobar, F.; Dias, C. L. GRADE: A code to determine clathrate hydrate structures. *Computer Physics Communications* **2019**, 244, 385–391.

Chapter 6

Future Directions

Current work highlights the role of third gases in enhancing CO₂ selectivity in different systems at 250K and 15MPa. Argon is one of the promising third gases for enhancing CO₂ selectivity in the absence of hydrate promoter at low temperature and high pressure and Xe shows the poorest CO₂ selectivity in sI NGHs. However, the trend is reversed in the presence of hydrate promoter (EDTA Bisamides) where Xe showed the highest CO₂ selectivity. Moreover, few third gases like Kr and H₂S showed different trends in formation of hydrate under different conditions. Based on the current insights from the role of third gas in governing the CO₂ selectivity in sI-NGHs, we proposed the following aspects that could be explored in future.

ROLE OF CONCENTRATION OF THIRD GAS – In this thesis, we explored only two ratios of CO₂ and third gases, 3:1 and 2:2 for all the third gases except Ar. Future work would focus on exploring other CO₂ and third gas ranges and their effect in CO₂ selective sequestration in natural gas hydrates.

ROLE OF TEMPERATURE AND PRESSURE - sI-NGHs with methane or carbon dioxide as guest species have been explored over a wide range of temperature (250K to 280K) and pressure (1MPa to 15MPa) ¹. However, the temperature and pressure in realistic conditions at sea floors that favor methane hydrates are in range of 270K to 277K and pressure up-to 5MPa. The future works would explore the effect of third gases on CH₄-CO₂ exchange with different range of temperatures and pressures especially in temperature and pressure range which is feasible for ocean floors.

ROLE OF HYDRATE PROMOTER - The current work highlights the formation of gas clusters in presence of hydrate promoter, EDTA Bisamide. The future work would involve understanding into the role of length of alkyl chains of EDTA Bisamides in formation of gas hydrates with its effect on hydrate formation and CO₂ selectivity in presence of different third gases in CH₄-CO₂ exchange in sI-NGHs. The insights from these studies would be helpful to generate a library of novel, biodegradable hydrate promoters that could enhance selectivity of CO₂ at low concentrations of third gas species as to enhance more encapsulation of CO₂ in gas hydrate cages.

ROLE OF MIXTURE OF THIRD GASES – Chapter 4 explored the role of mixture of few of the monatomic and polyatomic gases in CH₄-CO₂ exchange in sI-NGHs. The future work would include simulation and analysis for other polyatomic gases (CO, N₂O and NO) and monatomic gases (Ne, Ar, Kr and Xe) in CH₄-CO₂ exchange in sI-NGHs.

References

 Circone, S.; Stern, L. A.; Kirby, S. H.; Durham, W. B.; Chakoumakos, B. C.; Rawn, C. J.; Rondinone, A. J.; Ishii, Y. CO₂ Hydrate: Synthesis, Composition, Structure, Dissociation Behavior, and a Comparison to Structure I CH4 Hydrate. *J. Phys. Chem. B* 2003, 107, 5529-5539.

Selective Sequestration of Carbon dioxide in Natural Gas Hydrates – Role of Third Gas

by Satyam Singh

.ibrarian

Indira Gandhi Memorial Library UNIVERSITY OF HYDERABAD Central University P.O.

HYDERABAD-500 046.

Submission date: 17-Aug-2023 10:07AM (UTC+0530)

Submission ID: 2146918081

File name: Satyam_Singh.pdf (810.04K)

Word count: 22425

Character count: 106063

Selective Sequestration of Carbon dioxide in Natural Gas Hydrates - Role of Third Gas ORIGINALITY REPORT STUDENT PAPERS **PUBLICATIONS** INTERNET SOURCES SIMILARITY INDEX **PRIMARY SOURCES** digitalcommons.njit.edu Internet Source Liwei Cheng, Kai Liao, Zhi Li, Jinlong Cui, Bei Liu, Fengguang Li, Guangjin Chen, Changyu Sun. "The invalidation mechanism of kinetic hydrate inhibitors under high subcooling conditions", Chemical Engineering Science, 2019 Publication Yi, Lizhi, Deqing Liang, Shuai Liang, and Xuebing Zhou. "Molecular dynamics study of CH4 -CO2 mixed hydrate dissociation: Molecular Dynamics Study of CH4 -CO2", Asia-Pacific Journal of Chemical Engineering, 2015. Publication Alessandro Barducci. "Metadynamics", Wiley <1% Interdisciplinary Reviews Computational Molecular Science, 09/2011 Publication

5	Lizhi Yi, Deqing Liang, Xuebing Zhou, Dongliang Li. "Molecular dynamics simulations for the growth of CH4-CO2 mixed hydrate", Journal of Energy Chemistry, 2014 Publication	<1%
6	susi.usi.ch Internet Source	<1%
7	ir.lib.uwo.ca Internet Source	<1%
8	pubs.rsc.org Internet Source	<1%
9	Nianxiang Qiu, Xiaojing Bai, Ningru Sun, Xiaohui Yu, Longbin Yang, Yanjun Li, Minghui Yang, Qing Huang, Shiyu Du. "Grand Canonical Monte Carlo Simulations on Phase Equilibria of Methane, Carbon Dioxide, and Their Mixture Hydrates", The Journal of Physical Chemistry B, 2018	<1%
10	d-nb.info Internet Source	<1%
11	digitalassets.lib.berkeley.edu Internet Source	<1%
12	www.ourenergypolicy.org Internet Source	<1%

13	Xin Zheng, Limin Wang, Zhi Li, Weixin Pang, Qingping Li, Guangjin Chen, Bei Liu. "Molecular insight into the dissociation and re-formation of methane hydrate in silica nano-slit", Fuel, 2022 Publication	<1%
14	pubman.mpdl.mpg.de Internet Source	<1%
15	Alberto Maria Gambelli, Andrea Presciutti, Federico Rossi. "Review on the characteristics and advantages related to the use of flue-gas as CO2/N2 mixture for gas hydrate production", Fluid Phase Equilibria, 2021	<1%
16	Seungmin Lee, Yohan Lee, Jaehyoung Lee, Huen Lee, Yongwon Seo. "Experimental Verification of Methane–Carbon Dioxide Replacement in Natural Gas Hydrates Using a Differential Scanning Calorimeter", Environmental Science & Technology, 2013 Publication	<1%
17	Dong-Yeun Koh, Hyery Kang, Jong-Won Lee, Youngjune Park, Se-Joon Kim, Jaehyoung Lee, Joo Yong Lee, Huen Lee. "Energy-efficient natural gas hydrate production using gas exchange", Applied Energy, 2016 Publication	<1%

18	R.A. Latour. "3.14 Molecular Simulation Methods to Investigate Protein Adsorption Behavior at the Atomic Level &", Elsevier BV, 2017 Publication	<1%
19	digitalarchive.boun.edu.tr Internet Source	<1%
20	durham-repository.worktribe.com Internet Source	<1%
21	eprints.hud.ac.uk Internet Source	<1%
22	Lee, Yohan, Yunju Kim, and Yongwon Seo. "Enhanced CH4 Recovery Induced via Structural Transformation in the CH4 – CO2 Replacement that Occurs in sH Hydrates", Environmental Science & Technology Publication	<1%
23	Park, Kyoyeon, Wei Lin, and Francesco Paesani. "Fast and Slow Proton Transfer in Ice: The Role of the Quasi-Liquid Layer and Hydrogen-Bond Network", The Journal of Physical Chemistry B	<1%
24	coek.info Internet Source	<1%
25	www.coursehero.com	

Internet Source

Fernando de Azevedo Medeiros, Iuri Soter Viana Segtovich, Frederico Wanderley Tavares, Amadeu K. Sum. "Sixty Years of the van der Waals and Platteeuw Model for Clathrate Hydrates—A Critical Review from Its Statistical Thermodynamic Basis to Its Extensions and Applications", Chemical Reviews, 2020

< 1 %

Publication

Mohammad Tariq, David Rooney, Enas Othman, Santiago Aparicio, Mert Atilhan, Majeda Khraisheh. "Gas Hydrate Inhibition: A Review of the Role of Ionic Liquids", Industrial & Engineering Chemistry Research, 2014

<1%

dokumen.pub

<1%

Xiaodong Shen, Yang Li, Yanxia Li, Long Shen, Nobuo Maeda, Yinde Zhang, Heng Wang, Xiaoguang Wang. " Ultrarapid Formation and Direct Observation of Methane Hydrate in the Presence of -Tryptophan ", ACS Sustainable Chemistry & Engineering, 2023

Publication

Ya-Long Ding, Chun-Gang Xu, Yi-Song Yu, Xiao-<1% 30 Sen Li. "Methane recovery from natural gas hydrate with simulated IGCC syngas", Energy, 2017 Publication "Natural Gas Hydrates", Springer Nature, <1% 31 2013 Publication Titus V. Albu, José C. Corchado, Donald G. <1% 32 Truhlar. "Molecular Mechanics for Chemical Reactions: A Standard Strategy for Using Multiconfiguration Molecular Mechanics for Variational Transition State Theory with Optimized Multidimensional Tunneling", The Journal of Physical Chemistry A, 2001

Exclude quotes

On

Exclude matches

< 14 words

Exclude bibliography On

Publication